

Katharina Kodolitsch, BSc

Metal-organic frameworks with imidazole-carboxylate containing ligands

MASTER'S THESIS

to achieve the university degree of

Diplom-Ingenieurin

Master's degree programme: Technical Chemistry

submitted to

Graz University of Technology

Supervisor

Assoc.Prof. Dipl.-Ing. Dr.techn. Christian Slugovc

Institute for Chemistry and Technology of Materials

AFFIDAVIT

I declare that I have authored this thesis independently, that I have not used other than the declared sources/resources, and that I have explicitly indicated all material which has been quoted either literally or by content from the sources used. The text document uploaded to TUGRAZonline is identical to the present master's thesis.

Date

Signature

Danksagung

An dieser Stelle möchte ich meinen besonderen Dank nachstehenden Personen entgegen bringen, ohne deren Mithilfe die Anfertigung dieser Masterarbeit niemals zustande gekommen wäre:

Mein Dank gilt zunächst Herrn Prof. Dr. Christian Slugovc, für die Betreuung dieser Arbeit, der freundlichen Hilfe und der zahlreichen Ideengebungen, die mir einen kritischen Zugang zu dieser Thematik eröffnete.

Des Weiteren möchte ich mich bei Paolo Falcaro, Ana Trovisco, Raffaele Ricco, Franz Mautner, Josefine Hobisch und Petra Kaschnitz bedanken, für die Zeit die sie sich genommen haben, die Messungen und teilweise die Auswertungen für meine Arbeit durchzuführen.

Ein großer Dank gilt auch der gesamten Arbeitsgruppe, insbesondere Petra Hofstadler und Bettina Schafzahl, für die zahlreichen Hilfestellungen, Anregungen und Ideen, die mir meine Laborarbeit um einiges erleichtert haben. Danke für die angenehme Atmosphäre während meiner gesamten Zeit am Institut.

Abschließend möchte ich mich bei meinen Eltern bedanken für jegliche Unterstützung in meinem Leben insbesondere während meiner Studienzeit. Ich bin euch sehr dankbar, dass ihr mir all das ermöglicht habt. Danke an meine Schwester Elisabeth, die meine Launen während stressigen Zeiten ertragen hat. Du hast es immer geschafft mich wieder aufzubauen und zu motivieren. Damit hast du maßgeblich zu dieser Arbeit beigetragen.

Abstract

Metal-organic frameworks are widely regarded as promising materials for a huge variety of different applications. Compared to conventionally used microporous inorganic materials, like zeolites, these structures have the potential for a more flexible design.

In this work a truly green way to prepare potentially multidentate ligands namely 3-(1H-imidazol-1-yl)propanoic acid derivatives is disclosed. The synthesis of the ligands was done by an aza-Michael addition reaction with reaction conditions avoiding the use of a solvent and a catalyst. In a second step, the ligands have been saponified with NaOH. The obtained salts have been used for the assembly of metal-organic frameworks from water solutions of the precursors and laying the focus on zinc as the metal center.

Two of the obtained metal organic frameworks have been characterized in detail. The first is composed of zinc and 3-(1H-imidazol-1-yl)propanoate and initially forms an amorphous solid which slowly crystallizes under gentle heating to yield a crystalline material. The crystal is composed of 2D coordination polymer sheets linked to a 3D network by water molecules. It features an internal surface area of 190 m²/g. The second metal organic framework consists of zinc and 3-(2-methyl-1H-imidazol-1-yl)propanoate as the linker and forms directly as a microcrystalline powder, which under gentle heating grows in bigger single crystals. The crystals are composed by 1D coordination polymer chains which are linked by hydrogen bonding with additional water creating a 3D scaffold with an internal surface area of 110 m²/g.

Kurzfassung

Metall-organische Gerüstverbindungen werden weithin als vielversprechende Materialien für eine große Vielzahl von verschiedenen Anwendungen angesehen. Im Vergleich zu herkömmlich verwendeten mikroporösen anorganischen Materialien, wie Zeolithen, haben diese Strukturen das Potenzial für eine flexiblere Konstruktion.

In dieser Arbeit wird ein grüner Weg zur Herstellung potentiell mehrzähliger Liganden, nämlich 3-(1H-Imidazol-1-yl) propansäurederivaten, offenbart. Die Synthese der Liganden wurde durch eine Aza-Michael-Additionsreaktion durchgeführt mit Reaktionsbedingungen, bei denen die Verwendung eines Lösungsmittels und eines Katalysators vermieden wurde. In einem zweiten Schritt wurden die Liganden mit NaOH verseift. Die erhaltenen Salze wurden für den Aufbau metallorganischer Gerüste in wässriger Lösung verwendet und der Schwerpunkt wurde auf Zink als Metallzentrum gelegt.

Zwei der erhaltenen metall-organischen Gerüste wurden im Detail charakterisiert. Das erste besteht aus Zink und 3-(1H-Imidazol-1-yl)propanoat und bildet zunächst einen amorphen Feststoff, der sich unter leichtem Erwärmen langsam in ein kristallines Material umwandelt. Der Kristall besteht aus 2D-Koordinationspolymerschichten, die durch Wasserstoffbrückenbindungen von eingelagerten Wassermolekülen zu einem 3D-Netzwerk verbunden sind. Die Verbindung weist eine innere Oberfläche von 190 m²/g auf. Die zweite metall-organische Gerüstverbindung besteht aus Zink und 3-(2-Methyl-1H-imidazol-1-yl)propanoat als Linker und bildet sich sofort als mikrokristallines Pulver, welches unter sanfter Erwärmung zu größeren Einkristallen wächst. Die Kristalle bestehen aus 1D-Koordinationspolymerkettens, die durch Wasserstoffbrücken mit zusätzlichen Wassermolekülen, ein 3D-Gerüst mit einer inneren Oberfläche von 110 m²/g ausbilden.

Table of content

1. Introduction	1
2. General Aspects	2
2.1 Zeolitic imidazolate frameworks (ZIFs)	2
2.2 Metal-organic carboxylate frameworks	4
2.2 Metal - organic frameworks with multifunctional ligands	5
3. Results and Discussion	7
3.1 The aza-Michael reaction	8
3.1.1 Dependence of the pK _a value	14
3.1.2 Kinetic investigations.....	15
3.2 Saponification reaction	19
3.3 Metal-organic frameworks	21
3.3.1 Zinc-organic frameworks.....	21
3.3.1.1 Sodium 3-(2-methyl-1H-imidazol-1-yl)propanoate + Zn(NO ₃) ₂ (1AZn).....	21
3.3.1.2 Sodium 3-(1H-imidazol-1-yl)propanoate + Zn(NO ₃) ₂ (2AZn)	35
3.3.1.3 Sodium 3-(2-phenyl-1H-imidazol-1-yl)propanoate + Zn(NO ₃) ₂ (6AZn).....	46
3.3.1.4 Sodium 3-(2-methyl-1H-imidazol-1-yl)butanoate + Zn(NO ₃) ₂ (1BZn).....	50
3.3.1.5 Sodium 2-methyl-3-(2-methyl-1H-imidazol-1-yl)propanoate + Zn(NO ₃) ₂ (1CZn)	52
3.3.1.6 Sodium 3-(1H-pyrazol-1-yl)propanoate+ Zn(NO ₃) ₂ (3AZn)	52
3.3.2 Iron-organic frameworks.....	53
3.3.2.1 Sodium 3-(1H-imidazol-1-yl)propanoate + Fe ₂ SO ₄ (2AFe).....	53
4. Conclusion and Outlook	55
5. Experimental	56
5.1 Reagents	56
5.1.1 Chemicals.....	56
5.2 Instruments	56
5.2.1 NMR-spectroscopy	56
5.2.2 Infrared-spectroscopy	56
5.2.3 SC- XRD	56
5.2.4 XRD.....	56
5.2. Synthesis	58
5.2.1. Aza-Michael addition reaction	58
5.2.1.1. Methyl 3-(2-methyl-1H-imidazol-1-yl)propanoate (38)	58
5.2.1.2. Methyl 3-(1H-imidazol-1-yl)propanoate (12)	59
5.2.1.3. Methyl 3-(1H-pyrazol-1-yl)propanoate (8)	60
5.2.1.4. Methyl 3-(1H-1,2,4-triazol-1-yl)propanoate (9)	61
5.2.1.5. Methyl 3-(2-phenyl-1H-imidazol-1-yl)propanoate (67).....	62
5.2.1.6. Methyl 3-(2-methyl-1H-imidazol-1-yl)butanoate (33)	63
5.2.1.7. Methyl 2-methyl-3-(2-methyl-1H-imidazol-1-yl)propanoate (35).....	64
5.2.1.8. Dimethyl 2-(1H-imidazol-1-yl)succinate (50).....	65
5.2.1.9. 3-(2-Methyl-1H-imidazol-1-yl)propanenitrile (21).....	66
5.2.1.10. 3-(1H-Imidazol-1-yl)propanenitrile (22)	67

5.2.1.11. Methyl 3-(1H-benzo[d]imidazol-1-yl)propanoate (25)	68
5.2.1.12. Methyl 3-(1H-imidazol-1-yl)butanoate (27)	69
5.2.1.13. Methyl 3-(1H-imidazol-1-yl)-2-methylpropanoate (36)	70
5.2.2. Saponification reaction	71
5.2.2.1. Sodium 3-(2-methyl-1H-imidazol-1-yl)propanoate (20)	71
5.2.2.2. Sodium 3-(1H-imidazol-1-yl)propanoate (24)	72
5.2.2.3. Sodium 3-(2-phenyl-1H-imidazol-1-yl)propanoate (73)	73
5.2.2.4. Sodium 3-(2-methyl-1H-imidazol-1-yl)butanoate (62)	74
5.2.2.5. Sodium 2-methyl-3-(2-methyl-1H-imidazol-1-yl)propanoate (46)	75
5.2.2.6. Sodium 3-(1H-pyrazol-1-yl)propanoate (98)	76
5.2.3 Metal-organic frameworks	77
5.2.3.1 Sodium 3-(2-methyl-1H-imidazol-1-yl)propanoate + Zn(NO ₃) ₂ (1AZn)	77
5.2.3.2. Sodium 3-(2-methyl-1H-imidazol-1-yl)propanoate + Zn(Ac) ₂ (1AZn)	77
5.2.3.3. Sodium 3-(1H-imidazol-1-yl)propanoate + Zn(NO ₃) ₂ (1BZn)	78
5.2.3.4. Sodium 3-(2-phenyl-1H-imidazol-1-yl)propanoate + Zn(NO ₃) ₂ (6AZn)	78
5.2.3.5. Sodium 3-(2-methyl-1H-imidazol-1-yl)butanoate + Zn(NO ₃) ₂ (1BZn)	79
5.2.3.6. Sodium 2-methyl-3-(2-methyl-1H-imidazol-1-yl)propanoate + Zn(NO ₃) ₂ (1CZn)	79
5.2.3.7. Sodium 3-(1H-pyrazol-1-yl)propanoate + Zn(NO ₃) ₂ (3AZn)	80
5.2.3.8. Sodium 3-(1H-imidazol-1-yl)propanoate + Fe ₂ SO ₄ (2AFe)	80
6. List of Abbreviations	81
6. List of Figures	82
7. List of Tables	83
8. Appendix	84
8.1 NMR spectra	84
8.2 IR spectra	84
8.3 TGA	84
8.4 SC-XRD	84
8.5 XRD	84
8.6 BET	84

1. Introduction

Metal-organic frameworks (MOFs) have a fascinating variety of topologies, enthralling structures, interesting properties and potential applications. That is the reason why there is an increasing interest in the assembling and design of MOFs in the fields of coordination chemistry and crystal engineering.^[1] MOFs are comprised of metal ions and bridging ligands that form either two- or three-dimensional networks which may possess porosity.^[2] Because of this porosity and highly ordered structure they could be suitable for a wide range of applications—for example, gas sorption and separation,^[3] catalysis^[4] and ion transport.^[5] The preparation of these materials is adaptable and can be influenced among other things by the nature of the organic ligands, the coordination preference of the central metal ion, the crystallization conditions, the metal/ligand ratio and the solvent system. It is possible to use a great variety of organic ligands for the construction of MOFs with peculiar structures and properties. Currently, the imidazole-carboxylate ligands have attracted increasing attention in preparation due to their strong coordination affinity for various metal centers, versatile coordination modes and outstanding features of versatile coordination fashions.^[6,7] The underlying idea is the use of N donor ligands, usually nitrogen heterocyclic compounds such as pyridine, imidazole or triazole which are linked to a carboxylate group. The carboxylate functions as a spacer to increase the distance between the metal atoms. As a result the pore width should become larger. MOFs containing Zn(II) as the metal ion are remarkably fascinating as their d^{10} configuration facilitates a variety of coordination numbers and coordination geometries.^[1]

The focus in this master thesis lies on the assemblies and structures of Zn(II) MOFs with N and O donor ligands. The synthesis of the ligands was done with an aza-Michael addition reaction. There is a multitude of different donor and acceptor substrates used, leading to the focus on methyl acrylate as an acceptor and imidazole as a donor. After the aza-Michael addition reaction the synthesized ligands were saponified for the further use of the assembly of the metal organic frameworks with zinc salts and also with a variety of other metal salts.

¹ Y. Sun, W. Sun, Zinc and cadmium-organic frameworks with 1-imidazole-containing and 1-imidazole-carboxylate ligands, *CrystEngComm*, **2015**, 17, 4045-4063.

² S. Horike, S. Kitagawa, Unveiling liquid MOFs, *Nature Materials*, 16, **2017**.

³ J. W. Yoon, *et al.*, Selective nitrogen capture by porous hybrid materials containing accessible transition metal ion sites, *Nat. Mater.* 16, **2017**, 526-531.

⁴ J. Mondloch. *et al.*, Destruction of chemical warfare agents using metal-organic frameworks, *Nat. Mater.* 14, **2015**, 512-516.

⁵ S. Horike, D. Umeyama, S. Kitagawa, Ion conductivity and transport by porous coordination polymers and metal-organic frameworks, *Acc. Chem. Res.* 46, **2013**, 2376-2384.

⁶ R. Gaillac, Liquid metal-organic frameworks, *Nature Materials*, 16, **2017**.

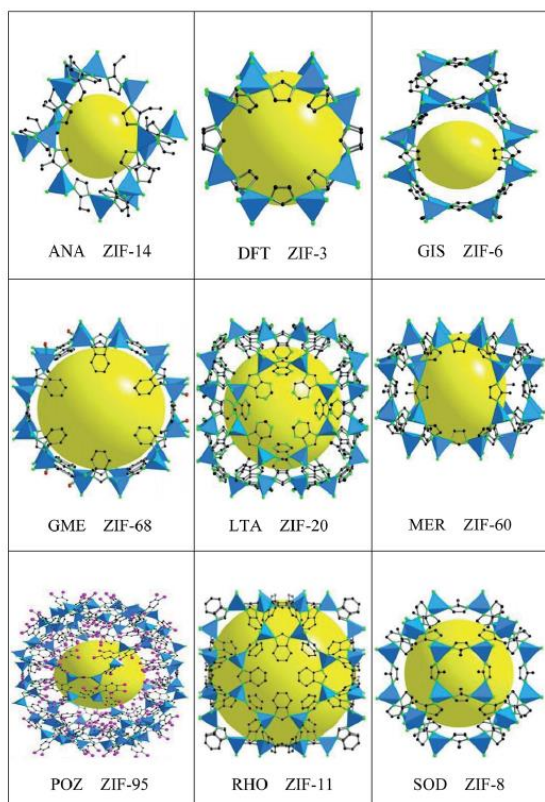
⁷ Z. Gu, *et al.*, Construction of Metal-Imidazole-Based Dicarboxylate Networks with Topological Diversity: Thermal Stability, Gas Adsorption and Fluorescent Emission Properties, *Crst. Growth Des.* **2012**, 12, 2178-2186.

2. General Aspects

2.1 Zeolitic imidazolate frameworks (ZIFs)

Crystalline microporous zeolites are used in a large segment for petrochemical cracking, ion-exchange, water softening and purification and in the separation of gases. They are composed of tetrahedral Si(Al)O₄ units which are covalently linked by oxygen atoms to create a framework.^[8] Zeolitic imidazolate frameworks (ZIFs) are comprised of imidazolate linkers and metal ions, with structures similar to these conventional aluminosilicate zeolites. The metal ions play the role of silicon and the imidazole anions forms bridges that mimic the role of oxygen in zeolites, with a metal – imidazole – metal angle of ~ 145°.^[9]

The imidazole group contains two nitrogen atoms; therefore the imidazole-containing compound can either act as neutral and monodentate ligand or as a negative and bidentate ligand, depending on the substitution position. Deprotonated imidazolate ligands coordinate with metal centers to generate frameworks.^[1]



ZIFs are built upon 4-connected nets of tetrahedral units, wherein metal ions like Zn²⁺ or Co²⁺ are linked through N atoms. Because of their high thermal and chemical stability, structural flexibility and rational design varieties they have already been proven as potential material for many different applications, like H₂ storage, CO₂ adsorption, alkane/alkene separation and heterogeneous catalysis.^[10] The representative ZIFs are shown in Figure 1. The first three capital letters under each example stand for the zeolite structure code.

Figure 1: Crystal structures of ZIFs^[9]

⁸ K. Park, Z. Ni Z, A. Côté, *et al.* Exceptional chemical and thermal stability of zeolitic imidazolate frameworks. *Proceedings of the National Academy of Sciences of the United States of America*, **2006**, 103 (27), 10186-10191.

⁹ C. Binling, Y. Zhuxian, Z. Yanqui, X. Yongde, Zeolitic imidazolate framework materials: recent progress in synthesis and applications. *J. Mater. Chem. A.*, **2014**, 2, 16811-16831.

¹⁰ Y. Lee, M. Jang, H. Cho, H. Kwon, S. Kim, W. Ahn, ZIF-8: A comparison of synthesis methods, *Chemical Engineering Journal*, **2015**, 271, 276-280.

They possess the characteristics of both MOFs and zeolites such as ultrahigh surface areas, unimodal micropores, high crystallinities and abundant functionalities.^[8,10]

ZIF-8 ($\text{Zn}(\text{mIM})_2$, mIM = 2-methylimidazolate) is currently the most investigated ZIF material. It consists of a 2-methylimidazole which is linked via the nitrogen to the zinc atoms. The structure has the regular zeolitic sodalite (SOD) topology which is shown in Figure 2. The yellow inscribed sphere represents the maximum size of any adsorbed molecule.^[8,10]

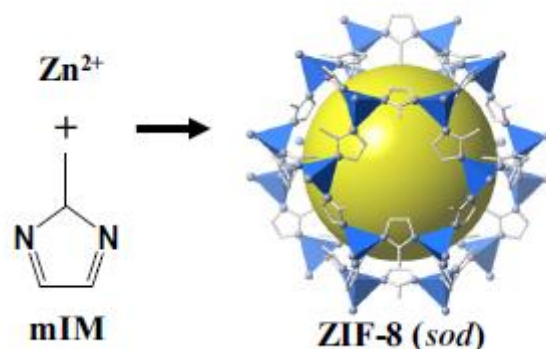


Figure 2: Crystal structure of ZIF-8

The preparation is traditionally done by hydrothermal or solvothermal synthesis routines in water or organic solvents respectively, with reaction temperatures varying from room temperature up to 200 °C and the reaction duration from hours to days. There is a variety of preparation methods including solvent-based and solvent-free methods, depending on the desired structure (powder, film/membrane etc.).^[9]

The architectural rigidity and permanent porosity of ZIF-8 were proven by gas-sorption analysis. With the Langmuir model surface areas from 1,810 m^2/g and with Brunauer-Emmett-Teller (BET) model surface areas from 1,630 m^2/g were obtained. These are the highest surface area values which ever have been reported for zeolites. The pore diameter is around 11.6 Å and the pore aperture diameter 3.4 Å. For the determination of the thermal stability, thermal gravimetric analysis (TGA) was performed. The TGA trace showed a gradual weight-loss step of 28.3% from a starting temperature of 25 °C till 450 °C. The chemical stability was examined by suspending the ZIF-8 in solvents like benzene, methanol, water and aqueous sodium hydroxide at the boiling point of each medium and found to be insoluble under these conditions.^[8]

2.2 Metal-organic carboxylate frameworks

Open metal organic frameworks are promising materials for catalysis, gas separation and storage and molecular recognition. By comparing them with the conventional used microporous inorganic materials like zeolites, they have the potential for a more flexible rational design.^[11]

Multidentate linkers like carboxylates can form such frameworks with a higher rigidity due to their ability to aggregate metal ions into M-O-C clusters. This rigidity arises because the metal ions are locked into their position by the carboxylates. These carboxylates can be joined by organic links to produce extended frameworks of high structural stability. There can be long links used that increase the spacing between the vertices in a net yields void space proportional to the length of the linker. Such expanded structures provide large pores, but they are often found to be highly interpenetrated and to have a low porosity.^[12]

A very important MOF is the $Zn_4O_{13}C_{24}H_{12}$ framework, also known as MOF-5. MOF-5 is a zinc based metal-organic framework that consists of $[Zn_4O]^{6+}$ clusters joined to an octahedral array of benzene-1,4-dicarboxylate groups (BDC) to form a cubic $Zn_4O(BDC)_3$ network, in which the centers of the clusters have a distance of 12.9 Å. The synthesis is normally performed by solvothermal methods. Therefore the mixture of organic linker and metal salt is in a solvent system, that usually contains formamide functionality, is heated up. Cubic crystals could be obtained with an ultra-high BET surface area up to 3400 m²/g.^[13,14]

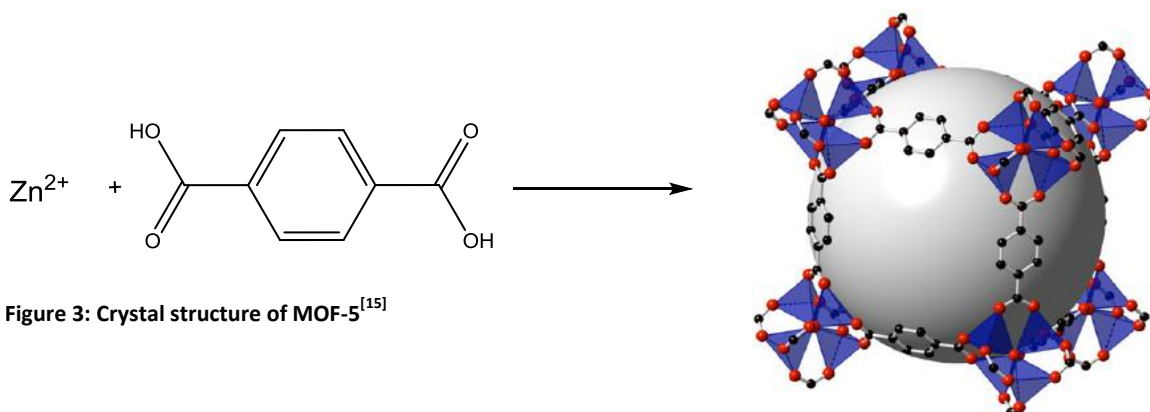


Figure 3: Crystal structure of MOF-5^[15]

The Zn-O-C clusters at the corners are linked through one benzene linker, as shown in Figure 3.

¹¹ H. Li, *et al.*, Design and synthesis of an exceptionally stable and highly porous metal-organic framework, *Nature*, 402, **1999**.

¹² M. Eddaoudi, *et al.*, Modular Chemistry: Secondary Building Units as a Basis for the Design of Highly Porous and Robust Metal-Organic Carboxylate Frameworks, *Acc.Chem.Res.* **2001**, 34, 319-330.

¹³ D. Tranchemontagne, J. Hunt, O. Yaghi, Room temperature synthesis of metal-organic frameworks, *Tetrahedron* 64, **2008**, 8553-8557.

¹⁴ L. Zhang, Y. Hu, Structure distortion of $Zn_4O_{13}C_{24}H_{12}$ framework (MOF-5), *Material Science and Engineering* 176, **2011**, 573-578.

¹⁵ Q. Li, T. Thonhauser, A theoretical study of the hydrogen-storage potential of $(H_2)_4CH_4$ in metal organic framework materials and carbon nanotubes, *J.Phys.: Condens. Matter* 24, **2012**.

2.2 Metal – organic frameworks with multifunctional ligands

Compared with these mono-functional organic ligands, bi-functional organic ligands, such as imidazole based-carboxylate ligands offer more possibilities to obtain higher dimensional coordination polymers and they are excellent candidates for preparing novel MOFs because of their versatile coordination modes and potential hydrogen bonding donors and acceptors. For example, benzimidazole-2-butanoic acid (H_2L) owns a flexible carboxylate arm with suitable length, which may exhibit various coordination modes with the nitrogen atoms from the benzimidazole and the oxygen atoms from the carboxylate coordinating metal ions. By using Zn^{2+} ions a 3D network with 3-connected etb topology is built in which each Zn^{2+} is tetrahedrally coordinated by two oxygen atoms and two nitrogen atoms from four different ligands (Figure 4a). There are small opened hexagonal channels formed in the 3D structure, providing the metal-organic framework with a suitable porosity (Figure 4b).^[16]

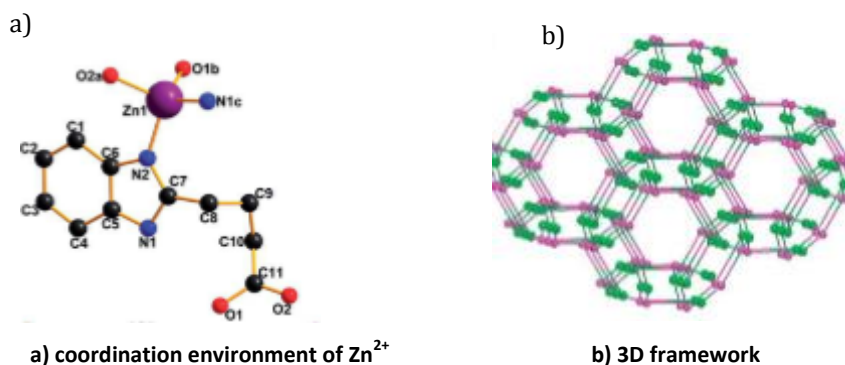


Figure 4: a) coordination environment of Zn^{2+}

b) 3D framework

Another metal-organic framework with a bi-functional organic ligand is disclosed in [17]. Here, imidazole-4,5-dicarboxylic acid (H_3IMDC) ligands and its derivatives, containing two nitrogen and four oxygen atoms providing them with multiple coordination sites for rigid and stable higher dimensional structures, were employed. The arrangement of the two nitrogen atoms with an N-metal-N angle of 144° is quite similar to the Si-O-Si angle which is typically found in zeolites and can favourably gear the coordination orientation. Furthermore, it has been found that the ligand can be partially or completely deprotonated, hence may exhibit very flexible coordination modes and a variety of different architectures. Up to now a great number of MOFs with similar ligands, which only differ in groups on the 2-position of the imidazole ring have been designed and studied, leading to the assumption that the group in the backbone modulates its coordination mode. By using ligands with different alkyl groups at the 2-position notable influences on the

¹⁶ Y. Zhang, Z. Du, X. Luo, Coordination Polymers with Different Dimensionalities: from 2D Layer to 3D Framework, *Z. Anorg. Allg. Chem.*, **2015**, 641 (15), 2637-2640.

¹⁷ Q. Zhai, R. Zeng, S. Li, Y. Jiang, M. Hu, Alkyl substituents introduced into novel d^{10} -metalimidazole-4,4-dicarboxylate frameworks: synthesis, structure diversities and photoluminescence properties, *CrystEngComm*, **2013**, 15, 965-976.

structure could be detected and whether a discrete compound, one-dimensional chain, two-dimensional layer or three dimensional framework is yielded.

Interesting for our work one MOF with a flexible alkyl-substituted ligand has been described - $[\text{Zn}(\text{H}_2\text{EIMDC})_2(\text{H}_2\text{O})_2] \cdot 2.25\text{H}_2\text{O}$ with $(\text{H}_3\text{EIMDC}) = 2\text{-ethyl-1H-imidazole-4,5-dicarboxylic acid}$. The preparation was done by dissolving both components in deionised water, mixing them and putting them into a Teflon-lined reactor at $180\text{ }^\circ\text{C}$ for 5 days. After cooling the mixture down to room temperature, colourless plate-like crystals have been obtained. The Zn^{2+} in compound is six coordinated by two nitrogen and two carboxylate oxygen atoms from the individual H_2EIMDC^- in the equatorial plane, and by two water oxygen atoms in axial position, leading to octahedral coordination geometry. The ligand anion acts as a chelating ligand through N and O atoms to form a five membered ring. The hydrogen bonds link the molecules to form a 1D chain along the b-axis (Figure 5a), which are further connected by crystallized water molecules via the hydrogen bonds to generate 2D layers and further a 3D supramolecular framework (Figure 5b).^[17]

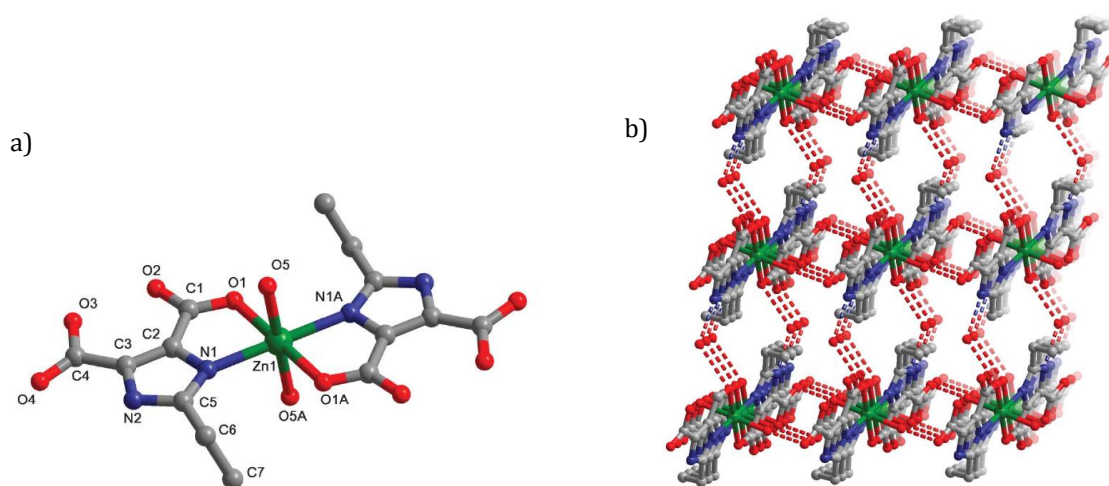


Figure 5: a) Coordination environment of Zn^{2+}

b) 3D framework formed by hydrogen bonds

3. Results and Discussion

The usage of multidentate ligands in constructing metal-organic frameworks has received increasing attention. Recently, the assembly based on carboxylate and/or N-heterocycles like imidazole and its derivate have triggered more interest due to structural diversities, wide potential applications and attractive physical and chemical properties. The ligands possess two N and two O potential binding centers and can serve as a class of superb multidentate ligands exhibiting a great variety of coordination modes. Furthermore the conjugated extent of the spacers spanned by the imidazole derivate and the carboxylate can be tunable.^[18] This might result in metal-organic frameworks with large cavities and thereby to a high porosity. The synthesis of the ligands was done by an aza-Michael addition reaction, which stands out as very facile and highly atom-efficient option for C-N bond formation. The reaction is normally performed under strongly acidic or basic conditions with high temperatures and requires long reaction times. Furthermore, the method is limited in substrate scope to aliphatic amine addition. In order to overcome these limitations a variety of Lewis acid metal catalysts have been disclosed for performing conjugate addition of aromatic amines to electron-deficient olefins under mild conditions.^[19] The use of this catalysts leads to a more efficient reaction completion, but they are often expensive, sensitive to air and moisture and they have to be removed at the end of the reaction.^[20]

The goal of this work was to perform the reaction with green reaction conditions and therefore it was performed without the addition of a solvent and without using a catalyst. Despite these unusual conditions there was the desired product, in quantitative yields and without any by-products, obtained. The effort of a work-up was minimized and there was no purification needed, as opposed to the synthesis in literature.^[20] Accordingly the ligands have been saponified with NaOH. There could be pure salts obtained in virtual quantitative conversion. Again there was no purification needed and the yielded ligand anion has been implemented with Zn²⁺ to receive a metal-organic framework.

¹⁸ M. Wu, *et. al.*, A diamond metal-organic framework with in situ generated 1H-tetrazolate-5-butyric acid ligand: Crystal structure, photoluminescence and high thermal stability, *Inorganic Chem. Comm.*, **2011**, 14, 333-336.

¹⁹ (a) D. Stevanovic, *et. al.*, Anodic generation of a zirconium catalyst for Ferrier rearrangement and hetero Michael addition, *Tetrahedron Lett.*, **2012**, 53, 6257-6260.

(b) D. Solè, Intramolecular α -Arylation of Sulfones: Domino Reactions in the Synthesis of Functionalized Tetrahydroisoquinolines, *Chem.Eur. J.*, **2015**, 21, 4580-4584.

²⁰ J. Gmach, L. Joachimiak, K.Blazewska, Aza-Michael Addition of Imidazole Analogues, *Synthesis*, **2016**, 48, 2681-2704.

3.1 The aza-Michael reaction

The aza-Michael reaction is a simple and accessible addition reaction performed at moderate temperature, normally done with the addition of a catalyst and a solvent. This addition reaction involves a nucleophile, more specifically an amine (Michael donor), and an electron deficient alkene molecule (Michael acceptor) such as acrylates or acrylamides.^[21]

In the current work a variety of donors (**1-12**) and acceptors (**A-F**) as shown in Figure 6 was used. As the Michael donor always a nitrogen heterocyclic compounds was selected in order to create N,O-coordinating ligands potentially useful for the generation of MOFs.

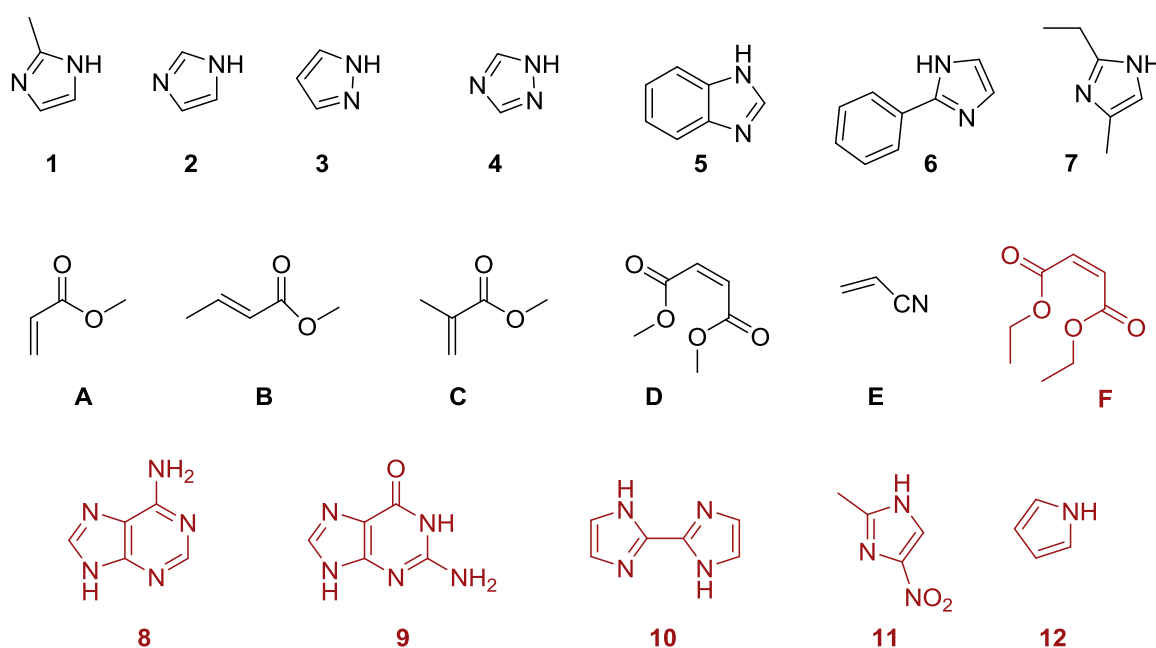


Figure 6: Donors and acceptors used for the Michael addition reaction

The reaction was performed without any additional solvent or catalyst at 80 °C, by combining both components with each other. There was an excess of the acceptor from 1.2 equivalents, in most cases. In some reactions the excess had to be larger, so that the donor was able to dissolve completely in the acceptor. The conversion was monitored by ¹H-NMR spectroscopy. After full conversion was detected, the reaction mixture was evaporated to get rid of the excess of the acceptor material and further dried under reduced pressure. It was possible to remove the whole excess in every case. All the products from the working reactions are given in Figure 7. The green marked ones have been further on used for the saponification reaction. The reactions

²¹ A. Genest, D. Portinha, E. Fleury, F. Ganachaud, The aza-Michael reaction as an alternative strategy to generate advanced silicon based (macro)molecules and material, *Progress in Polymer Science* 72, **2017**, 61-110.

of the blue compounds have worked as well with reasonable yields but they were not further studied within this work.

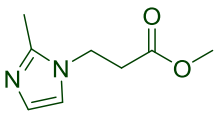
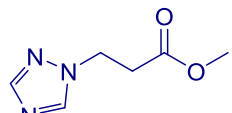
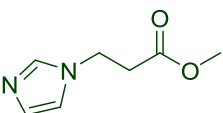
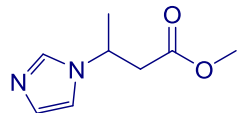
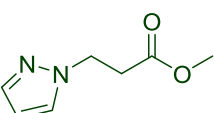
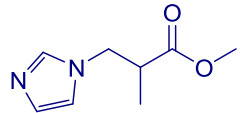
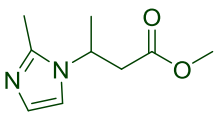
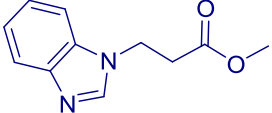
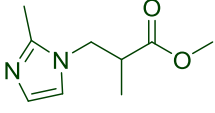
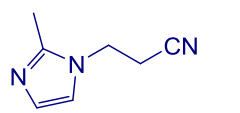
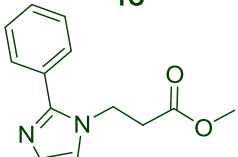
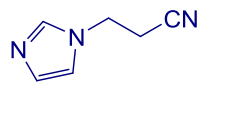
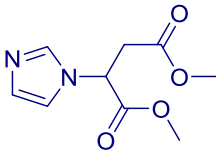
	Full conversion:	Yield:			
	6 h	>99 o.th.		2 h	>99% o.th.
1A			4A		
	5 h	>99% o.th.		24 h	>99% o.th.
2A			2B		
	4 h	>99% o.th.		24 h	>99% o.th.
3A			2C		
	24 h	>99% o.th.		48 h	>99% o.th.
1B			5A		
	24 h	>99% o.th.		4 h	>99% o.th.
1C			1E		
	72 h	>99% o.th.		3 h	>99% o.th.
6A			2E		
					80% o.th.
			2D		no full conversion not pure after column chromatography

Figure 7: Working aza-Michael addition reactions

The reaction is exemplarily described for 2-methylimidazole **1** and methyl acrylate **A** as the reactants (see Figure 8). The $^1\text{H-NMR}$ spectrum of the reaction mixture after drying under vacuum is shown for this particular case (Figure 9). The absence of peaks related to **1** indicates full conversion.

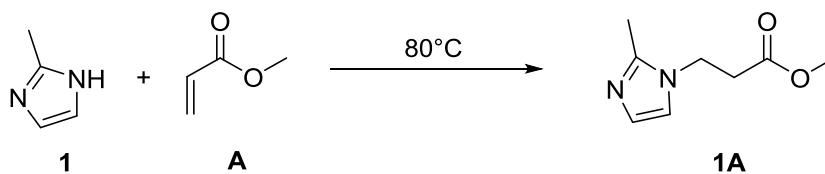


Figure 8: Michael addition reaction with 2-methylimidazole and methyl acrylate

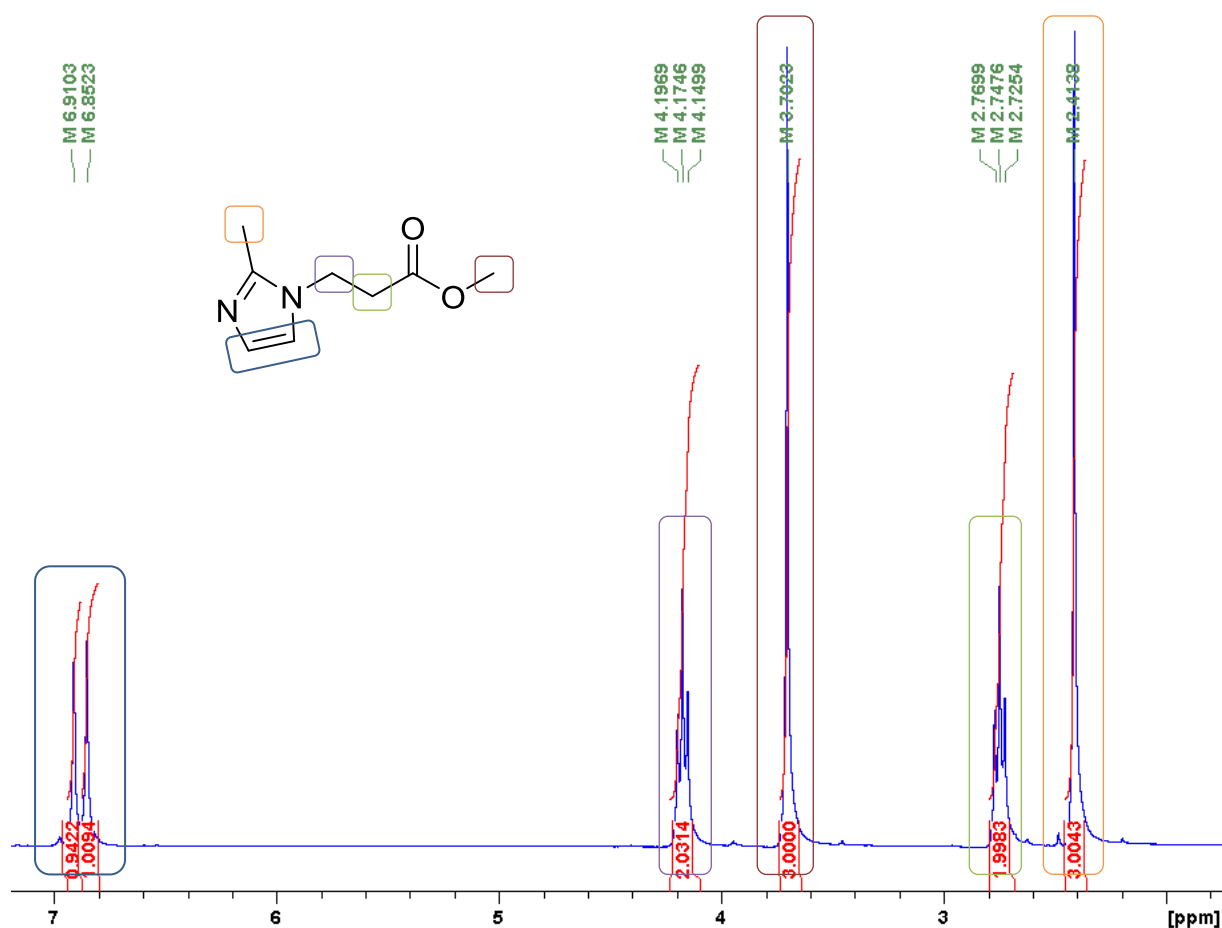


Figure 9: $^1\text{H-NMR}$ spectrum from 2-methylimidazole with methyl acrylate after full conversion

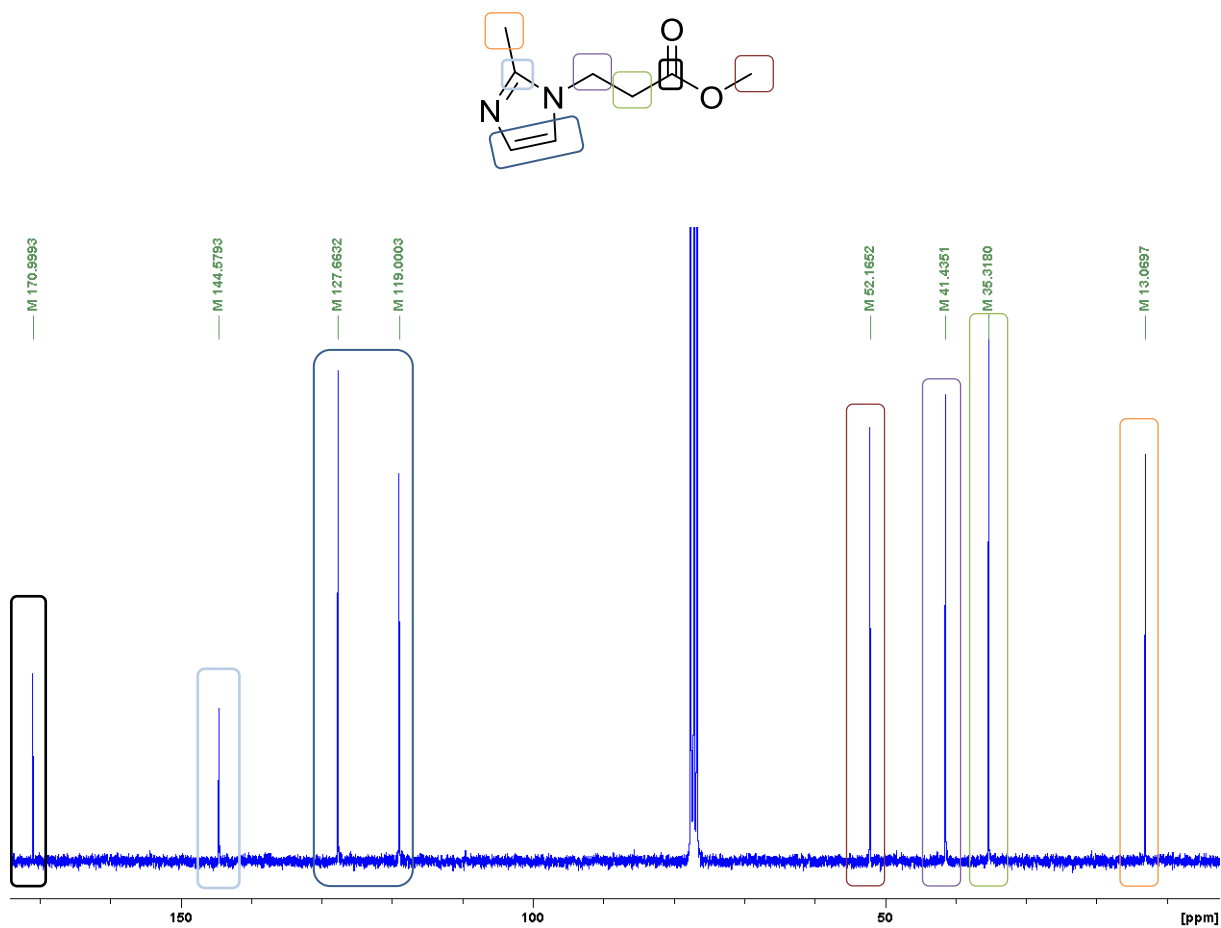


Figure 10: ^{13}C -NMR spectrum from 2-methylimidazole with methyl acrylate after full conversion

For the reaction with the red marked components (Figure 11), the desired product could not be obtained. The donor was either not soluble in the acceptor or no formation of the desired product could be detected with $^1\text{H-NMR}$ spectroscopy.

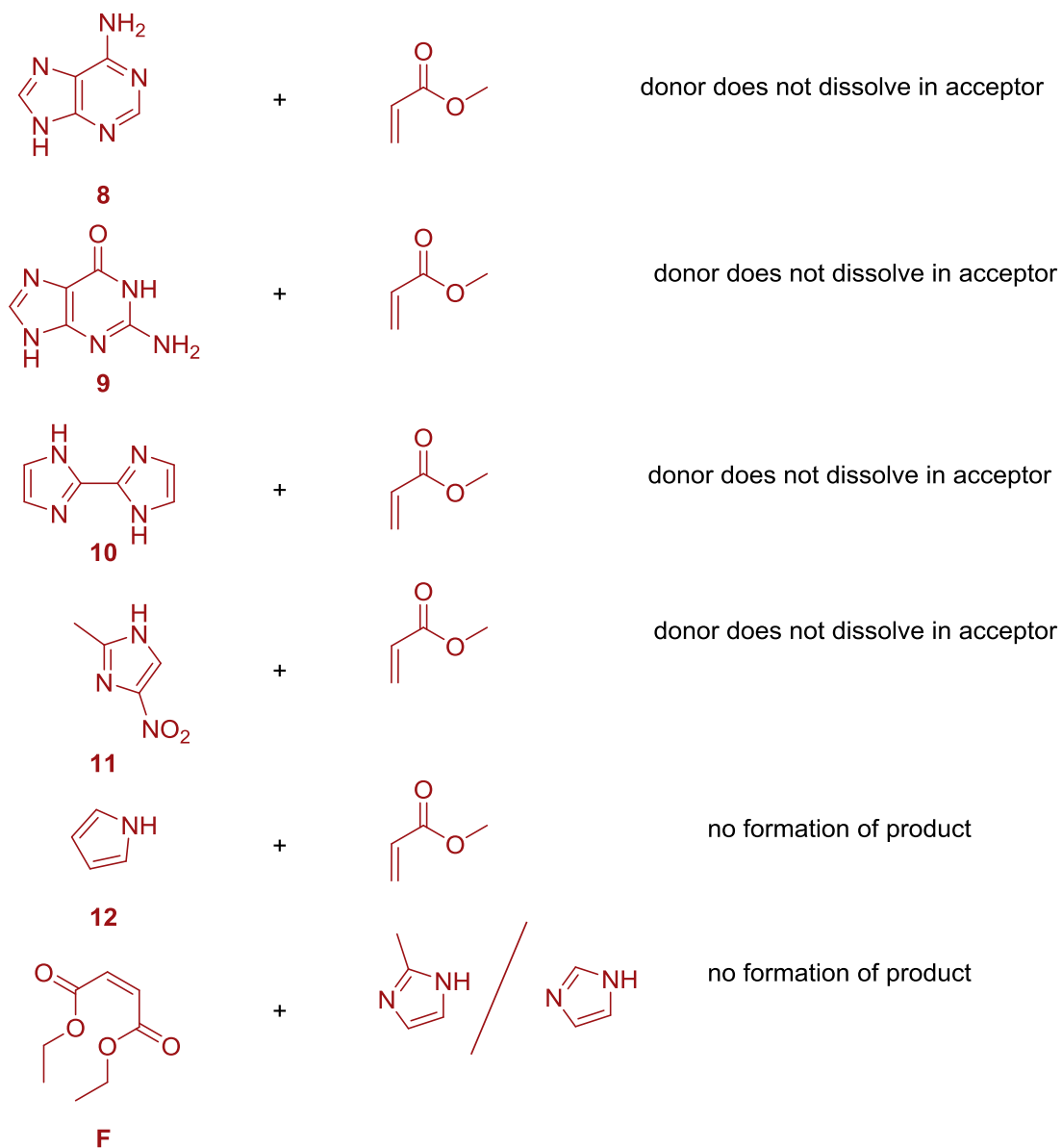


Figure 11: Unsuccessful aza-Michael addition reactions

In fact we have found preliminary support for the assumption, that the imidazole components are able to auto-catalyse themselves. There are quite a few different mechanisms described in literature. In the case of 2-methylimidazole a possible mechanism is formulated in [22], which proceed via abstraction of the N-H proton of the other N-heterocycle by the N¹ atom. Such an abstraction would enhance the nucleophilicity of the N-heterocycle for addition to electron deficient alkenes. If that is the case, the mechanism which takes place could proceed as shown in Figure 12.

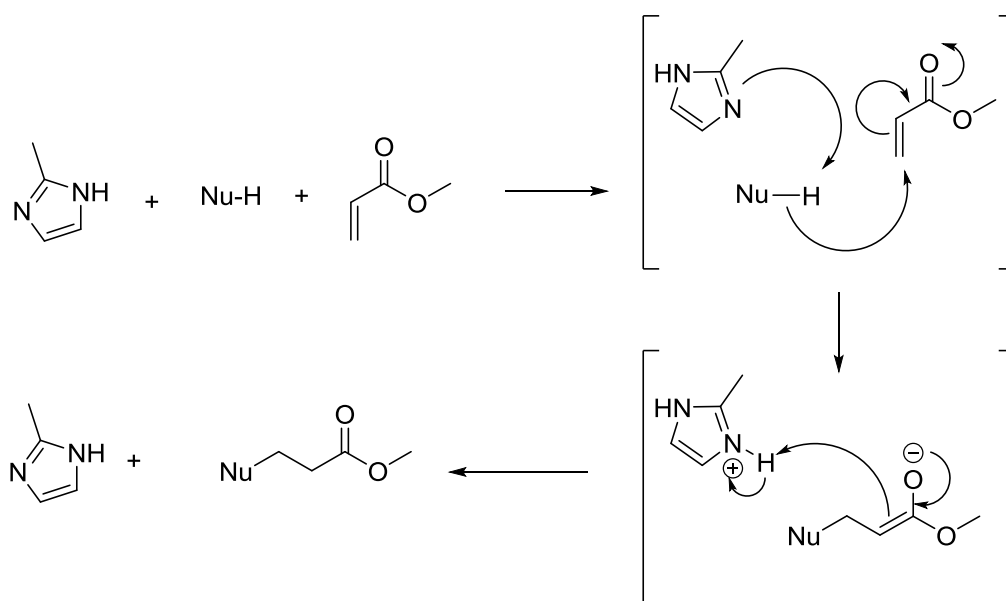


Figure 12: Mechanism for the nucleophile catalysed Michael addition^[22]

Most aza-Michael reaction protocols employ transition-metal catalysts such as SmI₂, CeCl₃, InCl₃, Cu(OTf)₃, LiClO₄ or heterogeneous solid acids.^[22] Having regard to the considerable cost and high toxicity of these metal complex catalysts, this utilised method completely avoids the use of them and makes the reaction atom economic.

²² B. Liu, Q. Wu, X. Qian, D. Lv, X. Lin, N-Methylimidazole as a Promising Catalyst for the Aza-Michael Addition Reaction of N-Heterocycles, *Synthesis* **2007**, 17, 2653-2659.

3.1.1 Dependence of the pK_a value

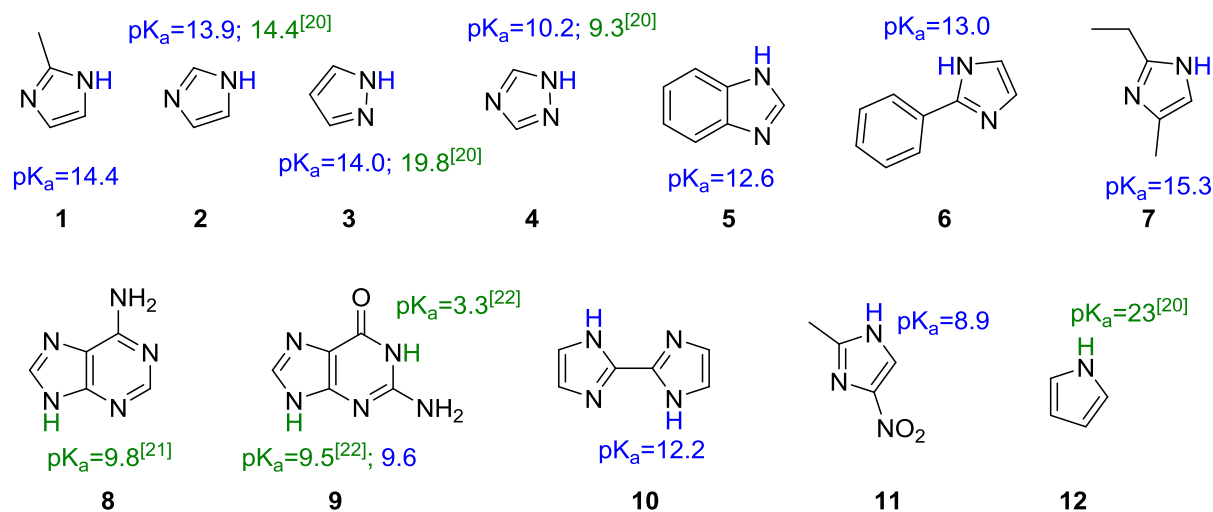


Figure 13: pK_a-values

- predicted with SciFinder
- value from literature^[23,24,25]

As shown before in Figure 6, the reaction with the N-heterocycles from the upper row (1-7) worked very well, in contrast to the N-heterocycles below (8-12). Figure 13 shows the pK_a-values for every compound. The pK_a values differ in the range between 9-23 and there could be no concrete value dependence detected. The only statement which could be made is that the donors have to be acidic and that it is likely that the reaction occurs faster the higher the acidity is. Therefore full conversion for the reaction of triazole **4**, which owns a pK_a value of approximately 10, could be detected after 2 h (Figure 7). Since compounds 8-11 are acidic as well, the failure of the reaction could be more likely caused by the limited solubility of the components, because all of them only dissolved partly in the acceptor component.

It was not possible to perform the reaction with pyrrole **12**. Pyrrole is a weak acid with a pK_a value of 23, which supports the assertion that the donor has to own a certain acidity. There was DMAP added as an additional catalyst, but the reaction could not be performed anyway.

²³ Baran, Richter, *Essential of Heterocyclic Chemistry-I*.

²⁴ Dawson, *et al.*, *Data for Biochemical Research*, Oxford, Clarendon Press, **1959**.

²⁵ R. Krishnamurthy, Role of pK_a of Nucleobases in the Origins of Chemical Evolution, *Accounts of Chemical Research*, **2012**, 45(12), 2035-2044.

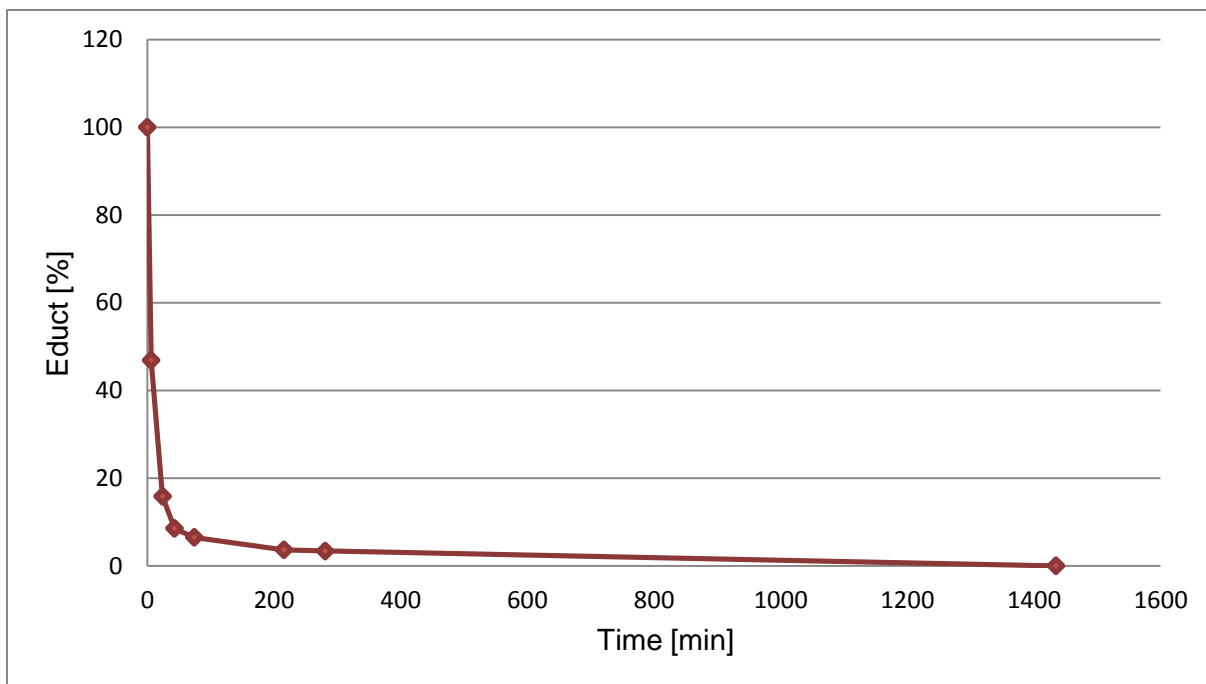


Figure 16: Decrease of the amount of educt against the time

Table 1: Degree of conversion

Time [min]	Educt: 2-Methylimidazole [%]
0	100
6	46.9
24	15.9
43	8.6
74	6.5
216	3.6
281 (~5 h)	3.4
1435 (~24 h)	0

The reaction proceeds quite fast as shown in Figure 16. After approximately six minutes half of the 2-methylimidazole was converted into the desired product. After about one hour there was only 6.5% educt left and the reaction got slower. The reason therefore could be the lack of solvent and the increased viscosity, and because of that it is more difficult for the two reacting components to reach each other for the interconversion.

For the determination of the reaction rate constant, $\frac{1}{[C_{educt}]}$ (for a second-order reaction) and $\frac{1}{[C_{educt}]^2}$ (for a third-order reaction) was plotted versus the time [min], in which c_{educt} means the concentration of educt. There were only the concentrations from 6-74 minutes used, because of their higher significance at the beginning of the reaction. The slope for the two different cases has a regression of 0.964 (2nd order) and 0.983 (3rd order). Because of this suitable plot for both cases the reaction order could not be determined exactly with this experiment.

Table 2: Concentration of educt

Time [min]	C_{educt} [%]	$1/[C_{educt}]$	$1/[C_{educt}]^2$
6	46.9	0.0213	$4.56 \cdot 10^{-4}$
24	15.9	0.0631	$3.98 \cdot 10^{-3}$
43	8.6	0.1169	$1.37 \cdot 10^{-2}$
74	6.5	0.1538	$2.37 \cdot 10^{-2}$

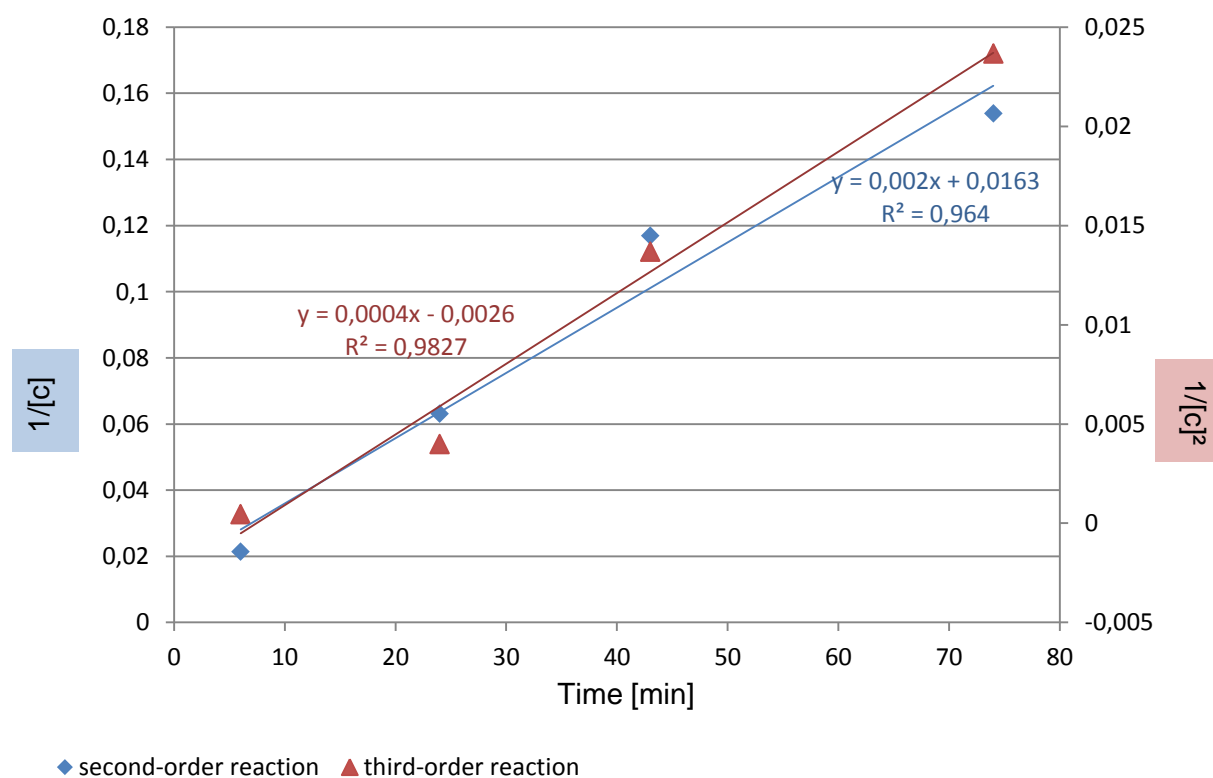


Figure 17: Plot $1/[c_{educt}]$ and $1/[c_{educt}]^2$ versus time [min]

The slope owns a gradient k , which could be determined with **0.002** in the case of a 2nd order reaction and **$4 \cdot 10^{-4}$** for a 3rd order reaction (Figure 17). If the reaction proceeds as a second-order reaction, the velocity of the reaction would only depend on the concentration of both educts. This differs from the case of the third-order reaction in which the formed imidazole-

carboxylate transition state intermediate is able to auto-catalyse the reaction and the reactions velocity depends on the concentration of the educts and the concentration of this intermediate. With the determined reaction rate constants the ideal courses of the reactions could be calculated (Formula 1) and are shown in Figure 18.

$$c_t(educt) = \frac{1}{2k * t + \frac{1}{c_0(educt)}}$$

Formula 1

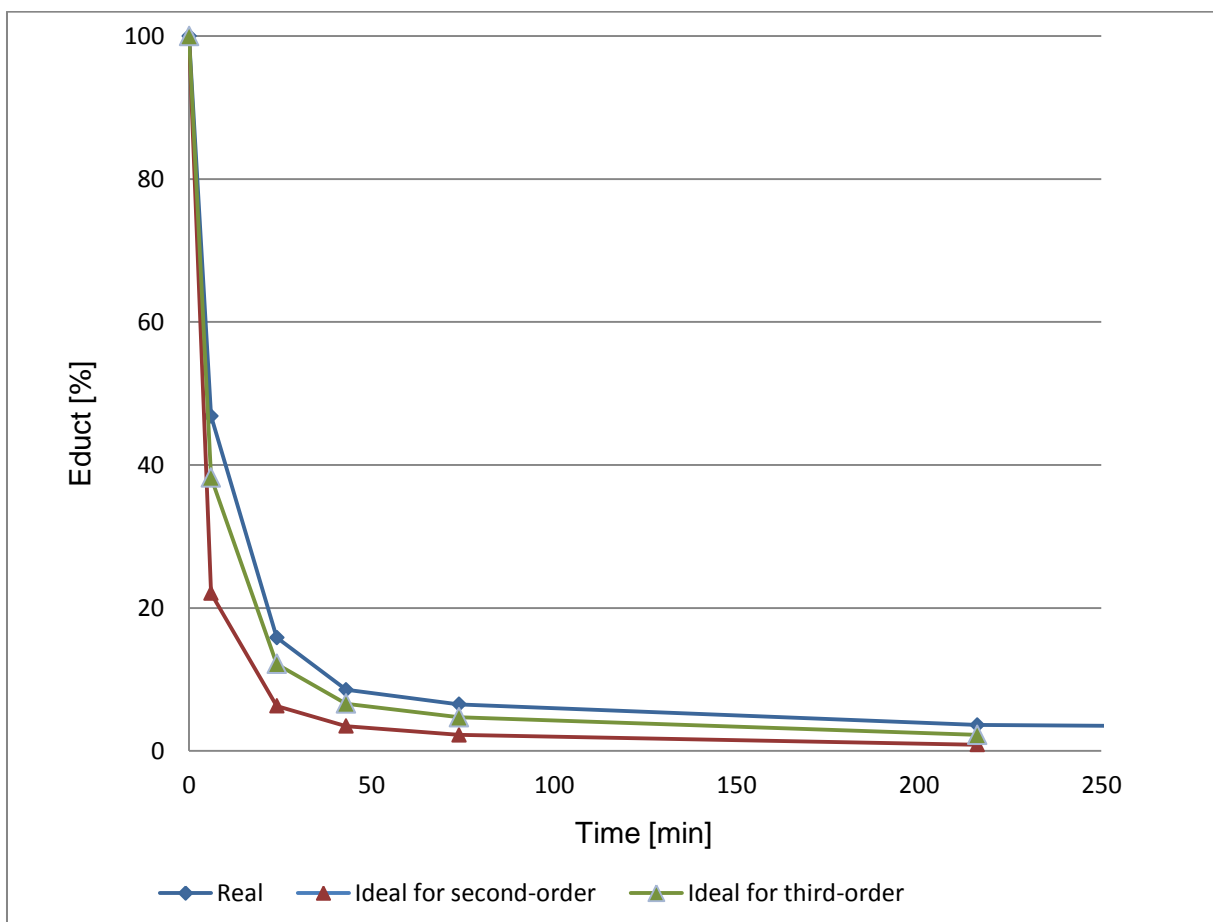


Figure 18: Ideal and real course of the reaction

The red curve shows the ideal course for a second-order reaction, which is faster than the real one. The green curve shows the ideal third-order reaction which is closer to the course of the real reaction, but should proceed faster as well. A conceivable reason therefore could be the lack of stirring.

3.2 Saponification reaction

For the saponification reaction a 5-6 M NaOH solution was used in an excess of 1.05 equivalents. The reaction was performed at 80 °C. The reaction vessel was unclosed to get rid of the resulting methanol and water. The formed product solidified after removing the heat. The reaction was done with all the synthesized ligands which are shown in Figure 7. In every case the pure colourless salt was obtained in virtual quantitative conversion (Figure 19).

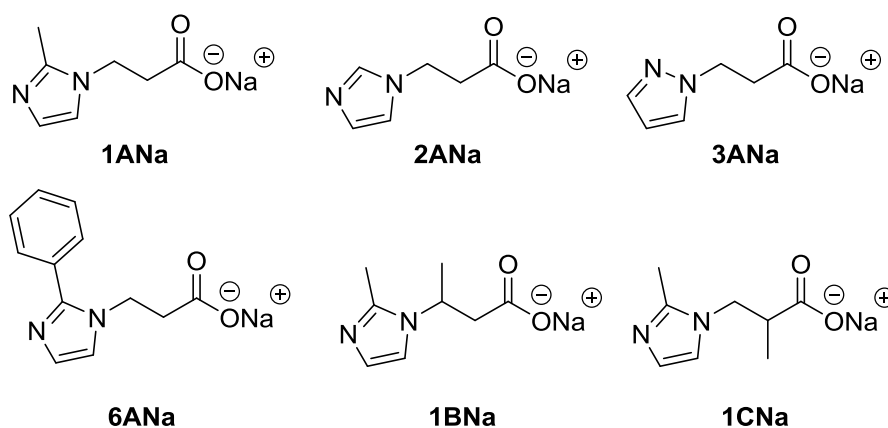


Figure 19: Compounds yielded after saponification

The suggested mechanism is shown below (Figure 20) in the case of methyl 3-(2-methyl-1H-imidazol-1-yl)propanoate with a sodiumhydroxid solution.

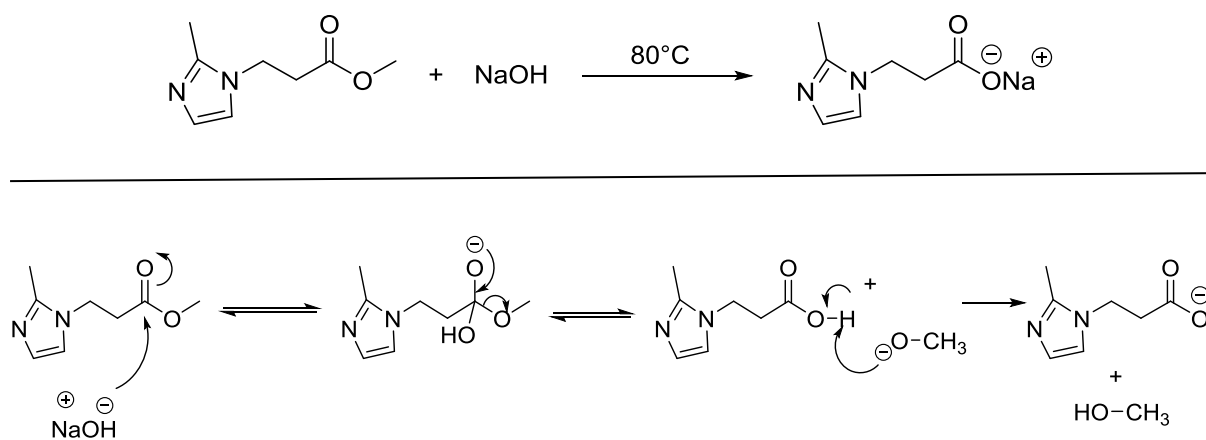


Figure 20: Mechanism of base hydrolysis^[26]

The hydroxide anion attacks the carbonyl group of the ester. Expulsion of the alkoxide generates a carboxylic acid. This alkoxide ion is a strong base so that the proton is transferred from the carboxylic acid to the alkoxide ion creating an alcohol, in this particular case methanol.^[26]

The conversion of the reaction was controlled with ATR-IR measurement (Figure 21). After the disappearance of the band from the ester group, which should occur approximately at a wavenumber of 1750-1735 cm^{-1} ^[28] the reaction was finished. The formed carboxylate group could be detected at a wavenumber of 1600 cm^{-1} , which is in the expected range.^[28]

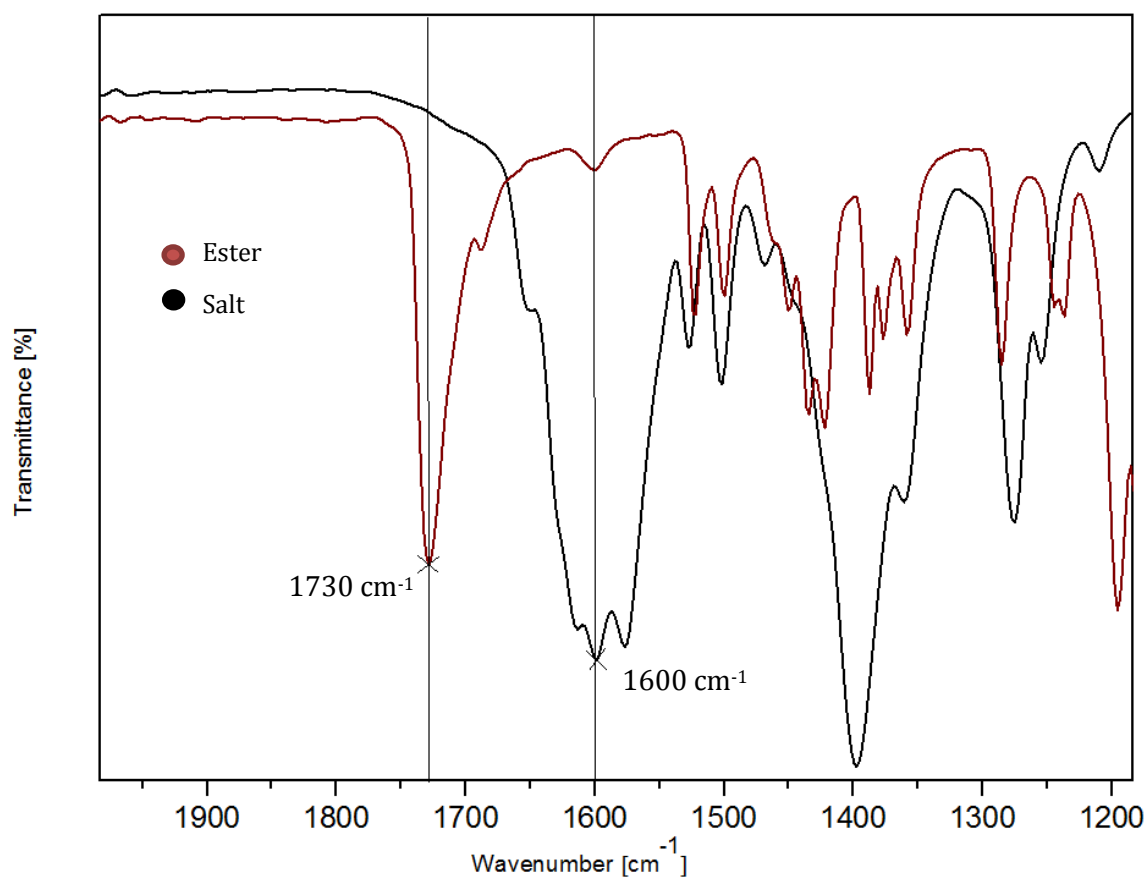


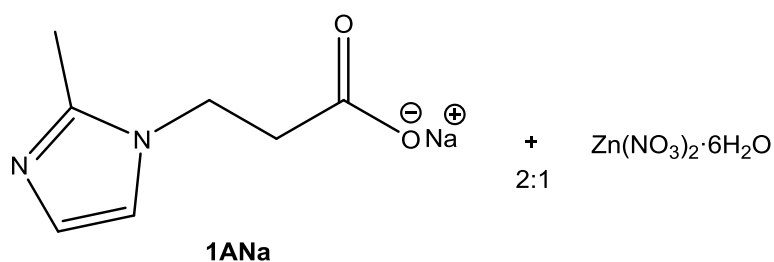
Figure 21: ATR-IR measurement from the ester and the salt

²⁶ Organikum, Wiley-VCH Verlag GmbH, 23. Auflage, 2009, 494-495

3.3 Metal-organic frameworks

3.3.1 Zinc-organic frameworks

3.3.1.1 Sodium 3-(2-methyl-1H-imidazol-1-yl)propanoate + Zn(NO₃)₂ (1AZn)



The reaction was done by dissolving the ligand (1.9 mmol) and the zinc salt (0.95 mmol) separately in respectively 5 mL water. The zinc solution was added to the ligand. Immediately a white fine precipitation was observed. The reaction mixture was heated up to 80 °C and a formation of clear cubic crystals could be detected after some hours. The supernatant, which should be water and NaNO₃, was removed and the crystals were washed with water. The precipitation (powder) which forms first and the crystals were analysed with different measurements (Figure 22) like XRD, SC-XRD, IR and TGA. The porosity was measured via BET measurement.

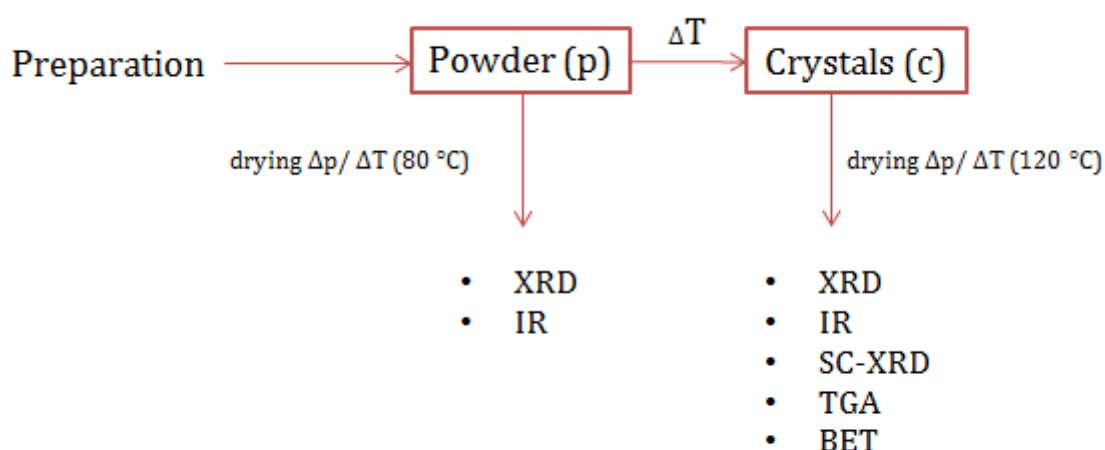


Figure 22: Measurements from the different prepared MOFs



Figure 23: Crystals (c) from the preparation with the methylimidazole ligand

The same crystals could be yielded by the preparation with $\text{Zn}(\text{Ac})_2 \cdot 2\text{H}_2\text{O}$. They have been characterized via SC-XRD as well and the same crystal structure could be determined.



Figure 24: Crystals from the preparation with $\text{Zn}(\text{Ac})_2 \cdot 2\text{H}_2\text{O}$

With the use of less solvent (water) no formation of clear crystals but a very fast formation of a fine white powder was observed. The obtained powder looked similar to the first formed precipitation. This leads to the assumption that the crystals arise when the crystallization process can occur slowly, which is given when enough water as a solvent is used.



Figure 25: Amorphous solid (powder (p))

By adding water to the powder and heating it up to 150 °C in the Monowave 50, the powder dissolves partly. The clear solution was separated from the powder residue and after some days there was a formation of the clear cubic crystals, which have been already described before.

Single crystal X-ray diffraction (SC-XRD):

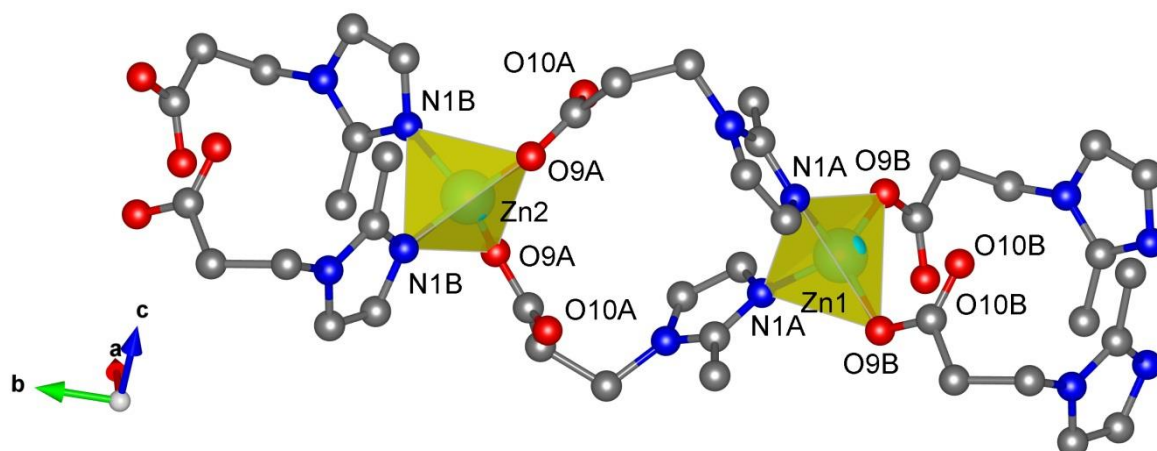


Figure 26: Crystal structure

The compound crystallizes in orthorhombic *Pcca* space group. The zinc atom is four coordinated and adopts a distorted tetrahedral geometry with angles around the metal centre ranging between 103.37 (7) ° and 128.59 (7) °. The zinc atom is coordinated to two oxygen atoms (O^{9a} and O^{9b}) and to two nitrogen atoms (N^{1a} and N^{1b}) from different ligand molecules. The Zn-O and Zn-N bond lengths are in the range of 1.9473 (11) and 2.0225 (13) Å (bonding) (Tab. 3). There is a formation of a grid structure through the linked ligands, which leads to the formation of cavities in the build 3D structure.

Table 3: Coordination around zinc

Coordination facility around Zn ^I		Coordination facility around Zn ^{II}	
Zn ^I —N ^{1a}	2.0225 (13) Å	Zn ^{II} —N ^{1b}	2.0177 (13) Å
Zn ^I —O ^{9b}	1.9473 (11) Å	Zn ^{II} —O ^{9a}	1.9419 (11) Å
Nonbonding:			
Zn ^{II} —O ^{10a}	3.0773 (12) Å		
Angles:			
O ^{9b} —Zn ^I —O ^{9b}	128.59 (7) deg	O ^{9a} —Zn ^{II} —O ^{9a}	123.51 (7) deg
N ^{1a} —Zn ^I —N ^{1a}	103.37 (7) deg	N ^{1b} —Zn ^{II} —N ^{1b}	103.21 (8) deg
N ^{1a} —Zn ^I —O ^{9b}	103.88 (5) deg	N ^{1b} —Zn ^{II} —O ^{9a}	103.06 (5) deg
Average bond length: 1.9849 Å		Average bond length: 1.9798 Å	
Distortion index (bond length): 0.01895		Distortion index (bond length): 0.01914	
Polyhedral volume: 3.8920 Å ³		Polyhedral volume: 3.8986 Å ³	

Quadratic elongation: 1.0210	Quadratic elongation: 1.0147
Bond angle variance: 94.8566 deg ²	Bond angle variance: 64.9615 deg ²
Effective coordination number: 3.9469	Effective coordination number: 3.9457

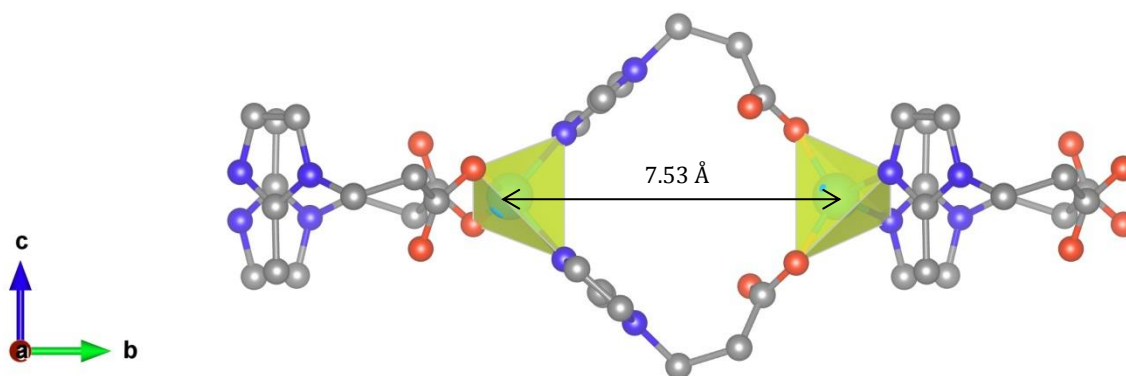


Figure 27: Coordination polymer chain seen along the a-axis

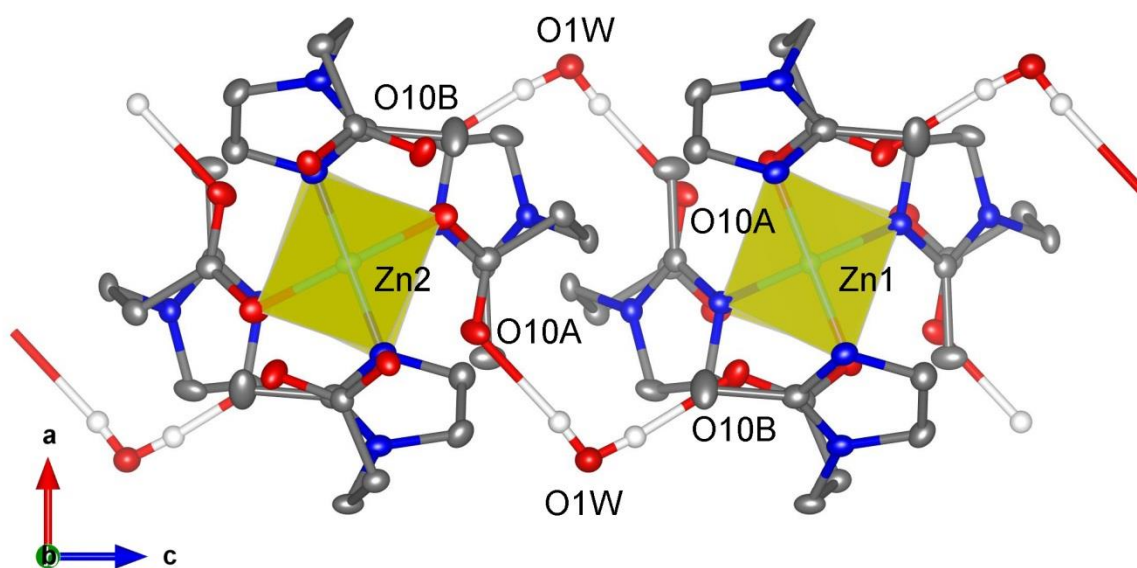


Figure 28: Chain seen along the b-axis

The compound crystallizes as 1D coordination polymer chains with additional water molecules (O1W) affording hydrogen bonding to the nonbonding oxygen atom of the carboxylate group creating a 3D scaffold. These electrostatic non-covalent intermolecular interactions and hydrogen bonds (C–H \cdots O, O–H \cdots O) fall within expected ranges for presented compounds. The methyl group of the opposing imidazole show in contrary direction. The distance between the zinc atoms in the in the coordination polymer chain along the a-axis are in the range of 7.53 Å and along the b-axis 9.12 Å.

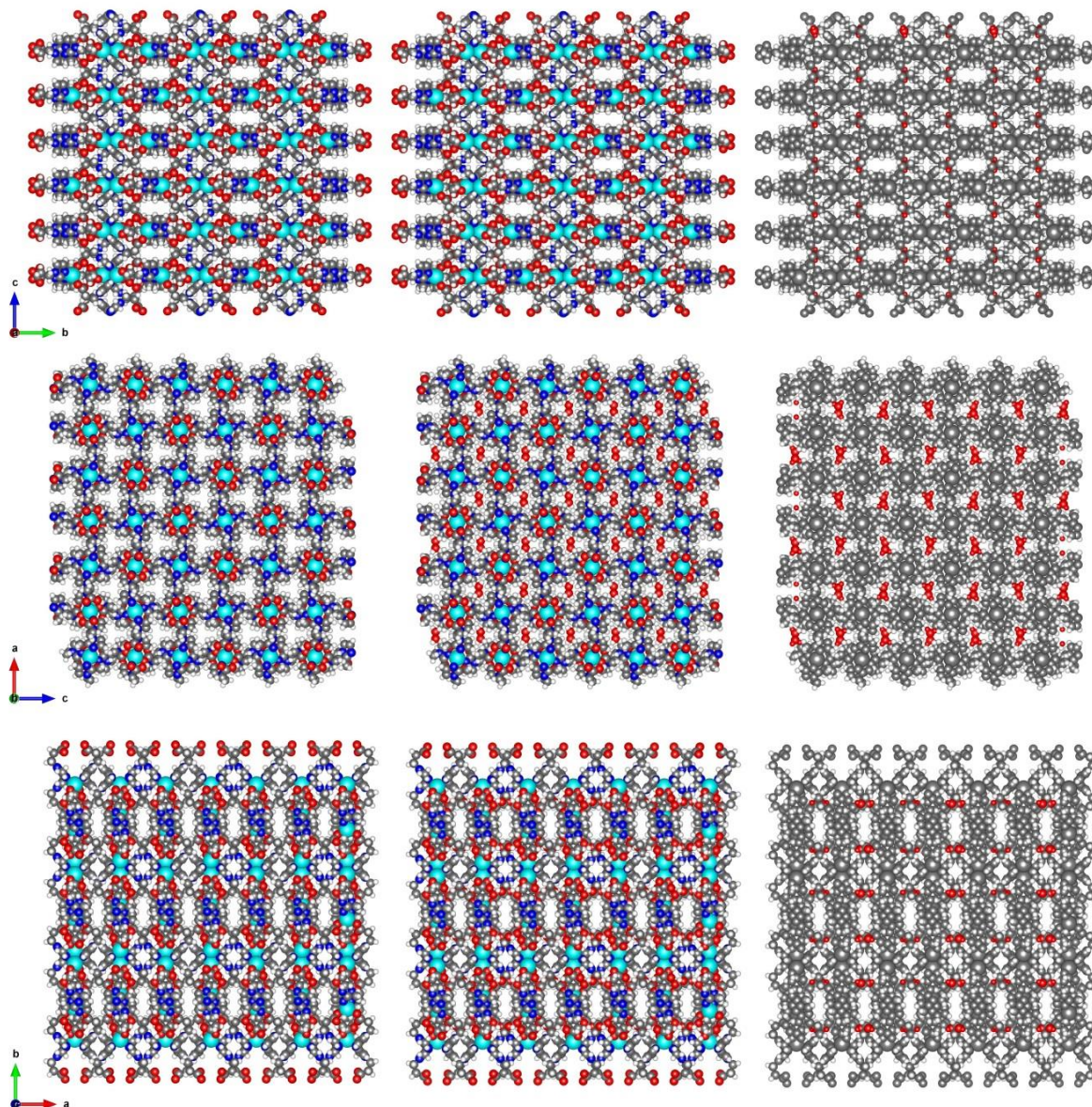


Figure 29: Solid state structures with water and without water

In Figure 29 the solid state structure with water omitted (left column), solid state structure with water in the pores (middle column) and the solid state structure with water enclosed in the structure (only water colored in red - right column) are shown. In the left column the water is theoretically subtracted and the middle and right column are only a different view of the water containing structure. The cavity size stays quite similar in every column, which means that the water does not close or clog the pores and therefore it does not affect the porosity. Only along the b-axis the cavity size decreases and is almost completely occupied by water molecules (middle row- right column). The most important information from SC-XRD measurement of the crystal are given in Table 4. Further crystallographic data and details of measurements are given in the appendix.

Table 4: Crystallographic data

Formula	C ₁₄ H ₁₈ N ₄ O ₄ Zn·H ₂ O	α , β , γ (°)	90
Fw (g mol ⁻¹)	389.73	Crystal size (mm)	0.05 × 0.05 × 0.04
a (Å)	15.1861 (13)	Crystal habit	Block, colourless
b (Å)	15.0082 (13)	Crystal system	Orthorhombic
c (Å)	15.0568 (13)	Space group	Pcca
d _{calc} (mg m ⁻³)	1.509		

X-ray diffraction (XRD):

Two different samples have been measured with XRD. The red curve shows the pattern from the crystals (Figure 30), which have been measured with SC-XRD as well. For the second sample the white fine precipitation, which forms immediately after adding the zinc salt to the ligand solution, was isolated. This precipitation is very fine and hard to filtrate by suction, but it was able to yield a small amount for the measurement.

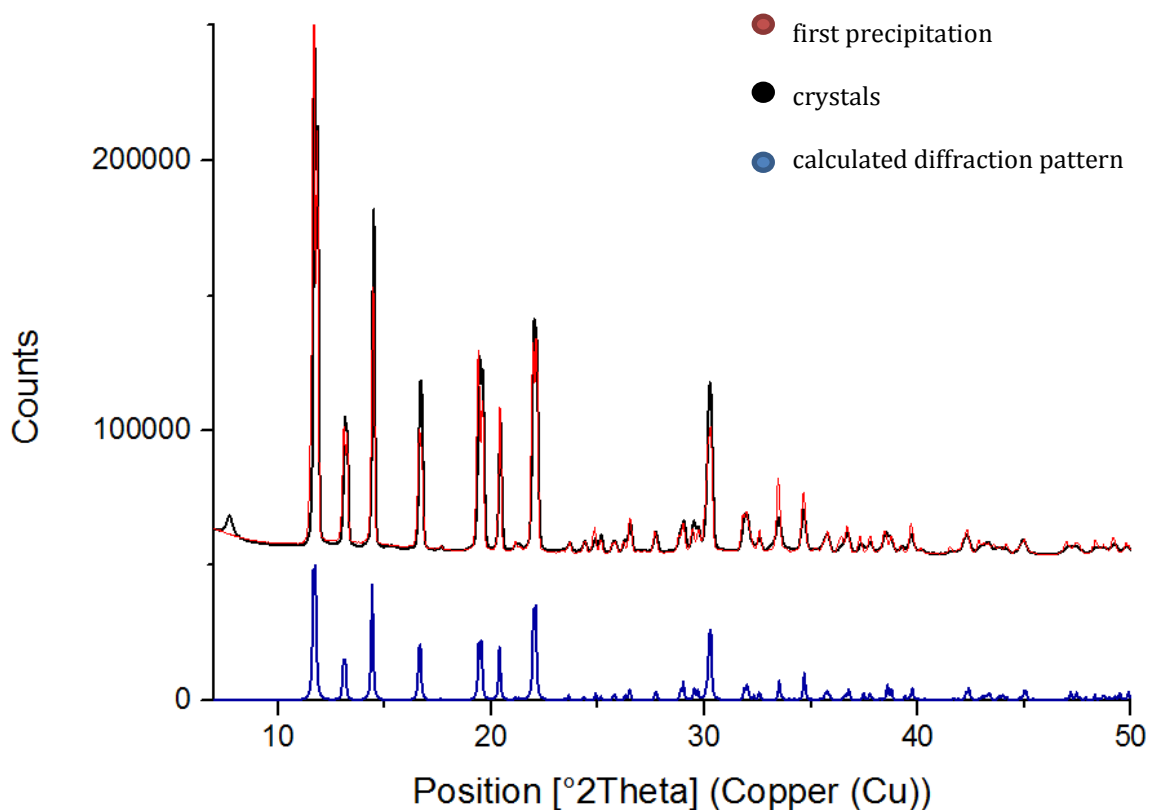


Figure 30: XRD pattern from the methylimidazole derivate

As shown in Figure 30 the two different samples (red and black curve) show the same reflexes in the XRD measurement. This leads to the assumption, that there is a formation of a crystalline solid state immediately and no amorphous form. These crystals only transform into bigger ones after a certain time. The reference (blue curve) is yielded by calculating the XRD diffraction pattern with the SC-XRD data.

In Tab. 5 the yielded reflexes from the XRD measurement for the real sample are given as well as the calculated reflexes. By comparing the diffraction patterns look the same and similar reflexes could be found.

Table 5: Reflexes from the XRD measurement from the methylimidazole derivate

Reflexes real sample [degree]	Calculated reflexes [degree]
11.7	11.6
13.1	13.0
14.5	14.4
16.7	16.6
19.4	19.4
20.4	20.5
22.0	22.03
30.3	30.3

XRD analysis is based on constructive interference of monochromatic X-rays and the crystalline sample. The interaction of the incident rays with the sample produces constructive interference when conditions satisfy Bragg's law (Formula 2):

$$n\lambda = 2d \sin\theta \quad \text{Formula 2}$$

This law relates the wavelength of electromagnetic radiation λ to the diffraction angle θ and the lattice spacing d in a crystalline sample. As already mentioned there was a XRD diffraction pattern calculated from the data of the SC-XRD measurement. From this data the distance between the atoms could be read out (VESTA) according to Bragg's law. The spacing is given in Table 6 for the most significant reflexes.^[27]

Table 6: Calculated lattice spacing from the SC-XRD data

Calculated reflexes [degree]	Lattice spacing [\AA]
11.6	7.59
13.0	6.78
14.4	6.14

The average distance between the Zn atoms from the crystal structure, measured with VESTA, is around 7.53 \AA (Figure 27). This leads to the assumption that the first reflex from the XRD diffraction pattern (Figure 30) at 11.6 $^\circ$ belongs to the Zn atoms.

²⁷ <http://particle.dk/methods-analytical-laboratory/xrd-analysis/>, 31.07.2018

Infrared-spectroscopy (IR):

An ATR-IR spectrum was recorded. The bands were assigned to the functionalities in Table 7 according to literature.^[28] The spectrum from the powder and the crystals looks the same.

Table 7: Bands of the metal-organic framework with the methylimidazole derivate

Wavenumber [cm ⁻¹]		
3115	Stretching vibration	Alkane (CH ₂)
1652	Stretching vibration	Imidazole
1618	Stretching vibration	Carboxylate (C=O ⁻)
1577	Stretching vibration	Ring C=C and N=C-N
1394, 1295	Deformation vibration	Alkane (CH ₂ , CH ₃)
1360	Stretching vibration	C-N
< 1000	Finger print area	Aromatic (CH)

The red curve in Figure 31 shows the bands of the metal-organic framework. The band from the carboxylate group occurs at a wavenumber of 1618 cm⁻¹. The black graph represents the free methylimidazole ligand. Therefore the band from the carboxylate group is found to be at a lower wavenumber.

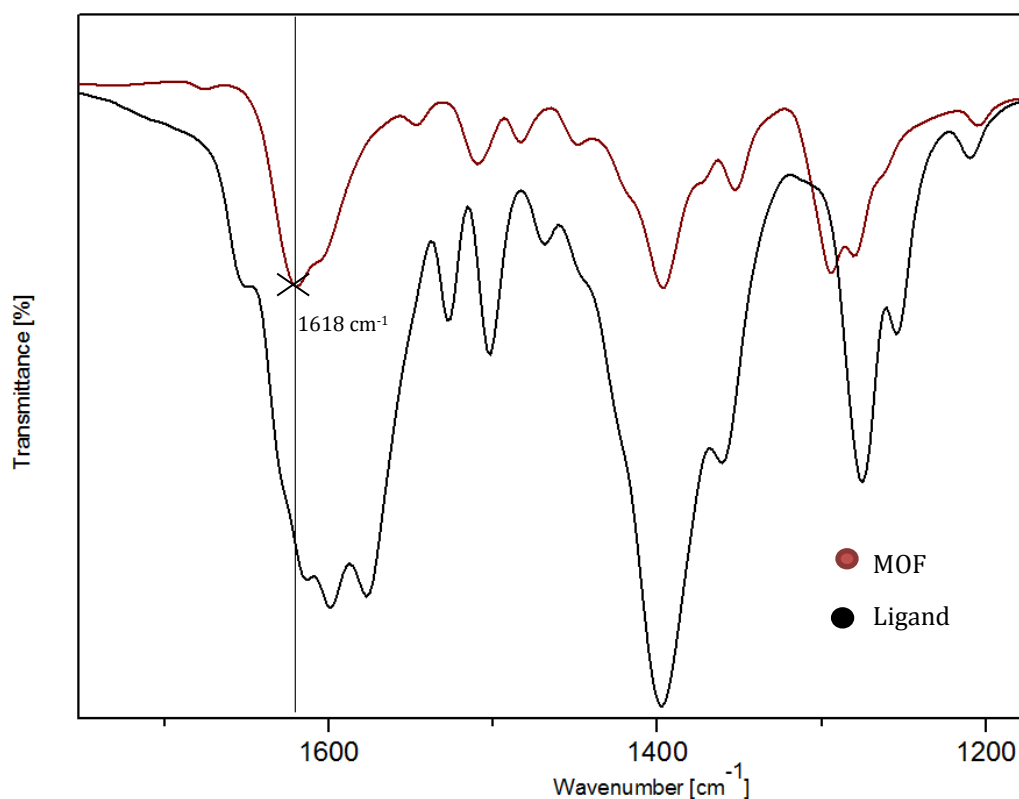


Figure 31: Comparison of the carboxylate group in the ATR-IR spectrum

²⁸ M. Hesse, H. Meier, B. Zech, Spektroskopische Methoden in der organischen Chemie, Thieme, 7. Auflage.

Thermogravimetric analysis (TGA):

To assess the thermal stability and structural changes as a function of temperature, TGA was carried out. The curve is given in Figure 32. The crystals have been dried under reduced pressure with 120 °C before the measurement was done. During the TGA heating process, the compound underwent a one-step weight loss of 35% and the entire structure remained stable up to a temperature of 295 °C. It is assumed that the organic ligand decomposes at this temperature range. In general, the decomposition of the organic components of the metal-organic frameworks typically begins at moderate temperatures in the range of 200-350 °C and leads to the decomposition of the synthesized materials. In literature there are metal-organic frameworks found with a higher thermal stability, depending on the organic linker and other factors. There are zinc complexes with a stability over 400 °C, because of their strong interaction between the metal-carboxylate group from the ligand that tightens the backbone and enhance the resistance to pyrolysis.^[29]

There is no dehydration of the sample detectable in the curve, meaning that there is no loss of crystal water as well.

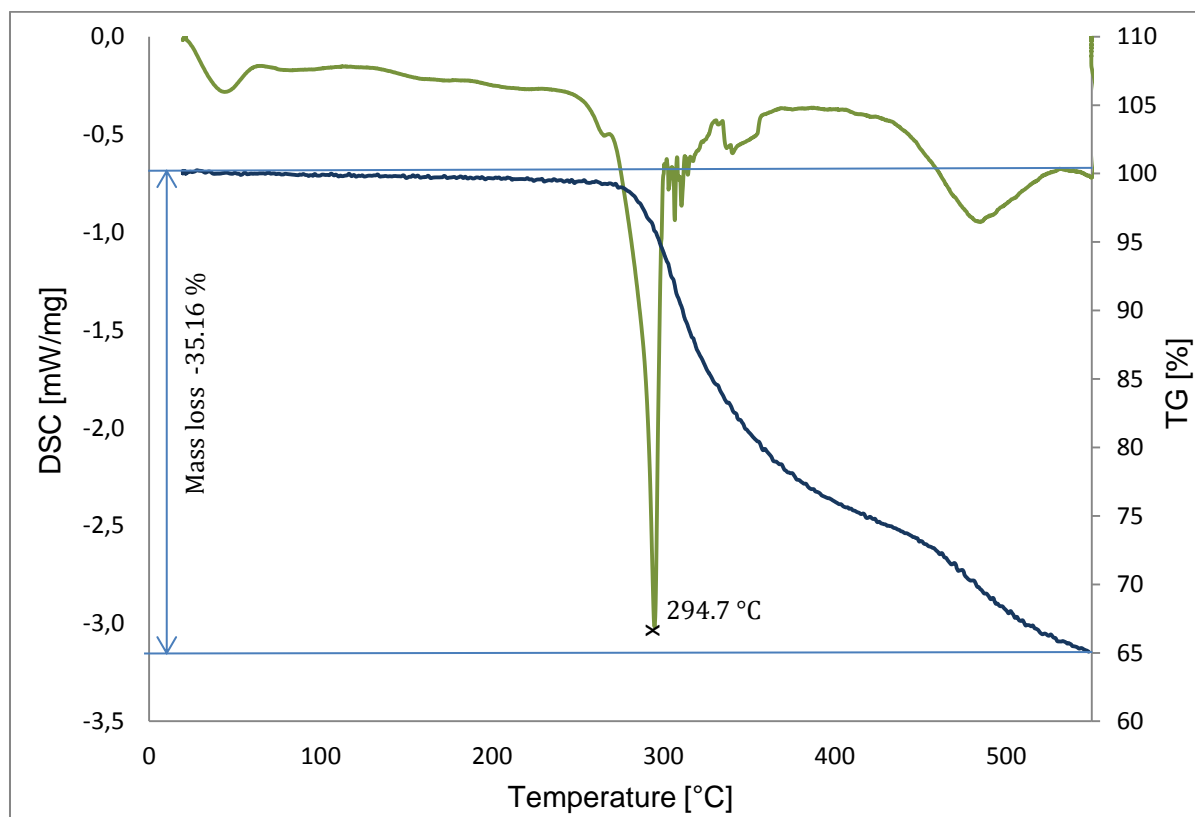


Figure 32: TGA from the MOF with the methylimidazole derivate

²⁹ R. Zou, *et.al*, Highly-thermostable metal-organic frameworks (MOFs) of zinc and cadmium 4,49-(hexafluoroisopropylidene)diphthalates with a unique fluorite topology, *Chem. Commun.*, **2007**, 2467-2469.

Brunauer-Emmett-Teller (BET) surface area analysis:

The solid has been dried under reduced pressure and temperature before the measurement was performed. In Table 8 the most important data from the measurement are given. The BET surface area is around 112 m²/g and the pore size is 56 Å.

Table 8: Data from the BET measurement from the MOF with the methylimidazole derivate

Surface area S _{BET}	[m ² /g]
BET surface area	111.57 ± 2.07
BJH Adsorption	88.72
BJH Desorption	91.29
Pore Volume	[cm ³ /g]
BJH Adsorption	0.125
BJH Desorption	0.126
Pore Size	[Å]
BJH Adsorption	56.33
BJH Desorption	55.06

The specific surface area of a solid could be determined by physical adsorption of a gas on the surface and by calculating the amount of adsorbate gas corresponding to a monomolecular layer on the surface. This physical adsorption results from relatively weak forces between the adsorbate gas molecules and the adsorbent surface area of the test powder. The concept of the theory is an extension of the Langmuir theory.

After measuring the amount of adsorbed gas the data are treated according to the Brunauer, Emmett and Teller (BET) adsorption isotherm equation:

$$\frac{1}{[V_a \left(\frac{P_0}{P} - 1 \right)]} = \frac{C - 1}{V_m C} * \frac{P}{P_0} + \frac{1}{V_m C}$$

Formula 3: BET isotherm equation

P	=	partial vapour pressure of adsorbate gas in equilibrium with the surface at 77.4 K (b.p. of liquid nitrogen) [Pa]
P_o	=	saturated pressure of adsorbate gas [Pa]
V_a	=	volume of gas adsorbed at standard temperature and pressure STP [273.15 K] and atmospheric pressure [1.013×10^5 Pa] [mm ³]
V_m	=	volume of gas adsorbed at STP to produce an apparent monolayer on the sample surface [mm ³]
C	=	dimensionless constant that is related to the enthalpy of adsorption of the adsorbate gas on the powder sample

The value of V_a is measured at different values of $\frac{P}{P_o}$. Then the BET value $\frac{1}{V_a(\frac{P}{P_o}-1)}$ is plotted against $\frac{P}{P_o}$ which leads to a straight line in the approximate relative pressure range 0.05 to 0.3 Pa. From this resulting linear plot the slope which is equal to $\frac{(C-1)}{V_m C}$ and the intercept, which is equal to $\frac{1}{V_m C}$ is evaluated by linear regression analysis to yield V_m which is $\frac{1}{(\text{slope} + \text{intercept})}$. From this value, the specific surface area S_{BET} in $\frac{m^2}{g}$ can be calculated with Formula 4.^[30]

$$S_{BET} = \frac{V_m N a}{m * 22400}$$

Formula 4: Specific surface area

N	=	Avogadro constant [6.022×10^{23} mol ⁻¹]
a	=	effective cross-sectional area of one adsorbate molecule [0.1620 nm ² for nitrogen]
m	=	mass of test powder [g]
22400	=	volume occupied by 1 mole of the adsorbate gas at STP allowing for minor departures from the ideal [mm ³ /mol]

³⁰ <http://particle.dk/methods-analytical-laboratory/surface-area-bet-2/>, 31.07.2018

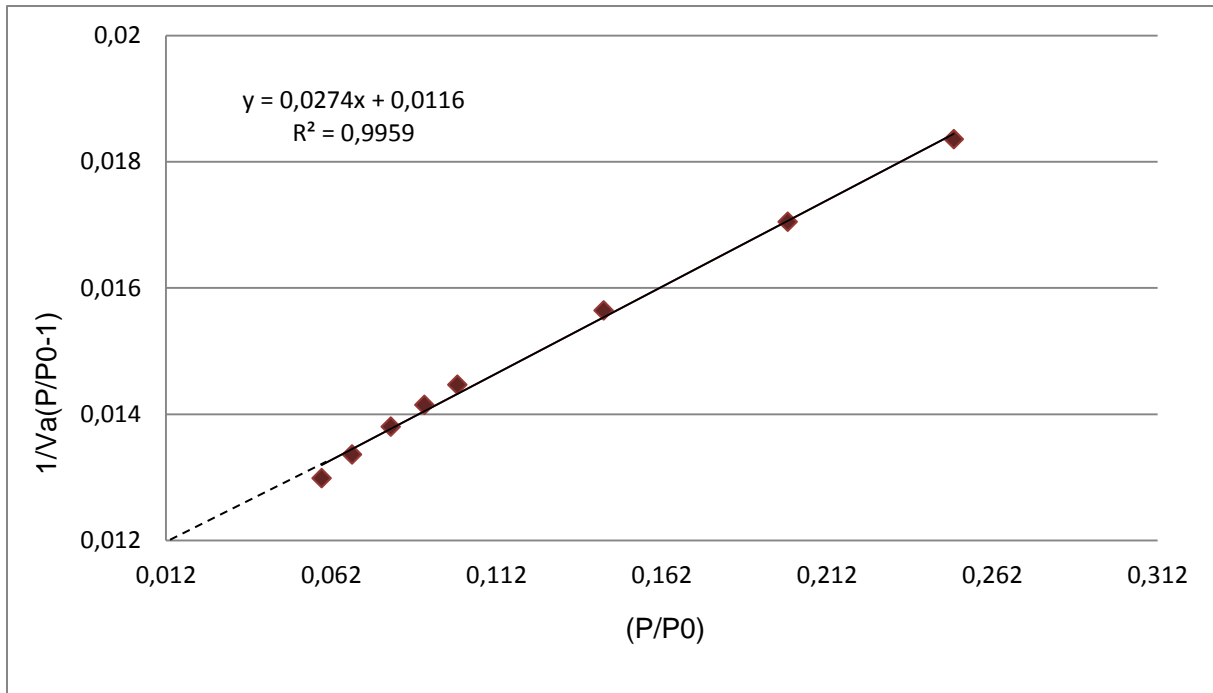


Figure 33: BET plot

In Figure 33 the BET plot is shown for the case of the zinc-methylimidazole framework. The value of the slope k could be determined with 0.0274 and the y-intercept d with 0.0116 which leads to a value of 25.6 cm³/g for V_m .

$$V_m = \frac{1}{(0.0274 + 0.0116)} = 25.6 \frac{\text{cm}^3}{\text{g}}$$

$$S_{BET} = \frac{(2.563 \cdot 10^{-5}) \cdot N \cdot (1.62 \cdot 10^{-19})}{0.022414} = 111.6 \frac{\text{m}^2}{\text{g}}$$

By using Formula 4 a surface area from 111.6 m²/g could be calculated.

The volume of voids contained in a particulate material is usually expressed by the porosity or the void ratio. Even with a constant value of void ratio, however, different arrangements of particles do occur, corresponding to different pore size distributions (Figure 34).^[31] The determination of the pore size distribution was done with the method of Barrett-Joyner-Halenda. The method uses the Kelvin model of pore filling for the calculation of the pore sizes from the experimental isotherms. The average pore size was determined to be in a range between 55-56 Å (Table 8).

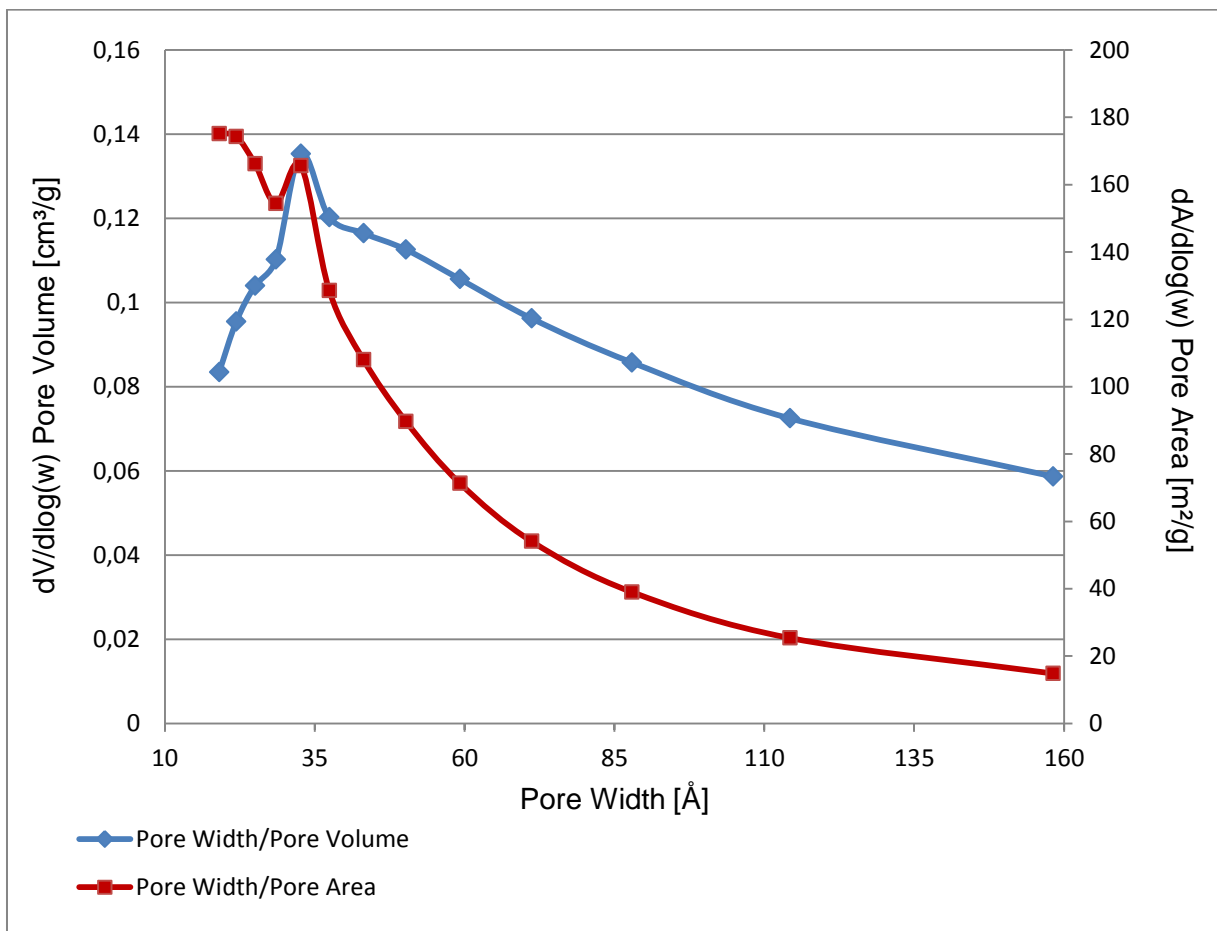
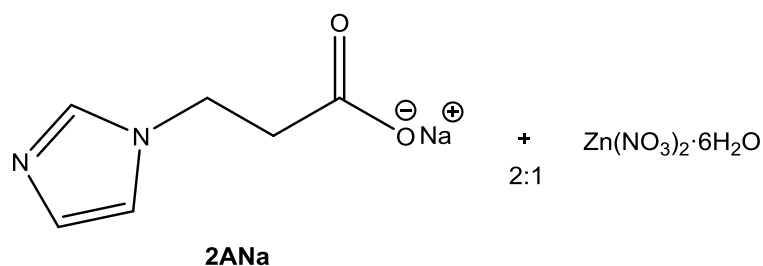


Figure 34: Plot of pore size distribution

³¹ A. Musso, F. Federico, Pore size distribution in filtration analyses

3.3.1.2 Sodium 3-(1H-imidazol-1-yl)propanoate + Zn(NO₃)₂ (2AZn)



The reaction was done by dissolving the ligand and the zinc salt separately in respectively 3 mL water. The zinc solution was added to the ligand and the reaction mixture turned cloudy immediately. It was heated up to 80 °C. There was a formation of an oily layer at the bottom of the reaction vessel. For the analysis of the oil, the supernatant was removed and the oil was dried in the oven at 80 °C. For the preparation of the crystals, the oil in solution was left 24 h in the oven and a formation of a yellow, clear crystal could be detected. The preparation procedure and the analysis techniques of the oil and the crystals were summarised in Figure 34.

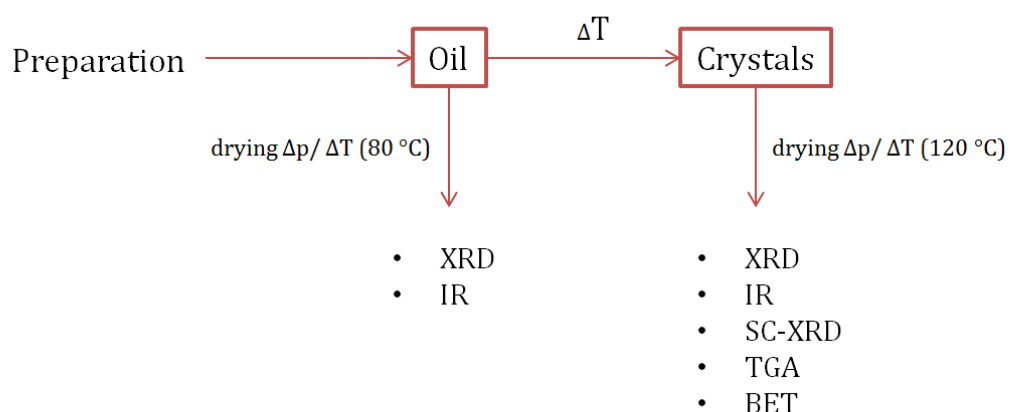


Figure 35: Measurements from the different prepared MOFs



Figure 36: Prepared crystals

Single crystal X-ray diffraction (SC-XRD):

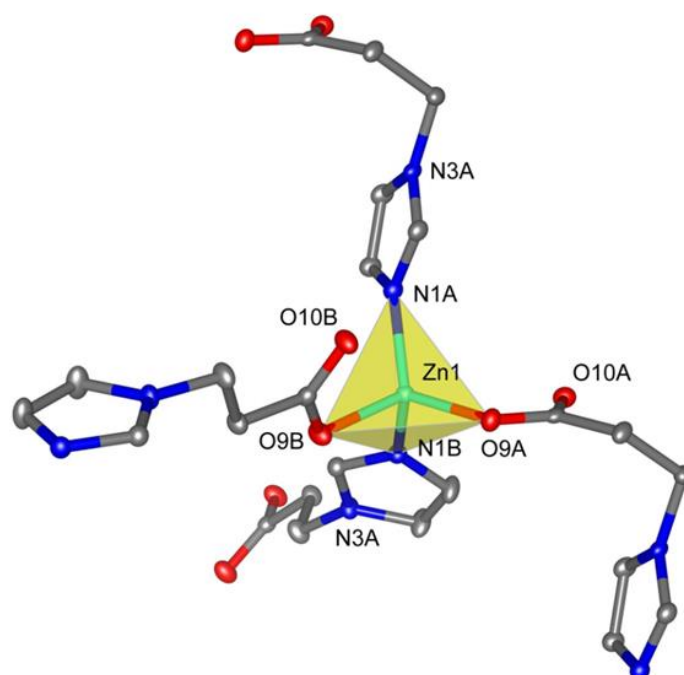


Figure 37: Crystal structure

Table 9: Coordination parameters

Zn ¹ —O ^{9a}	1.9653 (12) Å	Zn ¹ —N ^{1a}	1.9946 (13) Å
Zn ¹ —O ^{9b}	1.9617 (13) Å	Zn ¹ —N ^{1b}	2.0081 (13) Å
Nonbonding:			
Zn ¹ —O ^{10a}	2.9756 (13) Å		
Zn ¹ —O ^{10b}	2.8040 (15) Å		
Angles:			
O ^{9a} —Zn ¹ —O ^{9b}	103.19 (6) deg	N ^{1a} —Zn ¹ —N ^{1b}	105.94 (6) deg
O ^{9a} —Zn ¹ —N ^{1b}	113.67 (6) deg	N ^{1a} —Zn ¹ —O ^{9b}	114.13 (6) deg
N ^{1b} —Zn ¹ —O ^{9b}	100.07 (6) deg	N ^{1a} —Zn ¹ —O ^{9a}	118.49 (6) deg
Average bond length: 1.9824 Å		Quadratic elongation: 1.0137	
Distortion index (bond length): 0.00955		Bond angle variance: 52.1773 deg ²	
Polyhedral volume: 3.9181 Å ³		Effective coordination number: 3.9863	

The zinc atom exhibits a tetrahedral geometry and is coordinated to two oxygen atoms (O^{9a} and O^{9b}) and to two nitrogen atoms (N^{1a} and N^{1b}) from different ligand molecules (Figure 37). The angles between the metal centre range between 100.07 (6) ° and 118.49 (6) °. In Table 9 all coordination parameters are shown, in which the number in brackets means the deviation. The carboxylate anion coordinates to the metal centre in mono-dentate fashion, and as a result, the

other oxygen atom of the carboxylate group remains uncoordinated. The carboxylate distances are shorter with a range of 1.96-1.97 Å compared to the range of 1.99-2.00 Å for the imidazolates, but considering that the covalent radius of nitrogen is 0.05 Å then for oxygen (0.71 vs 0.66 Å) this difference is hardly significant.^[32] These values for Zn-O and Zn-N bond lengths are quite similar to already published ones. In *New J. Chem.*, **2015**, zinc metal-organic frameworks with a N(2-tetrazolethyl)-4-glycine spacer (TeGly)²⁻ have been designed. They have yielded Zn-N distances in the range of 2.039 (2)-2.099 (2) Å and Zn-O distances with values from 1.980 (2) and 2.185 (2) Å.^[33]

In comparison, the bond length from a cluster of ZnO₄ with a tetrahedral symmetry (T_d) would be 1.923 Å, a little bit smaller than in this case. For the ideal tetrahedral molecular geometry one can expect a bond angle from 109.5°, when all substituents are the same. The bond angles of the metal environment are in the range of 100-118 °

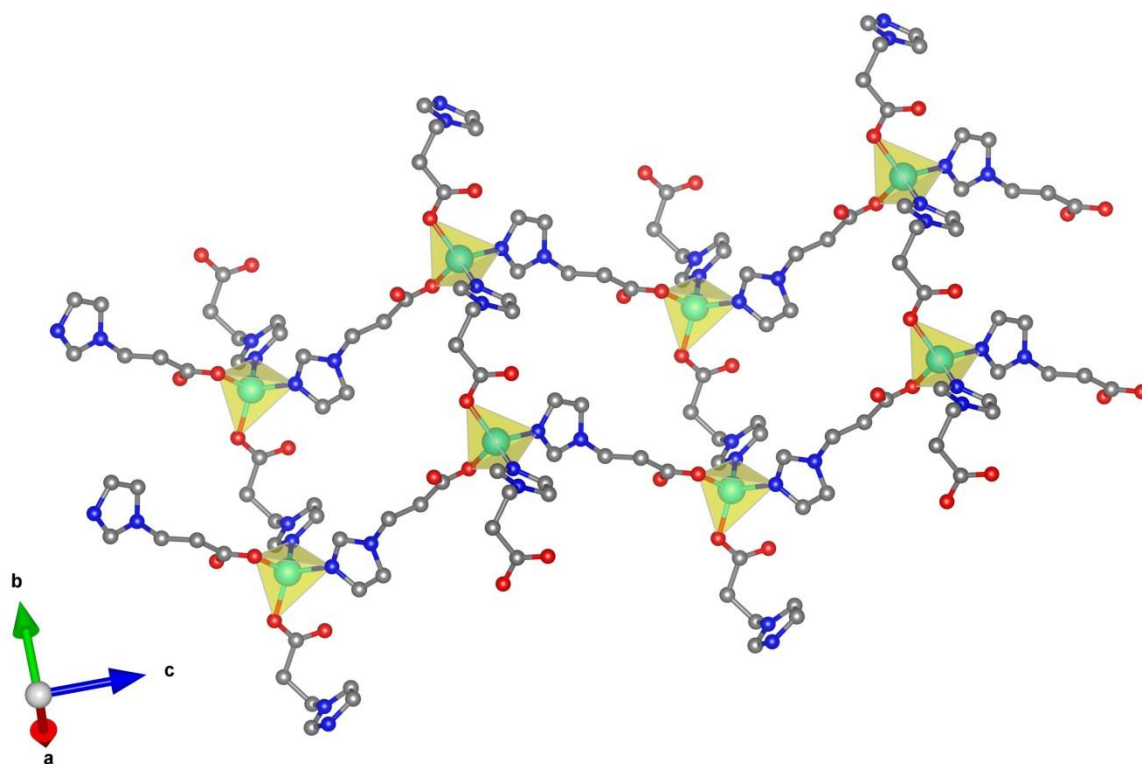


Figure 38: Crystal scaffold

The compound crystallizes as 2D polymer sheets (Figure 38). The Zn²⁺-Zn²⁺ distance in the b-axis direction is 8.2687 (3) Å and in c-axis direction 10.3972 (4) Å. There are square-shaped channels formed.

³² A. Nimmermark, L. Öhrström, J. Reedijk, Metal-ligand bond lengths and strengths: are they correlated, *Z. Kristallog.*, **2013**, 228, 311-317.

³³ A. Castillo, *et al.*, 2D-cadmium MOF and gismondine-like zinc coordination network based on the N-(2-tetrazolethyl)-4-glycine linker, *New J. Chem.*, **2015**, 39, 3982-3986.

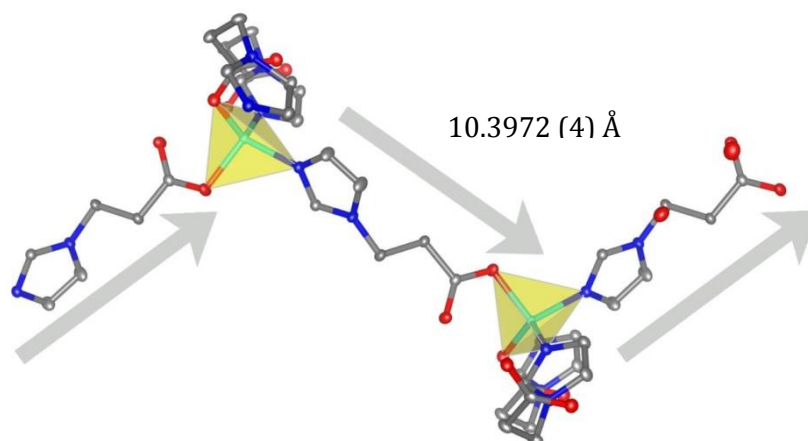


Figure 39: Part of the twisted 2D-network seen in the direction of the c-axis

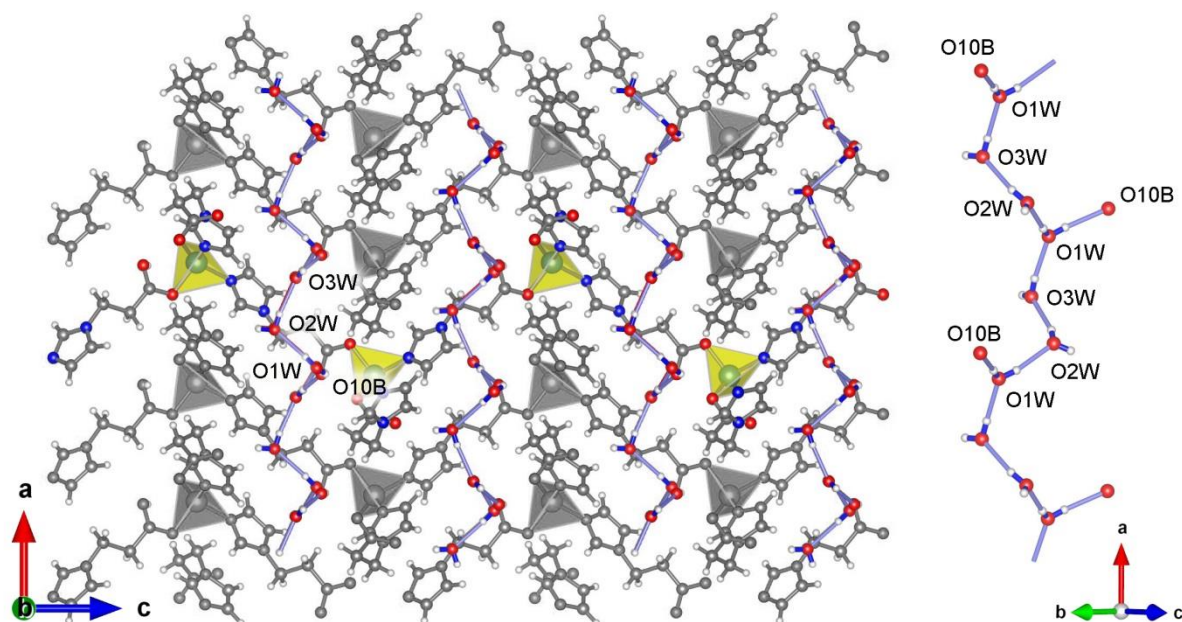


Figure 40: 3D network via hydrogen bonding

A 3D network is formed from the 2D polymer sheets via hydrogen bonding. Therefore three water molecules form a chain in which every third water molecule shows hydrogen bonding to the O^{10b} (non-bonding) atom of the carboxylate group from the ligand. The distance between the zinc atoms of the different sheets are approximately 5.93 Å.

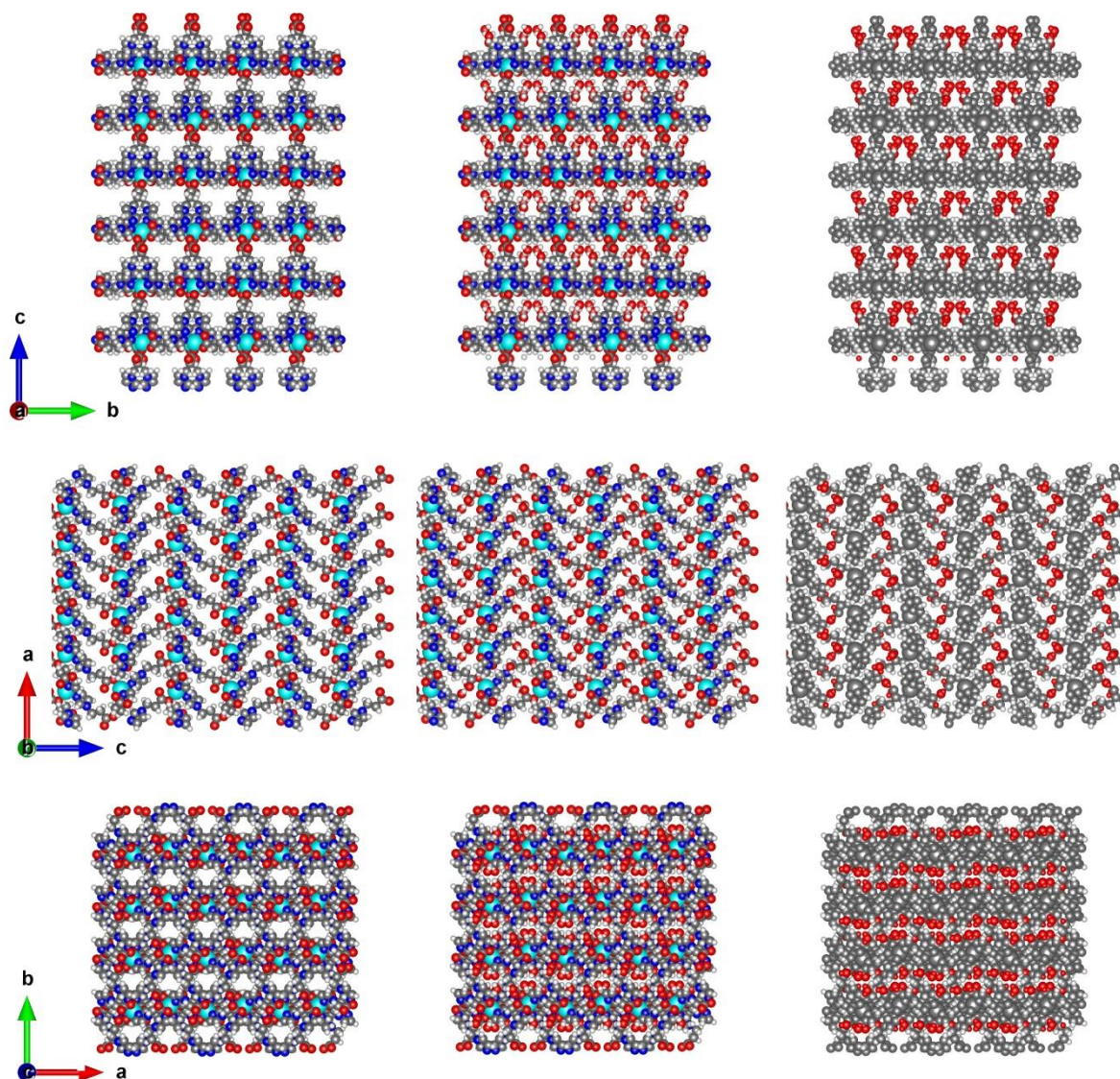


Figure 41: Solid state structures with water

In Figure 41 the solid state structure with water omitted (left column), solid state structure within the pores (middle column) and the solid state structure with water enclosed in the structure (right column) are shown. The water is responsible for the structure formation. In the left column the water is theoretically subtracted and channels can be detected. If the structure is shown with the water molecules (middle and right column) there are hardly any opened pores left. This differs from the methylimidazole derivate, where the water does only slightly affect the porosity. The key information from SC-XRD measurement of the crystal, are given in Table 10. Further crystallographic data and details of measurements are given in the appendix.

Table 10: Crystallographic data

Formula	$C_{12}H_{14}N_4O_4Zn \cdot 3H_2O$	α, β, γ ($^\circ$)	90
Fw ($g\ mol^{-1}$)	397.69	Crystal size (mm)	$0.09 \times 0.08 \times 0.08$
a (Å)	11.7285 (4)	Crystal habit	Block, colourless
b (Å)	8.2687 (3)	Crystal system	Orthorhombic
c (Å)	17.4803 (6)	Space group	Pca2 ₁
d_{calc} ($mg\ m^{-3}$)	1.558		

X-ray diffraction (XRD):

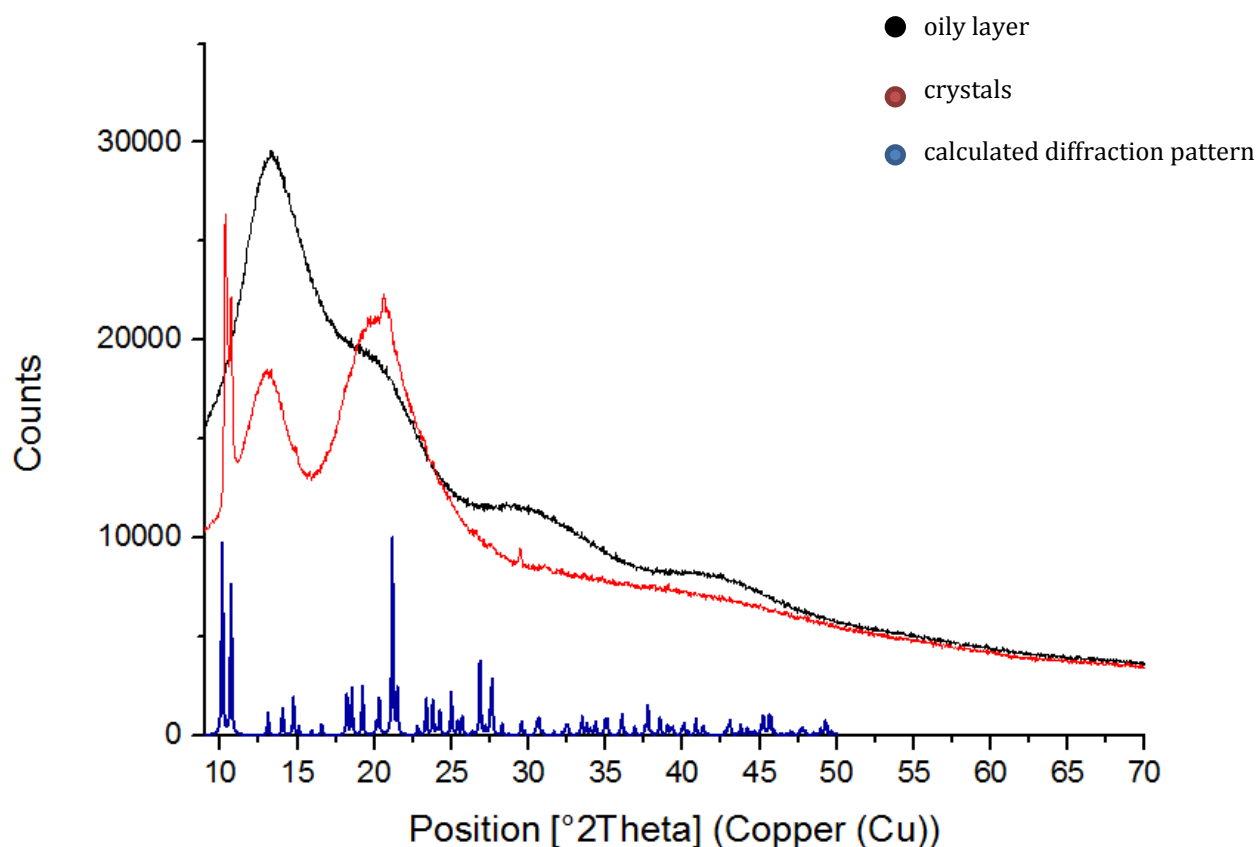


Figure 42: XRD pattern from the imidazole derivate

For the XRD measurement two samples have been prepared. The red curve arises from the already formed crystal, which is shown in Figure 42. The crystals have been dried under reduced pressure at 120 °C before the measurement was performed, leading to a loss of the clearness and to a decay of the crystals. The second sample (black curve) is the isolated oily layer, which forms after the zinc salt is added to the ligand solution. The X-ray powder diffraction pattern is essentially continuous in appearance for both samples. This type of powder patterns are

referred to as X-ray amorphous. Glassy materials are one example of solid state systems that will give rise to this form.^[34]

For the case of the crystal there are some small reflexes detectable, but the XRD diffraction pattern looks like an amorphous solid as well. It could be possible, that the compound lost its crystallinity during the drying process. This could explain why no small reflexes, which would indicate a crystalline structure are detectable in the diffraction pattern.

The ideal XRD diffractogram was calculated from the data of the Single-crystal XRD for the crystalline solid state (blue curve) in VESTA. There are reflexes at 10.1, 10.7, 14.1, 21.1 and 27.7°, which are indicated in the measured one as well.

Table 11: Calculated lattice spacing from the SC-XRD data

Calculated reflexes [°]	Lattice spacing [Å]
10.1	8.74
10.7	8.27
14.1	6.30
21.1	4.19

As already mentioned, the distance between the zinc atoms in the 2D polymer sheets along the b-axis (Figure 38) are 8.27 Å. This lattice spacing from these atoms could be responsible for the reflex at 10.1 degree, which is only visible in the pattern from the crystals. The spacing between the sheets in the 3D structure is 5.93 (measured with VESTA) which could fit with the reflex at 14.1 degree.

³⁴ S. Bates, Advanced Analysis of Non-Crystalline (X-ray Amorphous) Materials and Dispersions, TriclinicLabs.com/25.07.2018.

Infrared-spectroscopy (IR):

An ATR-IR spectrum was recorded. The bands were assigned to the functionalities in Table 12 according to literature.^[28]

Table 12: Bands of the metal-organic framework with the methylimidazole derivate

Wavenumber [cm ⁻¹]		
3113	Stretching vibration	Alkane (CH ₂)
1595	Stretching vibration	Carboxylate (C=O ⁻)
1381	Stretching vibration	C-N
1366, 1275	Deformation vibration	Alkane (CH ₂)
< 1000	Finger print area	Aromatic (CH)

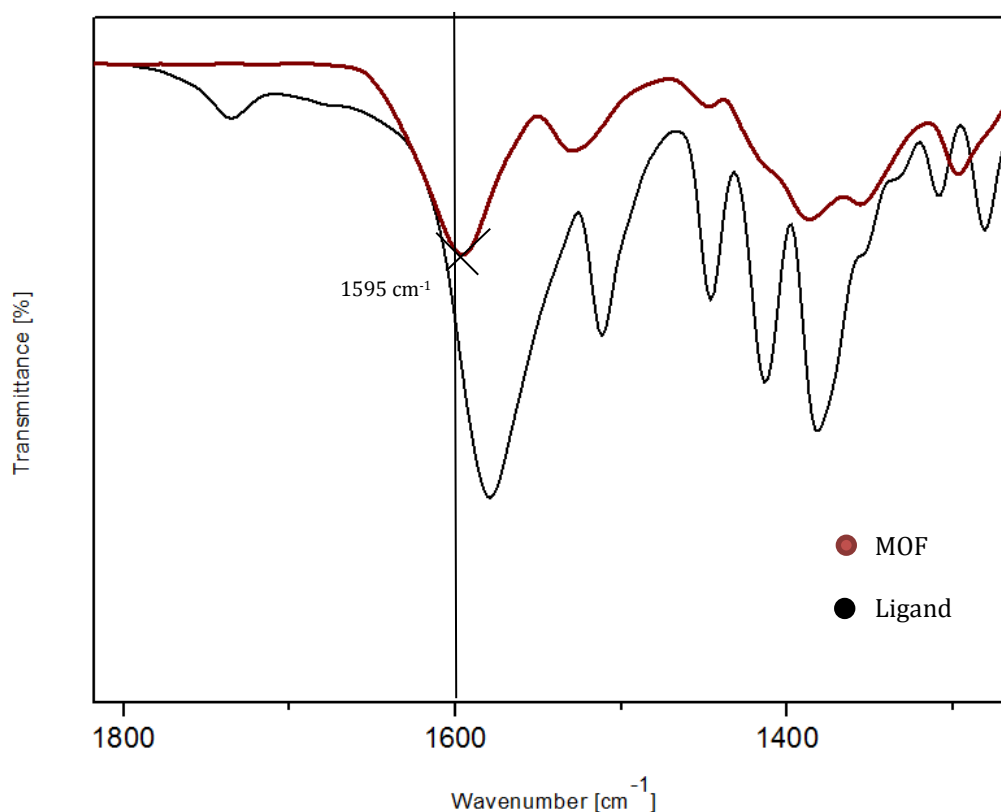


Figure 43: Comparison of the carboxylate group in the ATR-IR spectrum

The red curve in Figure 43 shows the bands of the metal-organic framework. The band from the carboxylate group is detectable at a wavenumber of 1595 cm⁻¹. The black graph represents the free imidazole ligand. As shown before in the case of the methylimidazole MOF the band from the carboxylate group is again found to be at a lower wavenumber.

Thermogravimetric analysis (TGA):

The TGA curve is shown in Figure 44. The crystals have been dried under reduced pressure, and 120 °C before the measurement was performed. Nevertheless there can be a loss of water at 100 °C detected and it is presumed that this is crystal water. There is a significant endothermic processes occurring at 280 °C which leads to a considerable mass loss from nearly 38.7% of the overall mass.

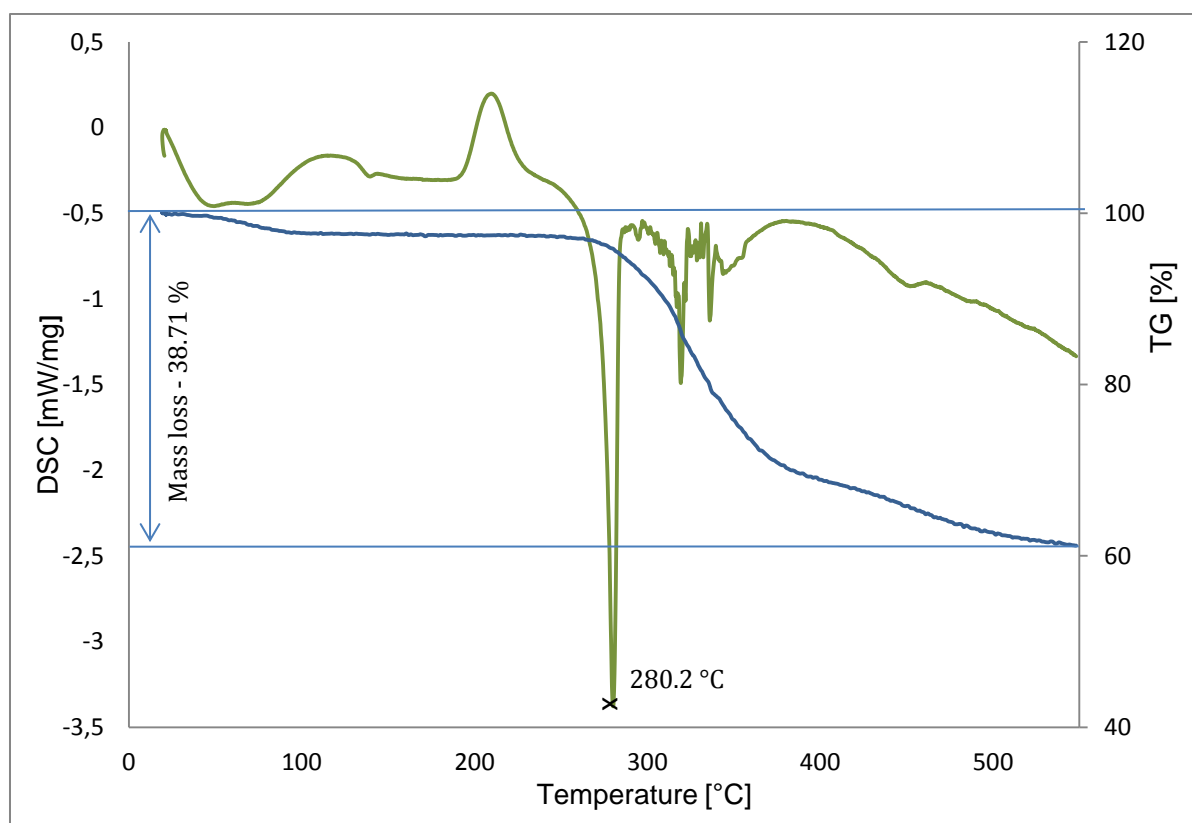


Figure 44: TGA from the MOF with the methylimidazole derivate

Brunauer-Emmett-Teller (BET) surface area analysis:

As already mentioned in the part of the XRD measurement, the crystals have been dried under reduced pressure and temperature. It could be detected, that the crystals lost their clearness and turned into a cloudy solid after the drying process. This leads to the assumption that the crystalline form degrades into the amorphous form. Furthermore the BET measurement would have been performed from the amorphous solid.

Table 13: BET measurement from the MOF with the imidazole derivate

Surface area	[m ² /g]
BET surface area	191.27 ± 1.62
BJH Adsorption	132.58
BJH Desorption	132.88
Pore Volume	[cm ³ /g]
BJH Adsorption	0.155
BJH Desorption	0.152
Pore Size	[Å]
BJH Adsorption	46.70
BJH Desorption	45.85

In Table 13 the most important parameters from the measurement are given. The specific BET surface area is around 191 m²/g and the pore size 47 Å.

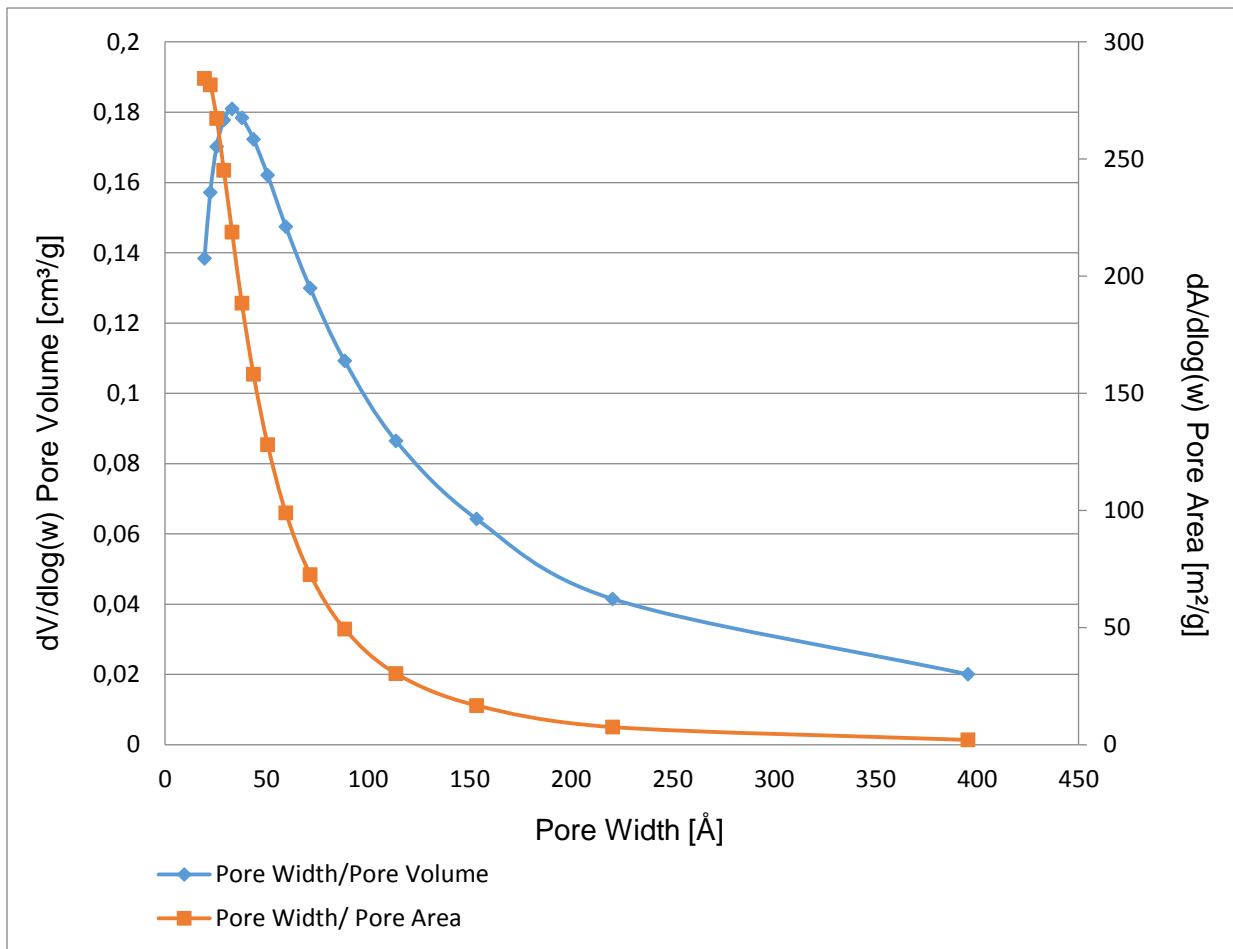
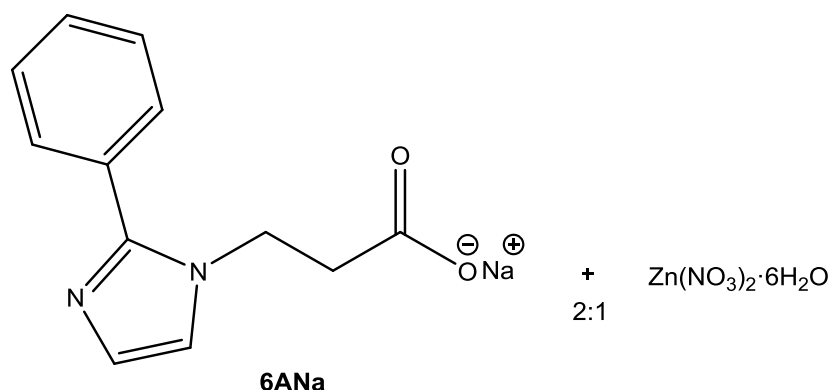


Figure 45: Plot of Pore Size Distribution

The average pore size was determined to be in a range between 46-47 Å (Table 13).

3.3.1.3 Sodium 3-(2-phenyl-1H-imidazol-1-yl)propanoate + Zn(NO₃)₂ (6AZn)



The reaction was done by dissolving the ligand and the zinc salt separately in respectively 2 mL water. The zinc solution was added to the ligand. There was a white, viscous precipitation immediately. The reaction mixture was put in the Monowave 50 at 150 °C for 45 min. There was a formation of a yellow solid layer at the bottom of the reaction vessel. The supernatant was removed into a new glass vial and heated up to 80 °C. After 24 h a formation of a white crystal could be detected. The crystals were analysed with SC-XRD.



Figure 46: Viscous precipitation after addition of the metal salt (left) and amorphous solid (right)



Figure 47: Crystalline form after heating up in the Monowave 50

The amorphous form, a yellow cloudy solid, could be yielded by heating the white viscous precipitation up to 80 °C.

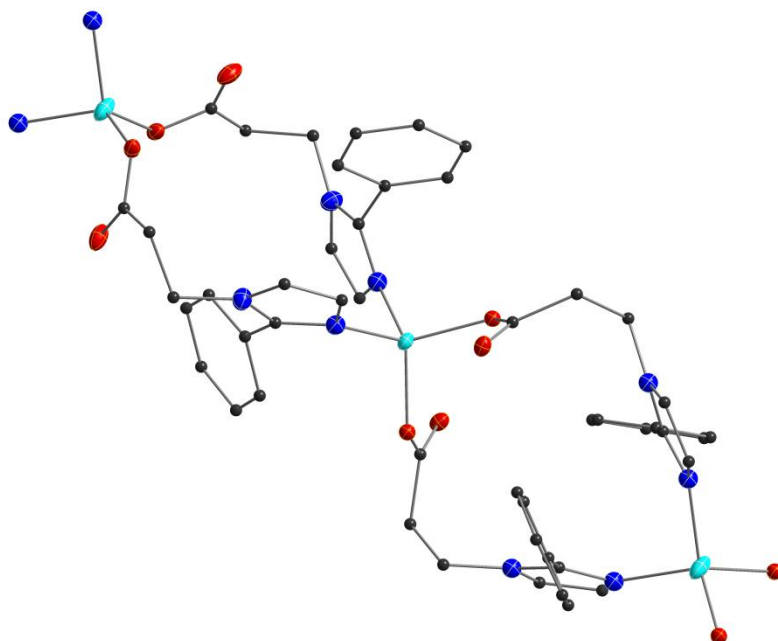


Figure 48: Crystal structure

Proper convergence of the refinement was not achieved and attributed to poor crystal quality and not incorrect atom assignments. Due to low crystal quality, in combination with disorder of the ligand and solvent water molecules, the crystallographic data are not publishable. The phenyl derivate crystallizes similar to the methyl derivate like a 1D coordination polymer.

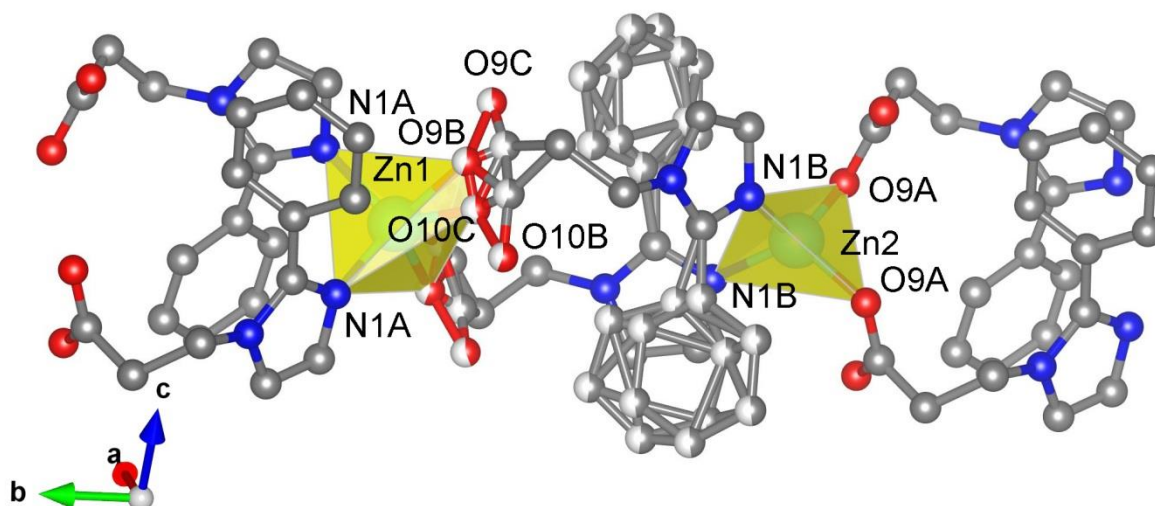


Figure 49: Crystal scaffold

The zinc atom is four coordinated and adopts a distorted tetrahedral geometry with angles around the metal centre ranging between 103.37 (7) ° and 128.59 (7) °. Furthermore it is coordinated to two oxygen atoms (O^{9a} and O^{9b}) and to two nitrogen atoms (N^{1a} and N^{1b}) from different ligand molecules. The Zn-O bond lengths are 1.947 (11) and 2.06 (3) and the Zn-N bond lengths are 2.029 (10) and 2.043 (11) Å (bonding) (Tab. 14). There is a formation of a grid structure through the linked ligands, which leads to the formation of cavities in the build 3D structure.

Table 14: coordination around zinc

Coordination facility around disordered Zn ^I		Coordination facility around Zn ^{II}	
Zn ¹ —N ^{1a}	2.029 (10) Å	Zn ² —N ^{1b}	2.043 (11) Å
Zn ¹ —O ^{9b}	2.06 (3) Å	Zn ² —O ^{9a}	1.947 (8) Å
Nonbonding:			
Zn ² —O ^{10c}	1.86 (3) Å		
Average bond length:	1.9859 Å	Quadratic elongation:	1.0210
Distortion index (bond length):	0.04073	Bond angle variance:	104.096 deg ²
Polyhedral volume:	6.5294 Å ³	Effective coordination number:	5.434

The key information from SC-XRD measurement of the crystal, are given in Table 15. Further crystallographic data and details of measurements are given in the appendix.

Table 15: Crystallographic data

Formula	C ₂₄ H ₂₂ N ₄ O ₄ Zn	β (°)	102.11(3)
Fw (g mol ⁻¹)	496.82	Crystal size (mm)	0.04 × 0.03 × 0.03
a (Å)	8.3300(7)	Crystal habit	Block, colourless
b (Å)	15.9200(12)	Crystal system	Monoclinic
c (Å)	17.5064(14)	Space group	P2/n
α, γ (°)	90	d _{calc}	1.451

Furthermore there has to be done further investigations to find a more efficient way of preparation, because the current one is very time consuming and gives only a very low yield.

Infrared-spectroscopy (IR):

Table 16: Bands of the metal-organic framework with the phenylimidazole derivate

Wavenumber [cm ⁻¹]		
3113	Stretching vibration	Alkane (CH ₂)
1624	Stretching vibration	Carboxylate (C=O ⁻)
1455, 1366, 1312	Deformation vibration	Alkane (CH ₂ , CH ₃)
1311	Stretching vibration	C-N
< 1000	Finger print area	Aromatic (CH)

The same spectrum for the crystalline and the amorphous structure was detected.

Thermogravimetric analysis (TGA):

The TGA curve is given in the appendix. The crystals have been dried under reduced pressure. There is a significant endothermal processes occurring at 247 °C which leads to a considerable mass loss from nearly 38.2% of the overall mass.

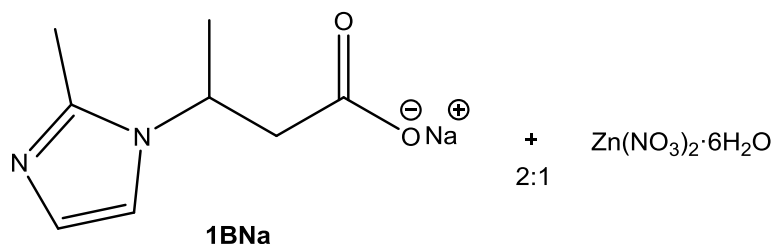
Brunauer-Emmett-Teller (BET) surface area analysis:

It has to be mentioned that the surface area was only measured for the amorphous form. The data from the measurement are given in Table 17. The BET surface area is around 328 m²/g and the pore size is 50 Å.

Table 17: Data from the BET measurement for the MOF with the phenylimidazole derivate

Surface area	m ² /g
BET surface area	328.36 ± 1.40
BJH Adsorption*	240.03
BJH Desorption*	241.32
Pore Volume	cm ³ /g
BJH Adsorption*	0.298
BJH Desorption*	0.298
Pore Size	[Å]
BJH Adsorption*	49.64
BJH Desorption*	49.45
*= cumulative surface area of pores between 17,000 and 3.000,000 Å width	

3.3.1.4 Sodium 3-(2-methyl-1H-imidazol-1-yl)butanoate + Zn(NO₃)₂ (1BZn)



The reaction was done by dissolving the ligand (**1BNa**) and the zinc salt separately in respectively 3 mL water. The zinc solution was added to the ligand. There was no precipitation. The clear reaction mixture was heated up to 80 °C. After some days there was still no formation of a solid detectable. The clear solution was evaporated under reduced pressure. A ¹H-NMR spectroscopy was performed in which the ligand could be detected, but the signals shifted to higher ppm except of the methyl group of the heterocycle which stayed the same. If a zinc complex was formed it could be possible, that the signals were shifted because of the new bonding situation and the formed coordination complex is water soluble.

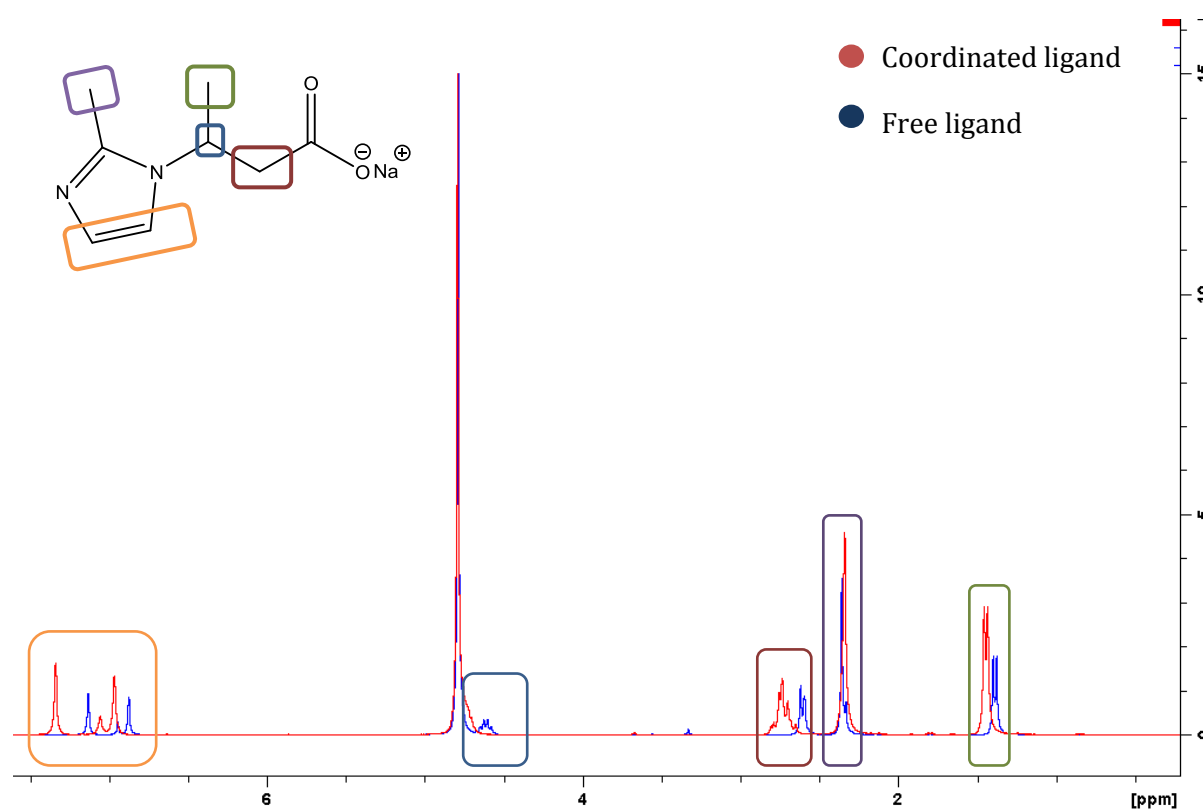


Figure 50: ¹H-NMR of the metal-organic framework and the free ligand

Because of the observed solubility, experiments were made for the use of the ligand for dissolving the other zinc-organic frameworks which were already discussed before (**1AZn**, **2AZn**).

Therefore a certain amount of zinc-organic framework was weighted in and covered with water. In the second sample was the crotonate ligand (**1BNa**) added and in the third the methylimidazole ligand as a crosscheck.(Table 18)

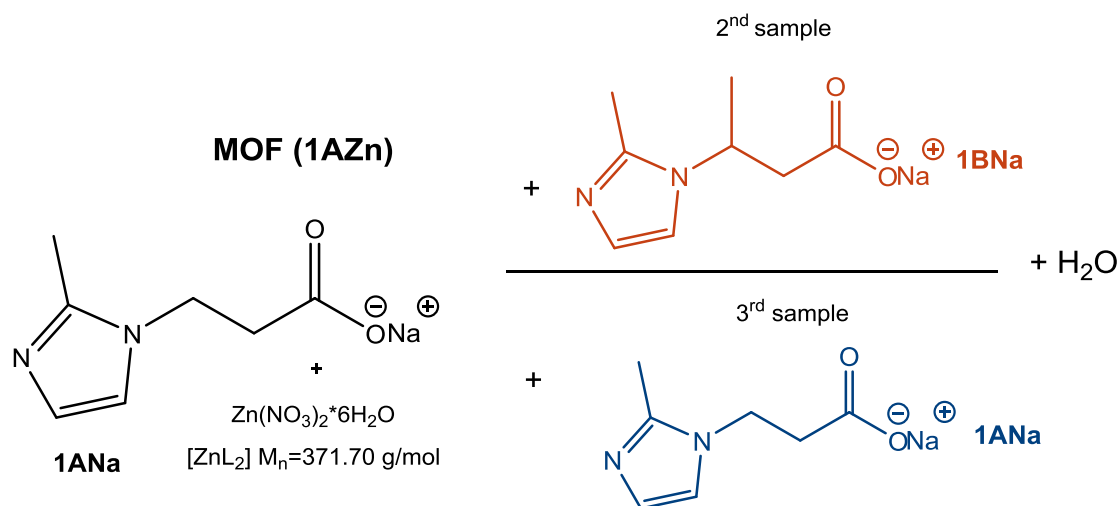


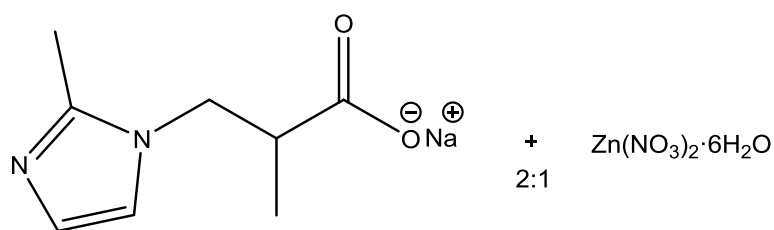
Table 18: Weight of sample taken

	MOF 1AZn concentration [mol/L]	Ligand [eq]	Dissolved fracture [mol%]
1.	5.05*10 ⁻²		18.4
2.	5.89*10 ⁻²	2.1 (1BNa)	84.7
3.	5.99*10 ⁻²	2.3 (1ANa)	25.9

After three days the supernatant of the crystals was removed, evaporated under reduced pressure and dried under vacuum and heat. The amount of the crystal and the residue was weighted out.

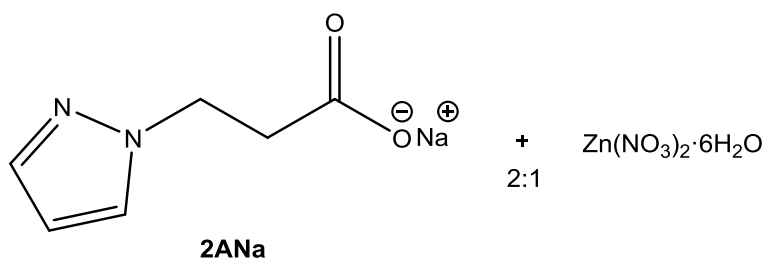
In the case of the first sample 18.4% of the crystals dissolved in the water. In the second case, with the addition of the crotonate ligand (**1BNa**), 84.7% of the crystal passed into solution. It is possible that there proceeds an exchange of the ligand (**1ANa**), which is coordinated in the metal-organic framework, with the free ligand (**1BNa**). That exchange leads to the formation of the soluble complex which was discussed before. It has to be mentioned that 7 mg mass was lost inexplicable in the second sample, maybe somehow in the form of crystal water. In the case of the crosscheck with the addition of the methylimidazole ligand (**1ANa**), 25.9% of the crystal dissolved.

3.3.1.5 Sodium 2-methyl-3-(2-methyl-1H-imidazol-1-yl)propanoate + Zn(NO₃)₂ (1CZn)



The reaction was done by dissolving the ligand (**1CNa**) and the zinc salt separately in respectively 3 mL water. The zinc solution was added to the ligand. There was no precipitation. The clear reaction mixture was heated up to 80 °C. On the next day there was a gelatinous precipitation at the bottom of the vial. The supernatant was evaporated under reduced pressure. A ¹H-NMR spectroscopy was performed in which the ligand could be detected. The behaviour from this component is very similar to component (**1BZn**). There were no further investigations or solubility experiments performed.

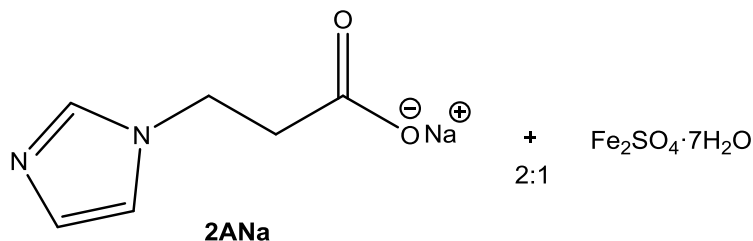
3.3.1.6 Sodium 3-(1H-pyrazol-1-yl)propanoate+ Zn(NO₃)₂ (3AZn)



The reaction was done by dissolving the ligand (**2ANa**) and the zinc salt separately in respectively 2.5 mL water. The zinc nitrate solution was slowly added to the ligand solution with a syringe. There was fine white precipitation and a clear solution. The vial was closed and heated up to 80 °C. After 24 h there was still a fine white precipitation at the bottom of the vial. It was not able to isolate it by filtration and because of that no further investigations were done.

3.3.2 Iron-organic frameworks

3.3.2.1 Sodium 3-(1H-imidazol-1-yl)propanoate + Fe₂SO₄ (2AFe)



The reaction was done by dissolving the ligand (**2ANa**) and the iron salt separately in respectively 3 mL water. The iron sulphate solution was slowly added to the ligand solution with a syringe. There was a dark green fine precipitation. The vial was closed and heated up to 80 °C. After 1 h there was a formation of a brown, thin solid layer at the water's surface. There were still dark green fine particles at the bottom. The solid platelet was lifted off, washed with deionised water and dried under reduced pressure.

It was not possible to obtain a SC-XRD from the solid and no XRD was measured as well.

Thermogravimetric analysis (TGA):

The TGA curve is given in the appendix. The crystals have been dried under reduced pressure. There is a significant endothermal processes occurring at 273 °C which leads to a considerable mass loss from nearly 14% of the overall mass.

Brunauer-Emmett-Teller (BET) surface area analysis:

With BET measurement a surface area from 973.3 m²/g could be yielded. This surface area is much higher than the determined surface areas from the prepared zinc-organic frameworks.

Table 19: BET measurement from the iron-organic framework

Surface area	[m ² /g]
BET surface area	973.2767 ± 14.0779
BJH Adsorption*	737.5697
BJH Desorption*	251.0165
Pore Volume	[cm ³ /g]
BJH Adsorption*	0.843254
BJH Desorption*	0.294245
Pore Size	[Å]
BJH Adsorption*	45.731
BJH Desorption*	46.889
* = cumulative surface area of pores between 17,000 and 3,000,000 Å width	



Figure 51: Solid plate formation on the water surface

4. Conclusion and Outlook

Different metal-organic frameworks have been prepared. The assembling focused on the use of zinc as a metal and a nitrogen and carboxylate containing ligand. These ligands have been prepared with an aza-Michael addition reaction and further have been saponified to yield a pure salt in virtual quantitative conversion. In the course of this work it was possible to determine the crystal structure from three different zinc-organic frameworks. They have been characterized with a multitude of measurements. The diffraction pattern was received with X-ray diffraction, thermal properties were obtained with thermogravimetric analysis and an ATR-IR spectrum was recorded as well. For the determination of the surface area, the pore size and the pore volume, Brunauer-Emmett-Teller measurement was done.

It was first assumed that the zinc-organic framework with the methylimidazole ligand forms an amorphous solid, but XRD measurement has shown that there is a formation of a crystalline form immediately. After drying the crystals there was no dehydration detectable in the TGA. BET measurement yielded a surface area from 112 m²/g.

The imidazole ligand forms an oily layer with the zinc salt first, which is converted into crystals with temperature and after some time. The solid was measured with SC-XRD from the crystals in solution yielding a crystal structure and the knowledge that there is an inclusion of crystal water. After drying the crystals they lose their clearness and crystalline structure, which could be shown with XRD measurement. This leads to the assumption that the water is much more important for the shaping of the crystalline structure for this component in comparison to the zinc-methylimidazole framework. There is a drying step before the BET measurement is performed and therefore the yielded 191 m²/g have also been measured from the degraded, amorphous form.

The zinc-phenylimidazole framework is possibly the most interesting one. Despite the fact that the crystal structure is disordered, the amorphous form is obtained very fast and owns the highest surface area from 328 m²/g.

The assembled zinc-organic frameworks have pore sizes in the range of 50-60 Å. This is pretty high in comparison to the ZIF-8, which owns a pore diameter of 11.6 Å. For this reason the idea behind is to try to encapsulate enzymes, or in general proteins, into these metal-organic frameworks to provide them with a thermal and chemical stability and to protect them against degradation. Therefore the zinc-phenylimidazole framework is the most promising one due to the high yielded porosity and surface area and the fast and easy preparation.

5. Experimental

5.1 Reagents

5.1.1 Chemicals

All chemicals have been purchased from Sigma-Aldrich, TCI or ABCR and were, unless specified otherwise, used as received. Used solvents for reactions, workup and purification were of analytical grade and also used as received.

For the purification of the synthesized compounds column chromatography was performed. Therefore Silica Gel 60 was used as stationary phase

5.2 Instruments

5.2.1 NMR-spectroscopy

The ^1H and ^{13}C NMR-spectra were recorded on a Bruker Ultrashield 300. The spectra were obtained in deuterated solvents, CDCl_3 and D_2O , at 300.36 MHz for ^1H and 75.53 MHz for ^{13}C . Chemical shifts for the ^1H -spectra are reported in points per million (ppm) relative to the singlet of CDCl_3 at 7.26 ppm and relative to the signal of D_2O at 4.79 ppm. The chemical shifts for the ^{13}C -spectra are reported relative to the triplet of CDCl_3 at 77.16 ppm and relative to the signal of TMS at 0 ppm for D_2O . The remaining peaks were identified according to literature. The shape of the occurring peaks is specified as follows: s (singlet), d (doublet), t (triplet), m (multiplet).

5.2.2 Infrared-spectroscopy

The infrared-spectroscopy measurements were taken on an Alpha FT-IR spectrometer from Bruker with the Platinum ATR single reflection diamond ATR module and the results are presented in cm^{-1} .

5.2.3 SC- XRD

The recording of the X-ray crystal structures was done by Ana Torvisco, Ph.D., Institute for Inorganic Chemistry, on an APEX II diffractometer from Bruker with Mo-K_α radiation.

5.2.4 XRD

X-ray powder diffraction profiles were measured with a Siemens D-5005 powder diffractometer with Bragg-Brentano θ/θ geometry, operated at 400 kV and 300 mA, using Cu K_α radiation, a graphite monochromator, a scintillation counter. The step width was 0.02° with constant counting times of 20 s/step.

5.2.5 Thermogravimetric analysis (TGA)

The TGA measurements were performed on a Netzsch STA 449 C. The purge and protective gases were helium, with a flow rate of 50 ml/min and as crucible one out of aluminum oxide was used. The temperature range of the experiments ranged from 20 to 550 K with a heating rate of 10 K/min.

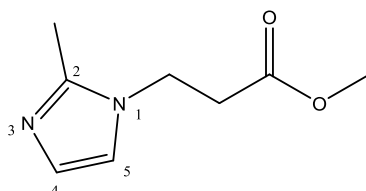
5.2.6 BET measurement

BET was measured at AIT using a Quantachrome® ASiQwin™ instrument. As adsorbate nitrogen was used at a bath temperature of 77.35 K using a cell diameter of 9 mm. The obtained data was analysed by multipoint BET and BJH. The used sample weight was between 50 and 100 mg.

5.2. Synthesis

5.2.1. Aza-Michael addition reaction

5.2.1.1. Methyl 3-(2-methyl-1H-imidazol-1-yl)propanoate (38)



3.3 mL methyl acrylate (0.0364 mol, 1.2 eq.) were added to 2.487 g of 2-methylimidazole (0.0303 mol, 1.0 eq.) in a 10 mL Schlenk tube. The suspension was heated up to 80 °C under reflux and was stirred continuously. The mixture was completely dissolved within 10 min. After 6 h a ¹H-NMR was performed and full conversion was detected. The heat was removed and the oil was dried under reduced pressure to get rid of the excess of methyl acrylate. The colourless oil solidified.

Yield: 4.97 g, (0.0295 mol), >99 % o.th., white solid.

C₈H₁₂N₂O₂ [168.19]

IR: 1729 cm⁻¹ (s), (Lit.^[35]: 1733 cm⁻¹)

¹H-NMR (300 MHz, CDCl₃) δ = 6.91, 6.85 (s, 2H, M.Im^{4,5}), 4.17 (t, J = 6.8 Hz, 2H, N-CH₂CH₂-COO), 3.70 (s, 3H, COO-CH₃), 2.75 (t, J = 6.8 Hz, 2H, N-CH₂CH₂-COO), 2.41 (s, 3H, Me) ppm.

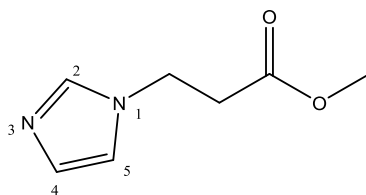
¹³C{¹H}-NMR (75 MHz, CDCl₃) δ = 170.9 (COO), 144.6 (M.Im²), 127.7 (CH, M.Im⁴), 119.0 (CH, M.Im⁵), 52.2 (CH₃, Me), 41.4 (CH₂), 35.3 (CH₂), 13.1 (CH₃, Me) ppm.

Literature:

- *Industrial & Engineering Chemistry Research*, **2007**, 46(25), 8614-8619.
- *Chemistry - An Asian Journal*, **2014**, 9(10), 2806-2813.
- *Tetrahedron Letters*, **2007**, 48(35), 6100-6104.

³⁵ Y. Cai, Q. Wu, Y. Xiao, D. Lv, X. Lin, *Journal of Biotechnology*, **2006**, 121, 330-337.

5.2.1.2. Methyl 3-(1H-imidazol-1-yl)propanoate (12)



3.6 mL methyl acrylate (0.0392 mol, 1.2 eq.) were added to 2.224 g of imidazole (0.0327 mol, 1.0 eq.) in a 10 mL Schlenk tube. The suspension was heated up to 80 °C under reflux and was stirred continuously. The mixture was completely dissolved within 3 min. After 5 h a ^1H -NMR was performed and full conversion was detected. The heat was removed and the oil was dried under reduced pressure to get rid of the excess of methyl acrylate. The yellowish oil solidified.

Yield: 4.97 g, (0.0295 mol), >99 % o.th., yellow-orange solid.

$\text{C}_7\text{H}_{10}\text{N}_2\text{O}_2$ [154.07]

IR: 1736 cm^{-1} (s), (Lit. 35: 1732 cm^{-1})

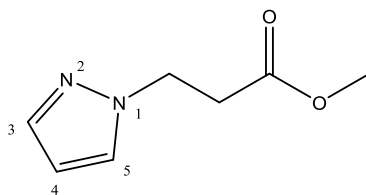
^1H -NMR (300 MHz, CDCl_3) δ = 7.50 (s, 1H, Im²), 7.03, 6.92 (s, 2H, Im^{4,5}), 4.26 (t, J = 6.5 Hz, 2H, N- $\text{CH}_2\text{CH}_2\text{-COO}$), 3.68 (s, 3H, COO-CH_3), 2.77 (t, J = 6.6 Hz, 2H, N- $\text{CH}_2\text{CH}_2\text{-COO}$) ppm.

$^{13}\text{C}\{^1\text{H}\}$ -NMR (75 MHz, CDCl_3) δ = 171.0 (COO), 137.4 (CH, Im²), 129.8, 118.9 (CH, Im^{4,5}), 52.2 (CH_3 , Me), 42.4 (CH_2), 35.9 (CH_2) ppm.

Literature:

- *Chemistry - An Asian Journal*, **2014**, 9(10), 2806-2813.
- *Ultrasonics Sonochemistry*, **2015**, 23, 376-384.
- *Synthetic Communications*, **2010**, 40(7), 973-979.

5.2.1.3. Methyl 3-(1H-pyrazol-1-yl)propanoate (8)



170 μ L methyl acrylate (1.876 mmol, 1.2 eq.) were added to 106.5 mg of pyrazol (1.564 mmol, 1.0 eq.) in a 4 mL glass vial. The suspension was heated up to 80 °C. The mixture was completely dissolved within 2 min. The colourless reaction mixture turned light brown after 1 h and further to yellow after 2 h. A $^1\text{H-NMR}$ was performed after 4 h and full conversion was detected. The heat was removed and the oil was dried under reduced pressure to get rid of the excess of methyl acrylate. A yellow oil was yielded.

Yield: 245 mg, (1.579 mmol), >99 % o.th.

$\text{C}_7\text{H}_{10}\text{N}_2\text{O}_2$ [154.07]

Boiling point^[36]: 110 – 112 °C

$^1\text{H-NMR}$ (300 MHz, CDCl_3) δ = 7.51, 7.44, 6.22 (s, 3H, Pyr^{3,4,5}), 4.44 (t, J = 6.6 Hz, 2H, N- $\text{CH}_2\text{CH}_2\text{-COO}$), 3.68 (s, 3H, COO-CH_3), 2.91 (t, J = 6.6 Hz, 2H, N- $\text{CH}_2\text{CH}_2\text{-COO}$) ppm.

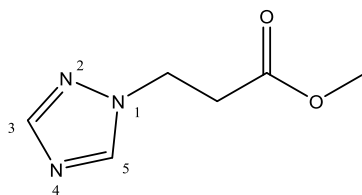
$^{13}\text{C}\{^1\text{H}\}\text{-NMR}$ (75 MHz, CDCl_3) δ = 171.7 (COO), 139.9, 129.8, 105.5 (CH, Pyr^{3,4,5}), 52.1 (CH_3 , Me), 47.4 (CH_2), 34.9 (CH_2) ppm.

Literature:

- *Research on Chemical Intermediates*, **2011**, 37(8), 883-890.
- *Tetrahedron Letters*, **2009**, 50(14), 1653-1657.

³⁶ Reimlinger, I.Hans, *Chemische Berichte*, **1964**, 97, 331-8.

5.2.1.4. Methyl 3-(1H-1,2,4-triazol-1-yl)propanoate (9)



170 μ L methyl acrylate (1.876 mmol, 1.23 eq.) were added to 105.28 mg of 1,2,4-triazole (1.524 mmol, 1.0 eq.) in a 4 mL glass vial. The suspension was heated up to 80 °C. The mixture was completely dissolved within 1 h. A reaction control was performed after 2 h via $^1\text{H-NMR}$ and full conversion was detected. The heat was removed and the slightly yellow oil was dried under reduced pressure to get rid of the excess of methyl acrylate.

Yield: 245 mg, (1.579 mmol), > 99 % o.th.

$\text{C}_6\text{H}_9\text{N}_3\text{O}_2$ [155.15]

Boiling point^[37]: 84 °C

$^1\text{H-NMR}$ (300 MHz, CDCl_3) δ = 8.14, 7.92 (s, 2H, Tri^{3,5}), 4.47 (t, J = 6.2 Hz, 2H, N- $\text{CH}_2\text{CH}_2\text{-COO}$), 3.67 (s, 3H, COO-CH_3), 2.91 (t, J = 6.2 Hz, 2H, N- $\text{CH}_2\text{CH}_2\text{-COO}$) ppm.

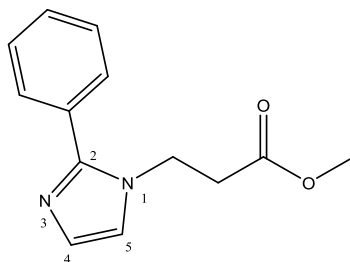
$^{13}\text{C}\{^1\text{H}\}$ -NMR (75 MHz, CDCl_3) δ = 171.0 (COO), 152.2, 143.8 (CH , Tri^{3,5}), 52.2 (CH_3 , Me), 44.9 (CH_2), 34.0 (CH_2) ppm.

Literature:

- *Synthetic Communications*, **2010**, 40(7), 973-979.
- *Tetrahedron Letters*, **2007**, 48(35), 6100-6104.

³⁷ F. Dallacker, *Chemiker-Zeitung*, **1986**, 110, 101-8

5.2.1.5. Methyl 3-(2-phenyl-1H-imidazol-1-yl)propanoate (67)



2.156 mL methyl acrylate (0.024 mol, 3.0 eq.) were added to 1.144 g of 2-phenylimidazole (7.93 mmol, 1.0 eq.) in a 10 mL Schlenk tube. The suspension was heated up to 80 °C under reflux and was stirred continuously. The mixture was completely dissolved within 3 h. After 72 h a ¹H-NMR was performed and almost completely conversion was detected. The heat was removed and the yellow oil was dried under reduced pressure to get rid of the excess of methyl acrylate.

Yield: 1.1983 g, (5.204 mmol), >99 % o.th., yellow oil.

C₁₃H₁₄N₂O₂ [230.27]

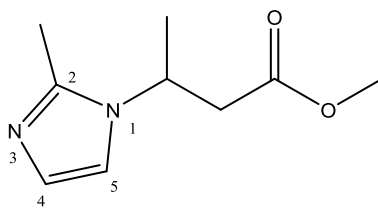
¹H-NMR (300 MHz, CDCl₃) δ = 7.56 – 7.44 (5H, Ph), 7.12, 7.04 (2H, Im^{4,5}), 4.34 (t, J = 7.0 Hz, 2H, N-CH₂CH₂-COO), 3.66 (s, 3H, COO-CH₃), 2.72 (t, J = 7.0 Hz, 2H, N-CH₂CH₂-COO) ppm.

¹³C{¹H}-NMR (75 MHz, CDCl₃) δ = 171.0 (COO), 147.9 (Im²), 130.8 - 128.8 (Ph), 125.8, 120.5 (Im^{4,5}), 52.2 (CH₃, Me), 42.3 (CH₂), 35.6 (CH₂) ppm.

Literature:

- From *Chemistry - An Asian Journal*, **2014**, 9(10), 2806-2813

5.2.1.6. Methyl 3-(2-methyl-1H-imidazol-1-yl)butanoate (33)



166.2 μL methyl crotonate (1.561 mmol, 1.2 eq.) were added to 107.21 mg of 2-methylimidazole (1.306 mmol, 1.0 eq.) in a 4 mL glass vial. The suspension was heated up to 80 $^{\circ}\text{C}$. The mixture was completely dissolved within 5 min. The colourless reaction mixture turned yellow after 10 min and brown after 1.5 h. A reaction control was performed after 24 h via $^1\text{H-NMR}$ almost completely conversion was detected. The heat was removed and the brown oil was dried under reduced pressure to get rid of the excess of methyl crotonate.

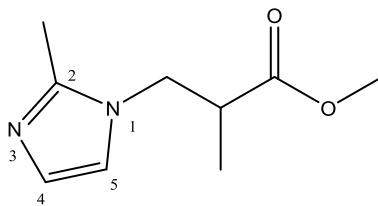
Yield: 238 mg, (1.31 mmol), > 99 % o.th.

$\text{C}_9\text{H}_{14}\text{N}_2\text{O}_2$ [182.22]

$^1\text{H-NMR}$ (300 MHz, CDCl_3) δ = 6.93, 6.84 (s, 2H, M.Im^{4,5}), 4.71–4.60 (m, J = 7.1 Hz, 1H, N-CH(CH₃)-CH₂), 3.63 (s, 3H, COO-CH₃), 2.73 (m, J = 6.7 Hz, 2H, N-CH(CH₃)CH₂-COO), 2.42 (s, 3H, Me) 1.46-1.44 (d, J = 6.8 Hz, 3H, N-CH(CH₃)-CH₂) ppm.

$^{13}\text{C}\{^1\text{H}\}$ -NMR (75 MHz, CDCl_3) δ = 170.5 (COO), 144.2 (M.Im²), 127.8, 114.6 (CH, M.Im^{4,5}), 52.0 (CH₃, COO-CH₃), 48.3 (CH, N-CH(CH₃)-CH₂), 41.9 (CH₂, N-CH(CH₃)-CH₂), 21.8 (CH₃, N-CH(CH₃)-CH₂), 13.1 (CH₃, Me) ppm.

5.2.1.7. Methyl 2-methyl-3-(2-methyl-1H-imidazol-1-yl)propanoate (35)



200 μ L methyl methacrylate (1.87 mmol, 1.2 eq.) were added to 128.10 mg of 2-methylimidazole (1.56 mmol, 1.0 eq.) in a 4 mL glass vial. The suspension was heated up to 80 °C. The mixture was completely dissolved within 1 h. A reaction control was performed after 24 h via $^1\text{H-NMR}$ and full conversion was detected. The heat was removed and the yellow oil was dried under reduced pressure to get rid of the excess of methyl methacrylate.

Yield: 280 mg, (1.54 mmol), 98 % o.th.

$\text{C}_9\text{H}_{14}\text{N}_2\text{O}_2$ [182.22]

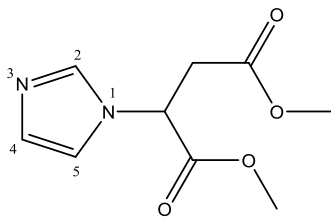
$^1\text{H-NMR}$ (300 MHz, CDCl_3) δ = 6.89, 6.79 (s, 2H, M.Im^{4,5}), 4.20–3.83 (m, 2H, N- $\text{CH}_2\text{-CH}(\text{CH}_3)\text{-COO}$), 3.66 (s, 3H, COO-CH_3), 2.89–2.82 (m, J = 7.2 Hz, 1H, N- $\text{CH}_2\text{-CH}(\text{CH}_3)\text{-COO}$), 2.38 (s, 3H, Me), 1.20–1.18 (d, 3H, N- $\text{CH}_2\text{-CH}(\text{CH}_3)\text{-COO}$) ppm.

$^{13}\text{C}\{^1\text{H}\}\text{-NMR}$ (75 MHz, CDCl_3) δ = 174.3 (COO), 144.7 (M.Im²), 127.5, 119.4 (CH , M.Im^{4,5}), 52.2 (CH_2 , N- $\text{CH}_2\text{-CH}(\text{CH}_3)\text{-COO}$), 48.4 (CH_3 , COO-CH_3), 41.1 (N- $\text{CH}_2\text{-CH}(\text{CH}_3)\text{-COO}$), 15.1, 13.1 (CH_3 , Me) ppm.

Literature:

- *Journal of Molecular Catalysis*, **2012**, 353– 354, 178– 184.

5.2.1.8. Dimethyl 2-(1H-imidazol-1-yl)succinate (50)



784 μL dimethyl crotonate (7.85 mmol, 1.05 eq.) were added to 508.7 mg of imidazole (7.47 mmol, 1.0 eq.) in a 4 mL glass vial. The suspension was heated up to 80 $^{\circ}\text{C}$. The mixture was completely dissolved within 1 h and changed the colour from colourless to. After 3 h a ^1H -NMR was performed and product could be detected. The heat was removed. For purification a column chromatography was performed. (CH:EE, 5:1; DCM:MeOH, 1:3). The product could not be yielded completely purified.

Yield: 1.26 g, (5.944 mmol), 80 % o.th.

$\text{C}_9\text{H}_{12}\text{N}_2\text{O}_4$ [212.21]

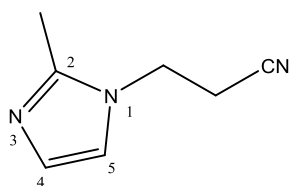
^1H -NMR (300 MHz, CDCl_3) δ = 7.57 (s, 1H, Im^2), 7.07, 6.99 (s, 2H, $\text{Im}^{4,5}$), 5.24 (t, J = 6.8 Hz, 1H, N- $\text{CH}(\text{CH}_2)$ -COO), 3.76 (s, 3H, COO- CH_3), 3.68 (s, 3H, COO- CH_3), 3.29–3.21 (m, 2H, N- $\text{CH}(\text{CH}_2)$ -COO) ppm.

$^{13}\text{C}\{^1\text{H}\}$ -NMR (75 MHz, CDCl_3) δ = 169.8 (COO), 169.0 (COO), 137.2, 130.0, 118.0 (CH, $\text{Im}^{2,4,5}$), 55.8 (CH, N- $\text{CH}(\text{CH}_2)$ -COO), 53.4 (CH_3 , Me), 52.5 (CH_3 , Me), 37.4 (CH_2 , N- $\text{CH}(\text{CH}_2)$ -COO) ppm.

Literature:

- Only the reaction from imidazole with diethyl crotonate.

5.2.1.9. 3-(2-Methyl-1H-imidazol-1-yl)propanenitrile (21)



90 μL acrylonitrile (1.357 mmol, 1.08 eq.) were added to 103.35 mg of 2-methylimidazole (1.259 mmol, 1.0 eq.) in a 4 mL glass vial. The suspension was heated up to 80 $^{\circ}\text{C}$. The mixture was completely dissolved within 20 min. After 3 h a $^1\text{H-NMR}$ was performed and full conversion was detected. The heat was removed and the colourless oil was dried under reduced pressure.

Yield: 168 mg, (1.24 mmol), >99% o.th.

$\text{C}_7\text{H}_9\text{N}_3$ [135.17]

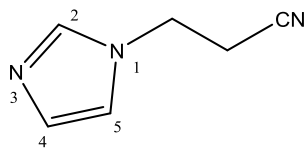
$^1\text{H-NMR}$ (300 MHz, CDCl_3) δ = 6.97, 6.90 (s, 2H, M.Im^{4,5}), 4.17 (t, J = 6.7 Hz, 2H, N- $\text{CH}_2\text{CH}_2\text{-CN}$), 2.75 (t, J = 6.7 Hz, 2H, N- $\text{CH}_2\text{CH}_2\text{-CN}$), 2.43 (s, 3H, Me) ppm.

$^{13}\text{C}\{^1\text{H}\}\text{-NMR}$ (75 MHz, CDCl_3) δ = 144.5 (M.Im²), 128.5, 118.8 (CH, M.Im^{4,5}), 116.6 (CN), 41.6 (CH₂), 20.1 (CH₂), 13.1 (CH₃, Me) ppm.

Literature:

- *Journal of Molecular Catalysis*, **2012**, 353-354, 178-184.
- *Industrial & Engineering Chemistry Research*, **2007**, 46(25), 8614-8619.

5.2.1.10. 3-(1H-Imidazol-1-yl)propanenitrile (22)



90 μ L acrylonitrile (1.357 mmol, 1.01 eq.) were added to 91.17 mg of imidazole (1.339 mmol, 1.0 eq.) in a 4 mL glass vial. The suspension was heated up to 80 $^{\circ}$ C. The mixture was completely dissolved within 20 min. After 3 h a 1 H-NMR was performed and full conversion was detected. The heat was removed and the colourless oil was dried under reduced pressure.

Yield: 170 mg, (1.4 mmol), > 99% o.th.

$C_6H_7N_3$ [121.14]

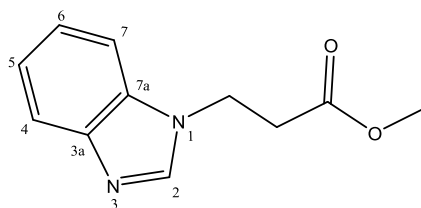
1 H-NMR (300 MHz, $CDCl_3$) δ = 7.58, 7.12, 7.02 (s, 3H, Im^{2,4,5}), 4.27 (t, J = 6.5 Hz, 2H, N-CH₂CH₂-CN), 2.81 (t, J = 6.6 Hz, 2H, N-CH₂CH₂-CN) ppm.

$^{13}C\{^1H\}$ -NMR (75 MHz, $CDCl_3$) δ = 137.1 (CH, Im²), 130.6, 118.7 (CH, Im^{4,5}), 116.6 (CN), 42.6 (CH₂), 20.8 (CH₂) ppm.

Literature:

- *Journal of Molecular Catalysis*, **2012**, 353–354, 178–184.
- *Industrial & Engineering Chemistry Research*, **2007**, 46(25), 8614-8619.

5.2.1.11. Methyl 3-(1H-benzo[d]imidazol-1-yl)propanoate (25)



300 μ L methyl acrylate (3.31 mmol, 3.7 eq.) were added to 106.04 mg of benzimidazole (0.898 mmol, 1.0 eq.) in a 4 mL glass vial. The suspension was heated up to 80 $^{\circ}$ C. The mixture was completely dissolved within 1.5 h. After 48 h a 1 H-NMR was performed and full conversion was detected. The heat was removed and the oil was dried under reduced pressure to get rid of the excess of methyl acrylate.

Yield: 184 mg, (0.9 mmol), > 99 % o.th., yellow-brownish oil.

$C_{11}H_{12}N_2O_2$ [204.23]

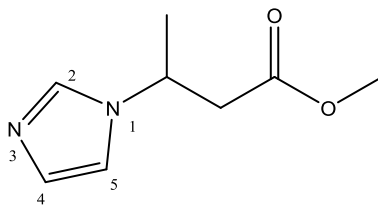
1 H-NMR (300 MHz, $CDCl_3$) δ = 7.93 (s, 1H, B.Im²), 7.77–7.20 (4H, B.Im^{4,5,6,7}), 4.46 (t, J = 6.4 Hz, 2H, N-CH₂CH₂-COO), 3.61 (s, 3H, COO-CH₃), 2.82 (t, J = 6.4 Hz, 2H, N-CH₂CH₂-COO) ppm.

$^{13}C\{^1H\}$ -NMR (75 MHz, $CDCl_3$) δ = 171.1 (COO), 143.9 (B.Im²), 143.4, 133.5 (B.Im^{3a,7a}), 123.2, 122.4, 120.7, 109.4 (B.Im^{4,5,6,7}) 52.2 (CH₃, Me), 40.4 (CH₂), 34.3 (CH₂) ppm.

Literature:

- *From Ultrasonics Sonochemistry*, **2015**, 23, 376-384.
- *Journal of Organic Chemistry*, **2012**, 77(8), 4079-4086.

5.2.1.12. Methyl 3-(1H-imidazol-1-yl)butanoate (27)



156.3 μL methyl crotonate (1.474 mmol, 1.2 eq.) were added to 85.63 mg of imidazole (1.228 mmol, 1.0 eq.) in a 4 mL glass vial. The suspension was heated up to 80 $^{\circ}\text{C}$. The mixture was completely dissolved within 30 min. A reaction control was done after 2 h via $^1\text{H-NMR}$ and almost completely conversion was detected. The heat was removed and the slightly yellow oil was dried under reduced pressure to get rid of the excess of methyl crotonate.

Yield: 207 mg, (1.23 mmol), > 99 % o.th.

$\text{C}_8\text{H}_{12}\text{N}_2\text{O}_2$ [168.20]

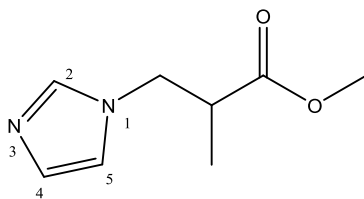
$^1\text{H-NMR}$ (300 MHz, CDCl_3) δ = 7.54, 7.05, 6.94 (s, 3H, $\text{Im}^{2,4,5}$), 4.76–4.65 (m, J = 6.9 Hz, 1H, $\text{N-CH}(\text{CH}_3)\text{-CH}_2$), 3.64 (s, 3H, COO-CH_3), 2.74 (m, J = 6.4 Hz, 2H, $\text{N-CHCH}_2\text{-COO}$), 1.55–1.53 (d, J = 6.8 Hz, 3H, $\text{N-CH}(\text{CH}_3)\text{-CH}_2$) ppm.

$^{13}\text{C}\{^1\text{H}\}\text{-NMR}$ (75 MHz, CDCl_3) δ = 170.5 (COO), 135.9 (CH , Im^2), 129.6, 116.5 (CH , $\text{Im}^{4,5}$), 52.1 (CH , $\text{N-CH}(\text{CH}_3)\text{-CH}_2$), 50.1 (CH_3 , Me), 42.6 (CH_2 , $\text{N-CH}(\text{CH}_3)\text{-CH}_2$), 21.7 (CH_3 , $\text{N-CH}(\text{CH}_3)\text{-CH}_2$) ppm.

Literature:

- *Synthetic Communications*, **2010**, 40(7), 973-979.

5.2.1.13. Methyl 3-(1H-imidazol-1-yl)-2-methylpropanoate (36)



266 μ L methyl methacrylate (2.496 mmol, 1.2 eq.) were added to 141.62 mg of imidazole (2.08 mmol, 1.0 eq.) in a 4 mL glass vial. The suspension was heated up to 80 °C. The mixture was completely dissolved within 1 h. A reaction control was performed after 24 h via $^1\text{H-NMR}$ and almost completely conversion was detected. The heat was removed and the yellow oil was dried under reduced pressure to get rid of the excess of methyl methacrylate.

Yield: 340 mg, (2.02 mmol), >99% o.th.

$\text{C}_8\text{H}_{12}\text{N}_2\text{O}_2$ [168.20]

$^1\text{H-NMR}$ (300 MHz, CDCl_3) δ = 7.46, 7.04, 6.88 (s, 3H, Im^{2,4,5}), 4.28–3.97 (m, 2H, N- CH_2 -CH(CH_3)-COO), 3.67 (s, 3H, COO- CH_3), 2.91–2.84 (m, J = 6.8 Hz, 1H, N- CH_2 -CH(CH_3)-COO), 1.19-1.18 (d, 3H, N- CH_2 -CH(CH_3)-COO) ppm.

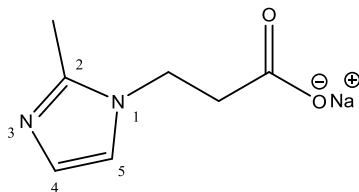
$^{13}\text{C}\{^1\text{H}\}$ -NMR (75 MHz, CDCl_3) δ = 174.3 (COO), 137.7 (CH, Im²), 129.7, 119.3 (CH, Im^{4,5}), 52.3 (CH₂, N- CH_2 -CH(CH_3)-COO), 49.4 (CH₃, COO- CH_3), 41.5 (N- CH_2 -CH(CH_3)-COO), 15.0 (CH₃ N- CH_2 -CH(CH_3)-COO) ppm.

Literature:

- *Journal of Molecular Catalysis*, **2012**, 353–354, 178–184.
- *Tetrahedron*, **2007**, 63(4), 904-909.

5.2.2. Saponification reaction

5.2.2.1. Sodium 3-(2-methyl-1H-imidazol-1-yl)propanoate (20)



4.77 mL of a 5.86 M NaOH solution (0.028 mol, 1.0 eq.) were added to 4.736 g of methyl 3-(2-methyl-1H-imidazol-1-yl)propanoate **38** (0.028 mol, 1.0 eq.) in a 10 mL Schlenk tube. The suspension was heated up to 80 °C under reflux and was stirred continuously. The mixture was completely dissolved within 10 min. After 6 h a ¹H-NMR was measured and full conversion was detected. The heat was removed and the colourless oil became a white solid under drying with reduced pressure.

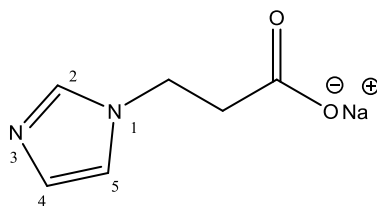
Yield: 4.93 g, (0.0295 mol), > 99 % o.th.

C₇H₉N₂NaO₂ [176.15]

¹H-NMR (300 MHz, D₂O) δ = 7.04, 6.86 (s, 2H, M.Im^{4,5}), 4.15 (t, J = 6.8 Hz, 2H, N-CH₂CH₂-COO), 2.60 (t, J = 6.9 Hz, 2H, N-CH₂CH₂-COO), 2.35 (s, 3H, Me) ppm.

¹³C{¹H}-NMR (75 MHz, D₂O) δ = 182.1 (COO), 148.7 (M.Im²), 128.0, 123.0 (CH, M.Im^{4,5}), 46.0 (CH₂), 41.0 (CH₂), 14.3 (CH₃, Me) ppm.

5.2.2.2. Sodium 3-(1H-imidazol-1-yl)propanoate (24)



4.7 mL of a 6.88 M NaOH solution (0.032 mol, 1.0 eq.) were added to 5 g of methyl 3-(1H-imidazol-1-yl)propanoate **12** (0.032 mol, 1.0 eq.) in a 10 mL Schlenk tube. The suspension was heated up to 80 °C under reflux and was stirred continuously. The mixture was completely dissolved within 15 min. After 3 h a ¹H-NMR was measured and full conversion was detected. The heat was removed and the orange oil solidified under drying with reduced pressure.

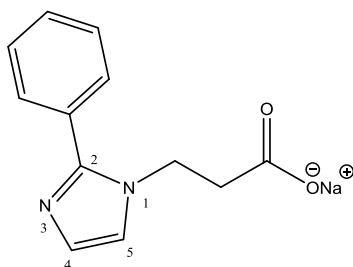
Yield: 6.309 g, (0.0389 mol), > 99 % o.th.

C₆H₇N₂NaO₂ [162.12]

¹H-NMR (300 MHz, D₂O) δ = 7.66, 7.15, 6.98 (s, 3H, Im^{2,4,5}), 4.24 (t, J = 6.6 Hz, 2H, N-CH₂CH₂-COO), 2.64 (t, J = 6.6 Hz, 2H, N-CH₂CH₂-COO) ppm.

¹³C{¹H}-NMR (75 MHz, D₂O) δ = 182.2 (COO), 140.8, 130.3 122.8 (CH, Pyr^{3,4,5}), 47.0 (CH₂), 41.6 (CH₂) ppm.

5.2.2.3. Sodium 3-(2-phenyl-1H-imidazol-1-yl)propanoate (73)



1.056 mL of a 5.17 M NaOH solution (5.46 mmol, 1.05 eq.) were added to 1.198 g of methyl 3-(2-phenyl-1H-imidazol-1-yl)propanoate **67** (5.2 mmol, 1.0 eq.) in a 20 mL glass vial. The emulsion was heated up to 80 °C. After 24 h a ¹H-NMR was measured and full conversion was detected. The heat was removed and the yellow solid was dried under reduced pressure.

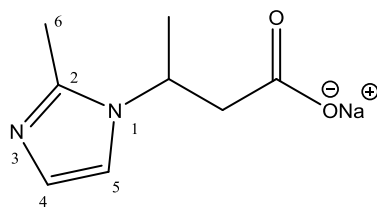
Yield: 1.24 g, (5.2 mmol), > 99 % o.th.

C₁₂H₁₁N₂NaO₂ [238.22]

¹H-NMR (300 MHz, D₂O) δ = 7.57 (s, 5H, Ph), 7.28, 7.09 (s, 2H, Im^{4,5}), 4.27 (t, J = 7.0 Hz, 2H, N-CH₂CH₂-COO), 2.56 (t, J = 6.8 Hz, 2H, N-CH₂CH₂-COO) ppm.

¹³C{¹H}-NMR (75 MHz, D₂O) δ = 181.7 (COO), 150.6 (Im²), 132.6 - 124.3 (Ph), 128.1, 125.9 (Im^{4,5}), 46.7 (CH₂), 41.1 (CH₂) ppm.

5.2.2.4. Sodium 3-(2-methyl-1H-imidazol-1-yl)butanoate (62)



151 μL of a 5.17 M NaOH solution (0.77 mmol, 1.03 eq.) were added to 135.36 mg of methyl 3-(2-methyl-1H-imidazol-1-yl)butanoate **33** (0.75 mmol, 1.0 eq.) in a 4 mL glass vial. The emulsion was heated up to 80 $^{\circ}\text{C}$ without closing the vial to get rid of the resulting methanol. After 24 h a ^1H -NMR was measured and full conversion was detected. The heat was removed and the yellowish, toughly oil became a yellow solid under drying with reduced pressure.

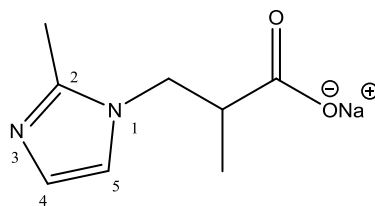
Yield: 143 mg, (0.75 mmol), >99% o.th.

$\text{C}_8\text{H}_{11}\text{N}_2\text{NaO}_2$ [190.18]

^1H -NMR (300 MHz, D_2O) δ = 7.13, 6.87 (s, 2H, M.Im^{4,5}), 4.78–4.57 (m, J = 7.1 Hz, 1H, N-CH(CH₃)-CH₂), 2.61–2.59 (d, J = 7.3 Hz, 2H, N-CH(CH₃)CH₂-COO), 2.36 (s, 3H, Me), 1.39–1.37 (d, J = 6.8 Hz, 3H, N-CH(CH₃)-CH₂) ppm.

$^{13}\text{C}\{^1\text{H}\}$ -NMR (75 MHz, D_2O) δ = 181.6 (COO), 148.2 (M.Im²), 128.6, 119.1 (CH, M.Im^{4,5}), 52.8 (CH, N-CH(CH₃)-CH₂), 47.8 (CH₂, N-CH(CH₃)-CH₂)-CH₂), 23.6 (CH₃, N-CH(CH₃)-CH₂), 14.5 (CH₃, Me) ppm.

5.2.2.5. Sodium 2-methyl-3-(2-methyl-1H-imidazol-1-yl)propanoate (46)



130 μL of a 6.33 M NaOH solution (0.822 mmol, 1.02 eq.) were added to 146.76 mg of methyl 2-methyl-3-(2-methyl-1H-imidazol-1-yl)propanoate **35** (0.805 mmol, 1.0 eq.) in a 4 mL glass vial. The emulsion was heated up to 80 $^{\circ}\text{C}$ without closing the vial to get rid of the resulting methanol. After 3 h the yellow oil solidified. A ^1H -NMR was measured and full conversion was detected. The heat was removed and the solid was dried under reduced pressure.

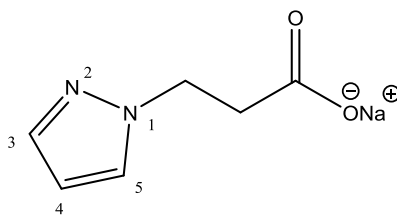
Yield: 153 mg, (0.8 mmol), >99% o.th.

$\text{C}_8\text{H}_{11}\text{N}_2\text{NaO}_2$ [190.18]

^1H -NMR (300 MHz, D_2O) δ = 6.99, 6.82 (s, 2H, M.Im^{4,5}), 4.08–3.82 (m, 2H, N- CH_2 -CH(CH_3)-COO), 2.72–2.63 (m, 1H, N- CH_2 -CH(CH_3)-COO), 2.31 (s, 3H, Me), 1.07-1.05 (d, J = 7.0 Hz, 3H, N-CH(CH_3) CH_2 -COO) ppm.

$^{13}\text{C}\{^1\text{H}\}$ -NMR (75 MHz, D_2O) δ = 184.0 (COO), 148.2 (M.Im²), 134.8, 123.3 (CH, M.Im^{4,5}), 51.9 (CH₂, N- CH_2 -CH(CH_3)-COO), 45.2 (CH₂, N- CH_2 -CH(CH_3)-COO), 17.0 (N- CH_2 -CH(CH_3)-COO), 13.0 (CH₃, Me) ppm. (referenced to KKO62- M.Im² because sample precipitates with standard)

5.2.2.6. Sodium 3-(1H-pyrazol-1-yl)propanoate (98)



3.820 mL of a 5.17 M NaOH solution (0.0197 mol, 1.0 eq.) were added to 3.066 g of methyl 3-(1H-pyrazol-1-yl)propanoate **90** (0.0198 mol, 1.0 eq.) in a 20 mL glass vial. The opened vial with the reaction mixture was heated up to 80 °C. After 24 h the orange mixture turned into a white, yellowish solid. A ¹H-NMR was performed and full conversion was detected.

Yield: 3.3209 g, (0.0205 mol), >99% o.th.

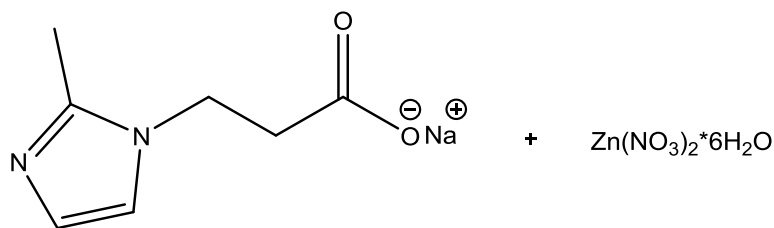
C₆H₇N₂NaO₂ [162.12]

¹H-NMR (300 MHz, D₂O) δ = 7.61, 7.53, 6.30 (s, 3H, Pyr^{3,4,5}), 4.35 (t, J = 6.7 Hz, 2H, N-CH₂CH₂-COO), 2.67 (t, J = 6.8 Hz, 2H, N-CH₂CH₂-COO) ppm.

¹³C{¹H}-NMR (75 MHz, D₂O) δ = 182.2 (COO), 142.3, 133.6, 108.3 (CH, Pyr^{3,4,5}), 51.3 (CH₂), 40.8 (CH₂) ppm.

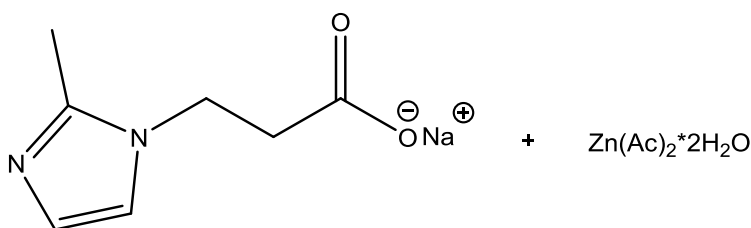
5.2.3 Metal-organic frameworks

5.2.3.1 Sodium 3-(2-methyl-1H-imidazol-1-yl)propanoate + Zn(NO₃)₂ (1AZn)



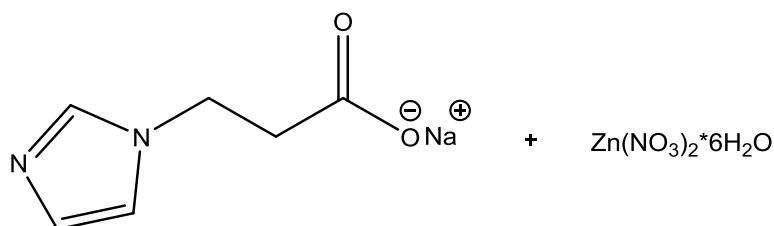
116.5 mg (0.66 mmol, 2.0 eq.) of the ligand sodium 3-(2-methyl-1H-imidazol-1-yl)propanoate **1ANa** were dissolved in 5 mL deionised water in a 20 mL glass vial. 93.6 mg (0.32 mmol, 1.0 eq.) of Zn(NO₃)₂*6H₂O were dissolved separately in 5 mL deionised water. The zinc nitrate solution was slowly added to the ligand solution with a syringe. There was a white finely crystalline precipitation immediately. The vial was closed and heated up to 80 °C. After 1 h a formation of colourless crystals could be detected. After another hour, the solution changed from cloudy into completely clear. After 72 h the solid was filtered by suction, washed with deionised water and dried under reduced pressure.

5.2.3.2. Sodium 3-(2-methyl-1H-imidazol-1-yl)propanoate + Zn(Ac)₂ (1AZn)



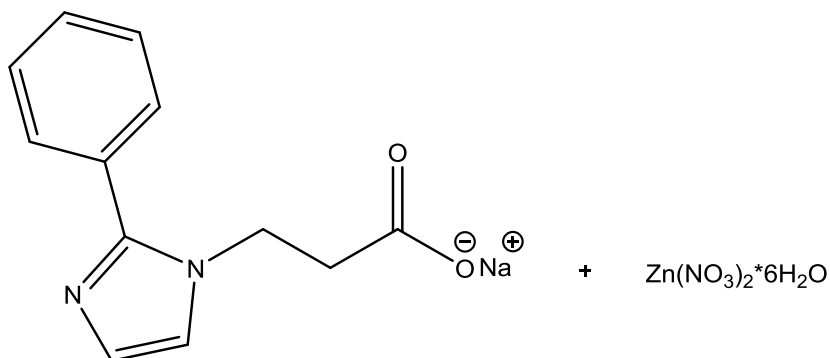
429.53 mg (2.44 mmol, 2.0 eq.) of the ligand sodium 3-(2-methyl-1H-imidazol-1-yl)propanoate **1ANa** were dissolved in 2 mL deionised water in a 20 mL glass vial. 272.43 mg (1.22 mmol, 1.0 eq.) of Zn(Ac)₂*2H₂O were dissolved separately in 2 mL deionised water. The zinc nitrate solution was slowly added to the ligand solution with a syringe. The clear, yellowish solution was heated up to 80 °C. After 1 h a formation of square, clear crystals could be detected. After 72 h the solid was filtered by suction, washed with deionised water and dried under reduced pressure. The filtrate was evaporated.

5.2.3.3. Sodium 3-(1H-imidazol-1-yl)propanoate + Zn(NO₃)₂ (1BZn)



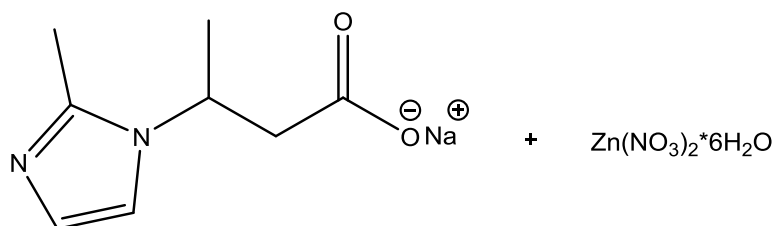
311.81 mg (1.92 mmol, 2.0 eq.) of the ligand sodium 3-(1H-imidazol-1-yl)propanoate **1BNa** were dissolved in 3 mL deionised water in a 20 mL glass vial. 286.04 mg (0.81 mmol, 1.0 eq.) of Zn(NO₃)₂*6H₂O were dissolved separately in 3 mL deionised water. The zinc nitrate solution was slowly added to the ligand solution with a syringe. There was a white finely crystalline precipitation immediately. The vial was closed and heated up to 80 °C. After 20 min the solution was completely clear and there was a thin, yellow, oily layer at the bottom. After 24 h this oily layer was still present. After 30 h there could be a formation of a single, yellow, clear crystal detected. The crystal was filtered by suction, washed with deionised water and dried under reduced pressure at 120 °C. The solid was cloudy and white after the drying process.

5.2.3.4. Sodium 3-(2-phenyl-1H-imidazol-1-yl)propanoate + Zn(NO₃)₂ (6AZn)



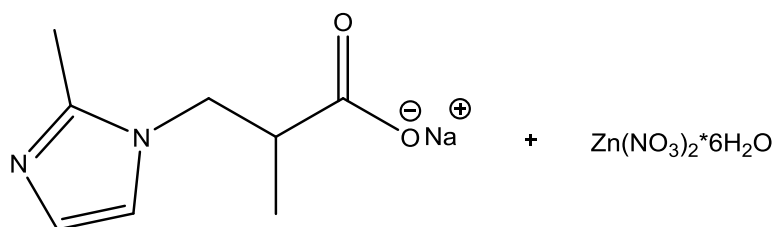
334.34 mg (1.403 mmol, 2.0 eq.) of the ligand sodium 3-(2-phenyl-1H-imidazol-1-yl)propanoate **6ANa** were dissolved in 2 mL deionised water. 205.1 mg (0.690 mmol, 1.0 eq.) of Zn(NO₃)₂*6H₂O were dissolved separately in 2 mL deionised water. The zinc nitrate solution was slowly added to the ligand solution with a syringe into a glass vial which was suitable for the Monowave 50. There was a white viscous precipitation immediately. The reaction mixture was put in the Monowave 50 at 150 °C for 45 min. There was a formation of a yellow solid layer at the bottom of the reaction vessel. The supernatant was removed into a new glass vial and heated up to 80 °C. After 24 h a formation of a white crystal could be detected.

5.2.3.5. Sodium 3-(2-methyl-1H-imidazol-1-yl)butanoate + Zn(NO₃)₂ (1BZn)



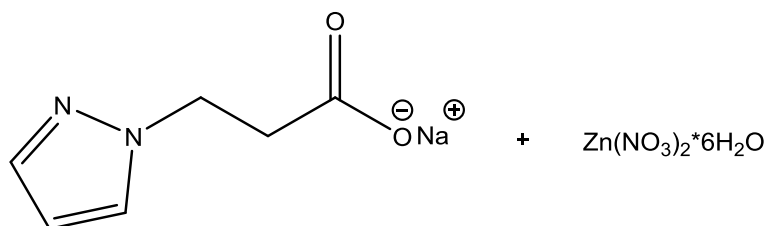
331.04 mg (1.741 mmol, 2.0 eq.) of the ligand sodium 3-(2-methyl-1H-imidazol-1-yl)butanoate **1BNa** were dissolved in 3 mL deionised water in a 20 mL glass vial. 257.92 mg (0.868 mmol, 1.0 eq.) of Zn(NO₃)₂·6H₂O were dissolved separately in 3 mL deionised water. The zinc nitrate solution was slowly added to the ligand solution with a syringe. There was a no precipitation. The solution was completely clear. The vial was closed and heated up to 80 °C. After 24 h there was a fine white precipitation at the bottom of the vial.

5.2.3.6. Sodium 2-methyl-3-(2-methyl-1H-imidazol-1-yl)propanoate + Zn(NO₃)₂ (1CZn)



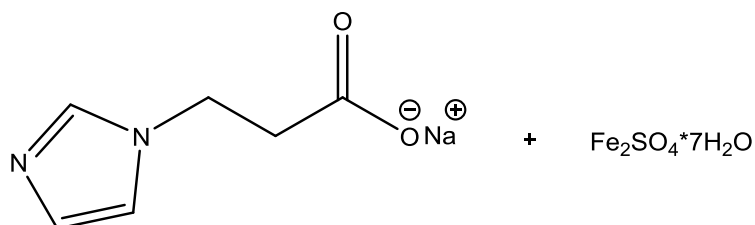
301.70 mg (1.586 mmol, 2.0 eq.) of the ligand sodium 2-methyl-3-(2-methyl-1H-imidazol-1-yl)propanoate **1CNa** were dissolved in 3 mL deionised water in a 20 mL glass vial. 232.20 mg (0.782 mmol, 1.0 eq.) of Zn(NO₃)₂·6H₂O were dissolved separately in 3 mL deionised water. The zinc nitrate solution was slowly added to the ligand solution with a syringe. There was a no precipitation. The solution was completely clear. The vial was closed and heated up to 80 °C. After 2 h there was a very small amount of solid at the bottom of the vial. After 24 h there was a gelatinous precipitation.

5.2.3.7. Sodium 3-(1H-pyrazol-1-yl)propanoate+ Zn(NO₃)₂ (3AZn)



213.53 mg (1.317 mmol, 2.0 eq.) of the ligand sodium 3-(1H-pyrazol-1-yl)propanoate **3ANa** were dissolved in 5 mL deionised water in a 20 mL glass vial. 201.11 mg (0.677 mmol, 1.0 eq.) of Zn(NO₃)₂*6H₂O were dissolved separately in 5 mL deionised water. The zinc nitrate solution was slowly added to the ligand solution with a syringe. There was fine white precipitation. The solution was clear. The vial was closed and heated up to 80 °C. After 24 h there was still a fine white precipitation.

5.2.3.8. Sodium 3-(1H-imidazol-1-yl)propanoate + Fe₂SO₄ (2AFe)



263.5 mg (1.56 mmol, 2.02 eq.) of the ligand sodium 3-(1H-imidazol-1-yl)propanoate **2AZn** was dissolved in 3 mL deionised water in a 20 mL glass vial. 216.05 mg (0.77 mmol, 1.0 eq.) of Fe₂SO₄*7H₂O were dissolved separately in 3 mL deionised water. The iron sulphate solution was slowly added to the ligand solution with a syringe. There was a dark green finely precipitation immediately. The vial was closed and heated up to 80 °C. After 1 h there was a formation of a brown, thin, solid layer at the water's surface. There was still a dark green precipitation at the bottom. After another hour the solid platelet was lifted off, washed with deionised water and tried under reduced pressure. The dark green residue was put in the oven to yield again a brown, solid layer on the next day.

6. List of Abbreviations

Analytical methods

<i>J</i>	Coupling constant
BET	Brunauer-Emmett-Teller model
BJH	Barrett-Joyner-Halender model
Hz	Hertz
IR	Infrared
MHz	Megahertz
NMR	Nuclear Magnetic Resonance
d	Doublet
m	Multiplet
q	Quadruplett
SC-XRD	Single-crystal X-ray diffraction
s	Singlet
t	Triplet
TGA	Thermogravimetric analysis
ppm	Parts per million
XRD	X-ray powder diffraction

Chemical formula

BDC	Benzene-1,4-dicarboxylate
CDCl ₃	Deuterated chloroform
D ₂ O	Deuterium oxide
DMAP	4-(Dimethylamino)pyridine
NaOH	Sodium hydroxide
Zn(NO ₃) ₂	Zinc nitrate

Others

MOF	Metal-organic framework
SOD	Sodalite
STP	Standard temperature and pressure
ZIF	Zeolitic imidazolate framework

6. List of Figures

Figure 1: Crystal structures of ZIFs ^[9]	2
Figure 2: Crystal structure of ZIF-8	3
Figure 3: Crystal structure of MOF-5 ^[1]	4
Figure 4: a) coordination environment of Zn ²⁺ b) 3D framework	5
Figure 5: a) Coordination environment of Zn ²⁺ b) 3D framework formed by hydrogen bonds	6
Figure 6: Donors and acceptors used for the Michael-addition reaction	8
Figure 7: Working aza-Michael addition reactions	9
Figure 8: Michael-addition reaction with 2-methylimidazole and methyl acrylate	10
Figure 9: ¹ H-NMR spectrum from 2-methylimidazole with methyl acrylate after full conversion	10
Figure 10: ¹³ C-NMR spectrum from 2-methylimidazole with methyl acrylate after full conversion	11
Figure 11: Unsuccessful aza-Michael addition reactions	12
Figure 12: Mechanism for the nucleophile catalysed Michael-addition ^[1]	13
Figure 13: pK _a -values	14
Figure 14: Determination of the kinetic in the case of 2-methylimidazole and methyl methacrylate	15
Figure 15: Reaction of methylimidazole with methyl acrylate	15
Figure 16: Decrease of the amount of educt against the time	16
Figure 17: Plot 1/[c _{educt}] and 1/[c _{educt}] ² versus the time [min]	17
Figure 18: Ideal and real course of the reaction	18
Figure 19: Compounds yielded after saponification	19
Figure 20: Mechanism of base hydrolysis ^[26]	19
Figure 21: ATR-IR measurement from the ester and the salt	20
Figure 22: Measurements from the different prepared MOFs	21
Figure 23: Crystals (c) from the preparation with the methylimidazole ligand	22
Figure 24: Crystals from the preparation with Zn(Ac) ₂ ·2H ₂ O	22
Figure 25: Amorphous solid (powder (p))	22
Figure 26: Crystal structure	23
Figure 27: Coordination polymer chain seen along the a-axis	24
Figure 28: Chain seen along the b-axis	24
Figure 29: Solid state structures with water and without water	25
Figure 30: XRD pattern from the methylimidazole derivate	27
Figure 31: Comparison of the carboxylate group in the ATR-IR spectrum	29
Figure 32: TGA from the MOF with the methylimidazole derivate	30
Figure 33: BET plot	33
Figure 34: Plot of pore size distribution	34
Figure 35: Measurements from the different prepared MOFs	35
Figure 36: Prepared crystals	35
Figure 37: Crystal structure	36
Figure 38: Crystal scaffold	37
Figure 39: Part of the twisted 2D-network seen in the direction of the c-axis	38
Figure 40: 3D network via hydrogen bonding	38
Figure 41: Solid state structures with water	39
Figure 42: XRD pattern from the imidazole derivate	40
Figure 43: Comparison of the carboxylate group in the ATR-IR spectrum	42
Figure 44: TGA from the MOF with the methylimidazole derivate	43
Figure 45: Viscous precipitation after addition of the metal salt (left) and amorphous solid (right)	46
Figure 46: Crystalline form after heating up in the Monowave 50	46
Figure 47: Crystal structure	47

Figure 48: Crystal scaffold	47
Figure 49: ¹ H-NMR of the metal-organic framework and the free ligand	50
Figure 50: Solid plate formation on the water's surface	54

7. List of Tables

Table 1: Degree of conversion	16
Table 2: Concentration of educt	17
Table 3: Coordination around zinc	23
Table 4: Crystallographic data	26
Table 5: Reflexes from the XRD measurement from the methylimidazole derivate	28
Table 6: Calculated lattice spacing from the SC-XRD data	28
Table 7: Bands of the metal-organic framework with the methylimidazole derivate	29
Table 8: Data from the BET measurement from the MOF with the methylimidazole derivate	31
Table 9: Coordination parameters	36
Table 10: Crystallographic data	40
Table 11: Calculated lattice spacing from the SC-XRD data	41
Table 12: Bands of the metal-organic framework with the methylimidazole derivate	42
Table 13: BET measurement from the MOF with the imidazole derivate	44
Table 14: coordination around zinc	48
Table 15: Crystallographic data	48
Table 16: Bands of the metal-organic framework with the phenylimidazole derivate	49
Table 17: Data from the BET measurement for the MOF with the phenylimidazole derivate	49
Table 18: Weight of sample taken	51
Table 19: BET measurement from the iron-organic framework	54

8. Appendix

8.1 NMR-spectra

The ^1H - and ^{13}C -NMR spectra of all synthesized compounds (part 5.2 Synthesis) from the aza-Michael addition reaction and saponification can be found in the file:

M:\ICTM\ANYONE\NMR\NMR Kodolitsch K

8.2 IR-spectra

The IR spectra from the metal organic frameworks (49), (65), (102) and the spectra from the corresponding free ligands can be found in file:

M:\ICTM\ANYONE\Katharina Kodolitsch\Master Thesis_Data\IR

8.3 TGA

The TGA curve from the metal organic frameworks (49), (65), (102) can be found in file:

M:\ICTM\ANYONE\Katharina Kodolitsch\Master Thesis_Data\TGA

8.4 SC-XRD

All the data from Single-crystal X-ray diffraction for compounds (49), (65) and (102) are given in:

M:\ICTM\ANYONE\Katharina Kodolitsch\Master Thesis_Data\SC-XRD

8.5 XRD

All the data from X-ray powder diffraction for compounds (49) and (65) are given in:

M:\ICTM\ANYONE\Katharina Kodolitsch\Master Thesis_Data\XRD

8.6 BET

The Exel files with all the data needed for the calculation of the BET surface area, the pore size and the pore volume for the compounds (49), (65) and (102) can be found in file:

M:\ICTM\ANYONE\Katharina Kodolitsch\Master Thesis_Data\BET